CMUG Phase 2 Deliverable

Reference: **D3.1: Quality Assessment Report**
Due date: **June 2015**
Submission date: **July 2015**
Version: **0.5**

Climate Modelling User Group

Phase 2 Deliverable 3.1

Quality Assessment Report

Centres providing input: Met Office, MPI-M, ECMWF, MétéoFrance, SMHI, DLR

Version nr.	Date	Status
0.1	21 Apr 15	Outline for partner comment
0.2	29 June 15	Partner contributions added
0.3	20 July 15	Partner contributions added
0.4	3 Sep 15	Section 4 added, figure & table numbering updated
0.5	23 Sep 15	Readability edits

CMUG Phase 2 Deliverable 3.1

Quality Assessment Report

Table of Contents

Quality Assessment Report

1. Purpose and scope of this report

The purpose of this document is to assess the quality of the CCI products and give feedback to ESA and the CCI teams. This assessment was conducted by the climate modelling and reanalysis centres in the CMUG consortium using CCI Phase 1 data (subsequent versions of this report will use Phase 2 data) and included a wide range of data and model interactions (assimilation, boundary conditions, optimisation, reanalysis, sensitivity studies etc). Some of the top level questions examined by the CMUG research are:

- Are the CCI data products of 'climate quality' i.e. is their quality adequate for use in climate modelling, reanalysis and for wider research applications?
- Are the error characteristics provided by CCI products adequate?
- Do the products meet the Global Climate Observing System (GCOS) quality requirements for satellite for Essential Climate Variables (ECV)?
- Is the quality of the products sufficient for climate service applications?

2. CMUG methodology and approach for assessing quality in CCI products

This report describes the results in the first 12 months of CMUG Phase 2 from CMUG Task 3 "Assessing consistency and quality of CCI products". The work is spread across twelve Work Packages (WP) listed in table 1, which includes the CCI product being assessed, the CMUG model being used to make the assessment, and the type of climate modeling experiment.

The CMUG results presented here provide information on the accuracy, consistency and usefulness of the CCI data sets. The analysis assessed the suitability of the CCI datasets for coupled climate model and reanalysis applications and evaluated the impact of the data products on model based studies, including quantification of the uncertainties associated with both the models and the observations (see table 1). This information is aimed at the CCI teams producing the data but will also be of use to other modelling centres who will use CCI data in the future.

The modeling experiments are described in the following sections of this report, and cover the following topics: assimilation of CCI data into climate models; cross assessments of CCI data (those which have physical links/interactions); applications for reanalysis; integrated assessment of CCI data in climate models; boundary condition forcing experiments; regional modeling; earth system process studies.

The CMUG work reported here was conducted with the CCI data available at the time, which in most cases were from the final Phase 1 Climate Record Data Packages produced by the CCI projects. Future versions of this report will cover studies using Phase 2 CCI data.

		CCI products												
		SST	SSH	Seaice	OC	Cloud	Ozone	Aerosol	GHG	LC	SM	Fire	Glacier	
CMUG Task 3: Assessing consistency and quality of CCI products														
WP	**CMUG Model**	**Ocean**				**Atmosphere**				**Land**				**Experiment Type**
3.1	FOAM	X	X	X	X									Assimilation
O3.1	NEMOVAR, ORA	X	X	X	X									Assimilation and Detection
3.2	ERA-Clim						X							Assimilation
3.3	MACC-II						X	X	X					Assimilation
3.4	JSBACH, TM3								X	X	X	X		Assimilation
O3.4	EC-Earth/CMIP5	X				X	X	X	X		X			Assessment, evaluation
3.5	LMDz, ORCHIDEE								X	X	X	X		Boundary Condition
3.6	MPI-OM, MPI-ESM	X		X	X	X								Assimilation (Polar Regions)
3.7	EMAC-MADE					X		X						Comparison
3.8	RCA HARMONIE	X				X					X			Comparison/Eval (CORDEX Africa)
3.9	Arctic HYPE		X							X			X	Assessment
3.10	CNRM-RCM	X	X			X		X			X			Comparison (Med CORDEX)

Table 1: Summary of the CMUG Work Packages, CMUG models, CCI products, and CMUG experiments for assessing quality of the CCI products, as given in this report.

3. Summary of CMUG assessment of Quality by WP

3.1 Assessment of Marine ECVs in FOAM Ocean Model [WP 3.1]

Aim

The aim of this research is to make an integrated assessment of marine ECVs to assess their consistency within a global and shelf seas regional data assimilation environment, and to provide an assessment of the uncertainty. It will address the following scientific questions:

- Are the individual marine CCI CDRs good enough for assimilation purposes?
- What are the changes made to the analyses by assimilating the CCI data?
- Are the uncertainties provided useful to assign observation errors to the measurements?
- Are the four marine ECVs mutually consistent from an ocean assimilation point of view?
- What should be recommended to EUMETSAT for Sentinel-3 processing to operational centres?

Summary of Results

Initial work has so far focused on assessment of the ocean colour CCI (OC-CCI) data for assimilation purposes. This will be extended to an integrated assessment of all four marine ECVs during the remainder of CMUG Phase 2.

At the end of Phase 1, a global ocean reanalysis was produced by assimilating OC-CCI V1 chlorophyll products into the FOAM-HadOCC coupled physical-biogeochemical ocean model (Storkey et al., 2010; Palmer and Totterdell, 2001; Hemmings et al., 2008; Ford et al., 2012), covering the period from September 1997 to July 2012. For comparison, a reanalysis was also produced assimilating the predecessor GlobColour products, as well as a control run with no data assimilation. A thorough assessment of the results has been performed during the first 12 months of Phase 2, and is summarised below. The work is being written up and will be submitted for publication in a peer-review journal. The methodology will then be extended to include all four marine ECVs, with appropriate assessment.

The OC-CCI products were found to be of sufficient quality for data assimilation purposes, and of at least equal quality to the GlobColour products (more detail on the comparison with GlobColour is included in the "Quality relevant outcomes" sub-section below). Assimilating OC-CCI chlorophyll data improved the model's representation of sea surface chlorophyll compared with both satellite data sets, and also a range of independent in situ observations. An example of this is shown in figure 1, which plots a time series of sea surface chlorophyll from all three model runs at the Hawaii Ocean Time Series (HOT) site in the North Pacific, along with in situ observations. The assimilation results in a much better match for both the magnitude and seasonality of the observations. It is also able to produce a reanalysis which is stable with time whilst displaying inter-annual variability.

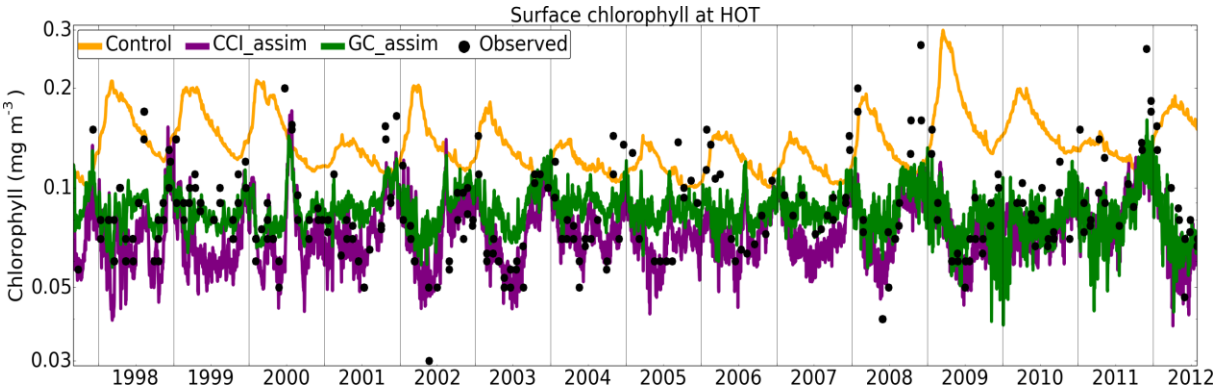

Figure 1: Time series of modelled and observed chlorophyll concentration in the surface 10 m at the HOT site. Observations have been obtained from http://hahana.soest.hawaii.edu/hot.

The largest impact of the assimilation was on sea surface chlorophyll, but an improved representation of chlorophyll was also found throughout the water column. Corresponding changes were found in phytoplankton and zooplankton biomass, although limited observational data are available for validation. Changes to nutrient concentrations were small, and largely neutral compared with observations. This is an important result, as some studies have found a degradation of nutrients due to chlorophyll assimilation.

Validation has also focused on the impact of the assimilation on the model carbon cycle, as this is of particular relevance for climate studies. Validation has been performed against surface fugacity of carbon dioxide (fCO_2) observations from the SOCAT V2 database (Bakker et al., 2014). Overall, the effect of the chlorophyll assimilation was small compared with the magnitude of model biases. In part, this is because there are large physical controls on the carbon cycle. The impact on these of additionally assimilating physical ECVs will be assessed as part of forthcoming Phase 2 activities. In regions of strong biological activity, the chlorophyll assimilation was found to have a beneficial impact on carbon variables, an example of which is shown in figure 2. In some areas, the assimilation was found to improve representation of the biological component of the carbon cycle, but overall degrade fCO_2 compared with observations due to compensating errors in the physical component of the carbon cycle. Again, the impact in these cases of combined assimilation of all marine ECVs will be assessed later in Phase 2.

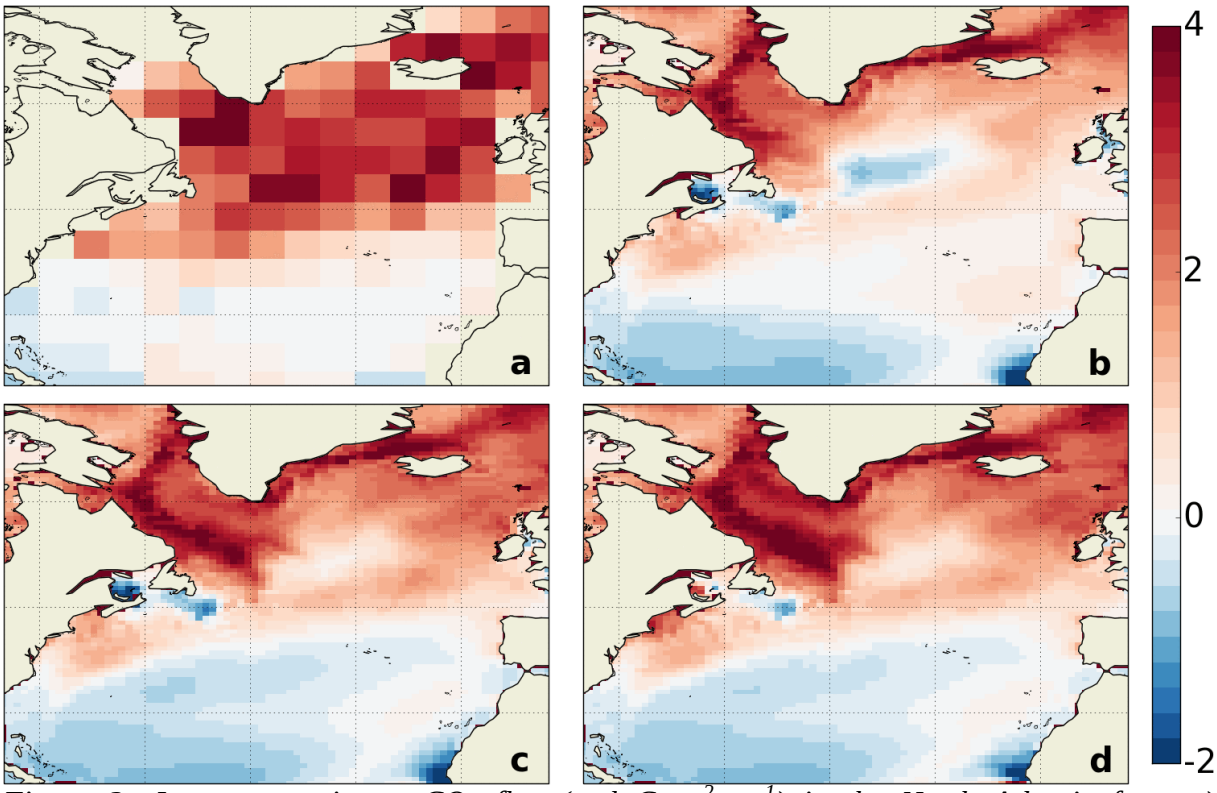

Figure 2: June mean air-sea CO_2 flux (mol C m^{-2} yr^{-1}) in the North Atlantic from a) climatology of Takahashi et al. (2009), b) FOAM-HadOCC control, c) reanalysis assimilating GlobColour data, d) reanalysis assimilating OC-CCI data. Positive values represent a flux into the ocean. The reduction in spurious outgassing in the centre of the domain in c) and d) compared with b) is due to the assimilation reducing the chlorophyll bias in this area.

Technical issues with the OC-CCI V1 products have already been reported on during Phase 1. OC-CCI V2 products have recently been released (although the release was not directly communicated to CMUG researchers), and testing will be performed to see if previous issues have been resolved. An initial reading of the Product User Guide suggests that the documentation has been improved, particularly regarding use of the uncertainty estimates.

Quality relevant outcomes

A comparison between the OC-CCI V1 and GlobColour observation products has been performed to assess their stability and spatial coverage, building on that reported on at the end of Phase 1. GlobColour has greater spatial coverage prior to 2002, as it uses an older NASA SeaWiFS processing which discards fewer data points. Between 2002 and 2012, OC-CCI has greater coverage as more use is made of MERIS data. This is of particular benefit to the assimilation in certain regions, such as the Mauritanian upwelling region and the Arabian Sea during the Asian monsoon period, which were poorly covered by GlobColour. There is a lack of *in situ* observations with which to validate the results in these areas, but the model fields when assimilating OC-CCI data are in line with qualitative expectations. The global mean and spatial standard deviation of the OC-CCI chlorophyll products are also more stable with time

than GlobColour, although a marked reduction in variability is noted when MERIS is introduced in 2002. This seems to suggest that the different sensors are not fully inter-calibrated. Such features are less clear in the reanalysis fields, as to some extent the model acts to smooth these out, and overall very similar results are obtained whether OC-CCI or GlobColour products are assimilated.

In the current line of work, the uncertainty estimates have been used to assign observation errors during the quality control stage, but not as part of the assimilation. The latter requires a development to the data assimilation scheme, which is expected to be included for future Phase 2 activities, allowing the uncertainty estimates to be assessed in this context. As part of the quality control, the only issue found was that not every observation had a corresponding uncertainty, as reported during Phase 1, which led to these observations being automatically rejected. This is a known issue which the OC-CCI team is aware of. Some use has been made of the uncertainties in a validation context, although a lack of documentation for the V1 products meant their appropriate usage was not entirely clear. As noted above, this appears to have been much improved for the V2 release, which should allow more, and improved, use of these uncertainties.

Assessment of the seasonal and inter-annual variability of the reanalyses has also been performed, including the impact of the data assimilation on this variability, as an assessment of the applicability of the end product to climate monitoring activities. As mentioned above, the assimilation has a beneficial impact on the variability of model chlorophyll, and has also been found to impact phenological indicators, for instance the start dates of the North Atlantic spring bloom. The effect of the assimilation on the carbon cycle variability is more subtle, with it impacting the magnitude more than the variability of the air-sea CO_2 flux. Nonetheless, the model is able to capture observed variability relating to climate drivers such as the El Niño Southern Oscillation (ENSO), the North Atlantic Oscillation and the Atlantic Meridional Overturning Circulation. An example is shown in figure 3, which plots time series of the Tropical Pacific mean air-sea CO_2 flux, along with the multivariate ENSO index. Anomalies are seen corresponding to El Niño and La Niña events, related to changes in upwelling.

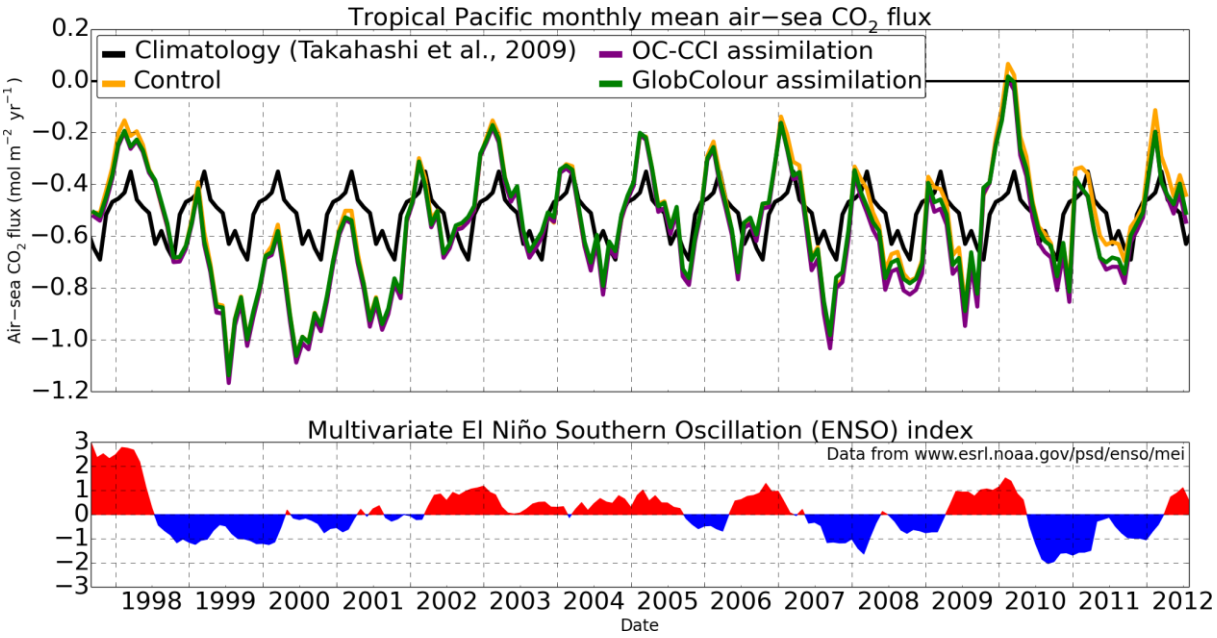

Figure 3. Top: Tropical Pacific mean air-sea CO_2 flux from the climatology of Takahashi et al. (2009) repeating in black, and each model run (coloured lines, as labeled). Bottom: multivariate ENSO index, as obtained from http://www.esrl.noaa.gov/psd/enso/mei.

3.2 Assimilation of several L2 ozone products in the ERA-Clim system [WP 3.2]

Aim

The aim of this study is to promote and facilitate the integration of as many O3-CCI products as possible in reanalysis systems in general and in the forthcoming ERA5 production in particular. A number of Observing System Experiments (OSEs) have been designed to provide a detailed assessment of the quality and of the impact of these O3-CCI products. The list of assessed datasets includes seven products encompassing the three lines of production of O3-CCI (total column, profiles from nadir instruments, and profiles from limb instruments).

For some of the European instruments considered by O3-CCI, alternative retrieval algorithms exist besides those developed within the CCI project. This enables users to download alternative datasets, but it may not be obvious which of the available datasets best suits their applications or models. A set of Round Robin (RR) assimilation exercises for algorithm selection were therefore performed to provide an objective and rigorous assessment of the impact of assimilating datasets retrieved from the same measurements but with competing retrieval schemes, thus giving the reanalysis community feedback on which datasets to use.

By inter-comparison with the results from some of the performed experiments, it is possible to provide user recommendations to space agencies and retrieval teams on the most useful characteristics of future satellite instruments for ozone measurement.

Summary of Results

The results from this study can be summarized as follows:

- The structure of observation uncertainties generally compare well with estimates obtained using the Desroziers method (Desroziers et al., 2005). The differences between estimated and provided uncertainties show up to 60% overestimation in the tropical mid stratosphere for GOME-2 NPO3 (this accounts for less than 4% of the observation values) and up to 100% underestimation in the tropics for the total columns (this difference is about 8% of the global mean total column ozone value).
- All the products exhibit negligible to very small biases.
- All assessed O3-CCI datasets lead to improved ozone analyses.
- Regarding the RR assimilation exercises, with the exception of OMI TCO3, the O3-CCI retrievals seem to better constrain the ozone analyses than retrievals obtained from the same radiances using alternative algorithms.
- The assimilation of the GOME-2 NPO3 show a clear improvement in the internal consistency of the data assimilation system in terms of better fit to the AIRS ozone-sensitive IR channels that in turn leads to statistically significant reduction (i.e. improvement) in the RMS of the geopotential forecast errors in the tropics.
- Assimilation User Requirements to Space Agencies and retrieval teams:
  - ❖ The comparison of the impact generated by the GOME-2 TCO3 and that of the GOME-2 NPO3 shows that the latter dataset can lead to a greater positive impact on the ozone analyses than the former.

- The comparison of the impact generated by the GOME-2 NPO3 and that of the MIPAS LPO3 shows that thanks to its higher vertical resolution limb observations can lead to a greater positive impact in the stratosphere and upper troposphere than the nadir ozone profiles. This is not always the case in the lower troposphere, where despite lacking visibility, the limb observations can still improve the ozone analyses compared to a control experiment if their synergy with other observations (in particular total column ozone products) can be exploited within the data assimilation system.

Based on the discussed results and conclusions, the following O3-CCI products are recommended to be assimilated in the forthcoming ERA5 reanalysis: SCIAMACHY TCO3; GOME and GOME-2 NPO3; MIPAS LPO3.

Datasets and experiment set-up

Table 2 lists all the assessed products from O3-CCI (in orange) and for some of them additional datasets retrieved from the same instrument measurements but with alternative algorithms (in blue). These additional datasets were used for the four RR assimilation exercises. All used datasets (included non CCI) were reprocessed products retrieved with the latest available algorithm at time the experiments were run though might not be the latest version available at time of writing. For instance, the O3M-SAF product was recently reprocessed with the GDP4.7 algorithm. Independent validation of the GDP4.6 and GDP4.7 GOME-2 products shows a roughly 1% underestimation of the TCO3 in the GDP4.6 version as opposed to a 1% overestimation found in the GDP4.7 product (D. Loyola, DLR, personal communication).

Experiments were run for the period July-October 2008 except for the ERS-2 GOME datasets that were assessed over the period July-October 1997. The data assimilation system consists of a reduced resolution version of the ECMWF Integrated Forecasting System (IFS) run at T511 (about 40 km grid resolution) on 91 vertical levels spanning the atmosphere from surface up to 0.01hPa.

A control experiment (referred to as *Exp/CTRL* hereafter) was run using the following observations:

- **L2 ozone data:** 1 TCO3 (SCIAMACHY or OMI depending on the assessment), 6-layer partial column O3 from three SBUV/2 instruments.
- **IR ozone sensitive channels:** HIRS for the 1997 experiments; HIRS, IASI, and AIRS for the 2008 experiments.
- **Other observations:** All other non-ozone sensitive observations used in ERA-Interim.

A perturbation experiment (referred to as *Exp/PERT* hereafter) was then run with exactly the same configuration of *Exp/CTRL* plus the assimilation of one of the datasets listed in table 2.

Satellite / Instrument	Production Lines for ozone products					
	TCO3			NPO3	LPO3	
ERS-2 / GOME	**CCI (fv0101)** Van Roozendael et al, 2012			**CCI (fv0101)** Miles et al, 2015	/	
MetOp / GOME-2	**O3M SAF (GDP4.6)** Loyola et al, 2013	**CCI (fv0101)** Van Roozendael et al, 2012		**CCI (fv0101)** Miles et al, 2015	/	
ENVISAT / SCIAMACHY	**KNMI (v2.0)** Eskes et al, 2005	**CCI (fv0101)** Van Roozendael et al, 2012		/	/	
Aura / OMI	**KNMI (DOAS v003)** Bhartia, 2002	**NASA (TOMS v003)** Bhartia, 2002	**CCI (fv0101)** Van Roozendael et al, 2012	/	/	
ENVISAT / MIPAS	/			/	**ESA (v6)** Carli et al, 2011	**CCI (fv0003)** Sofieva et al, 2013

Table 2: List of assessed CCI O3 products (orange) and alternative datasets used in the Round Robin assimilation exercises (blue) given by the instrument. The data version for each product is provided between brackets. References are also given.

Quality relevant outcomes

The comparisons between each O3-CCI dataset and the collocated ozone analyses from Exp/CTRL showed in general good agreement but also some differences that normally reduced after the assimilation (not shown). The following sub-sections will address specific aspects of the assessment, such as the characterization of the observation uncertainty and of their bias, the impact on the quality of the ozone analyses (including the results from the Round-Robin exercises), and the internal consistency. Furthermore, indications on how useful different observations are in a data assimilation system are provided by focusing on the impact of the vertical resolution and of the viewing geometry.

3.2.1 Uncertainty characterization

Uncertainty estimates are an essential element of any dataset as they give a measure on how reliable the dataset is. Thus, their characterization is an aspect of paramount importance for any applications. Although significant progress has been made in understanding and characterizing most sources of error, as well as in following best practises, limitations in those estimates still exist. This is either because some of the sources of uncertainty are particularly difficult to characterise or because they are (known and unknown) unknown. In data assimilation, the observation uncertainties determine the weight the observations have in the data assimilation system (DAS) and thus the impact on its products.

Here, the Desroziers' method (Desroziers et al, 2005) was used as a simple diagnostic to derive an estimate of the total observation error based on departure statistics from the DAS and then to assess the observation uncertainty provided with each ozone product. This method has been applied to hyperspectral infrared data in a range of assimilation systems in recent years (e.g. Bormann et al. 2010, 2015) to improve the error standard deviations of their channels, and to derive inter-channel or spatial error correlations. It is important to stress that although successfully used, this diagnostics depends on a number of assumptions, for instance, that the weights in the assimilation system are consistent with true weights. As these assumptions are not strictly valid, the error estimates will have themselves some uncertainty.

The top panels of figure 4a present vertical cross-sections of the mean provided uncertainty (left) and mean estimated error (right) for the CCI GOME-2 NPO3 product averaged during the period Jul-Oct 2008. The structure of the provided uncertainty is very similar to that estimated, although the overall values are somewhat larger than those computed with the Desroziers' method in most of the lower and middle stratosphere. Although in relative terms such an overestimation can be as large as 60% of the observation uncertainty (bottom right panel of figure 4a), it accounts for less than 4% of the observation values (bottom left panel of figure 4a).

The total column products seem to have uncertainties (on average less than 5 DU (Dobson Units)) that are systematically lower than the estimated values, with differences as high as 100% of the provided uncertainties in a wide channel across the equator up to mid-latitudes. In contrast, the provided uncertainties are larger than the estimated values at latitudes closer to the daily part of the instrument orbits. Two examples are shown in figure 4b where the hovmoeller plots of the estimated minus provided uncertainty difference relative to the provided value presented for the CCI SCIAMACHY and GOME-2 TCO3 products.

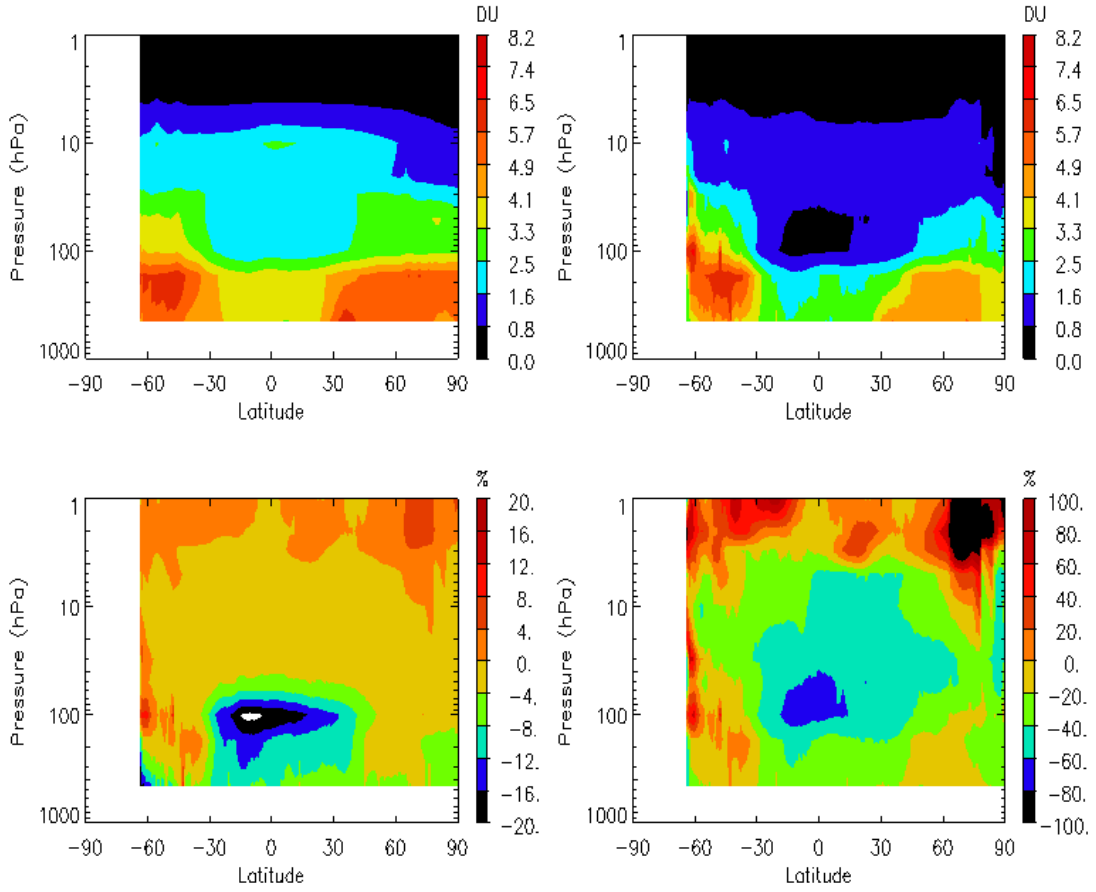

Figure 4a: ***Top panels:*** *Vertical cross-sections of the provided (left) and estimated (right) uncertainty for GOME-2 NPO3 for the period Jul-Oct 2008. Data are in DU.* ***Bottom panels:*** *Vertical cross-section of the difference between the estimated and the provided uncertainty relative to the observation (left) and to the provided uncertainty (right) for GOME-2 NPO3 over the period Jul-Oct 2008. Data are in %. Please note the different range between them.*

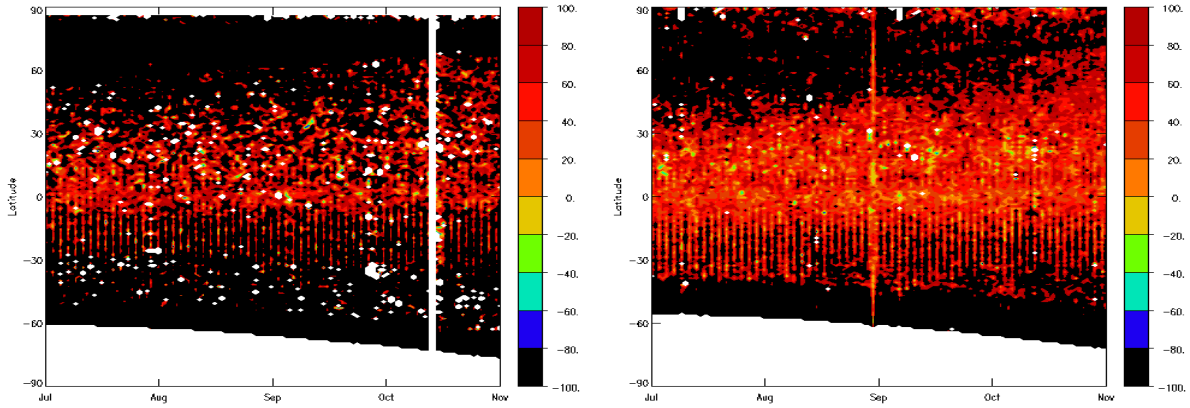

Fig 4b: Hovmoeller plot of the difference between the estimated and the provided uncertainty relative to the provided uncertainty for the CCI SCIAMACHY TCO3 (left) and the CCI GOME-2 TCO3 (right) products. Data are in %.

3.2.2 Bias characterization

Ozone is fully integrated into the ECMWF forecast model and analysis system (Dethof and Hólm 2004) as an additional three-dimensional model and analysis variable. Its data assimilation is performed together with all other observations using a 4D-Var scheme that provides two main 12 h 4D-Var analyses and forecasts at 0000 and 1200 UTC. A variational bias correction (VarBC) scheme for satellite radiances (Auligné et al., 2007; Dee 2005) and retrieved ozone products (Dragani 2009) is routinely used in the assimilation to automatically detect and correct for observation systematic biases. VarBC is formulated for all observations as linear regressions of a number of bias predictors that are observation type- and sensor-dependent, as well as geographically varying, e.g. depending on prescribed atmospheric air-mass predictors in the case of radiances. The coefficients of those regressions are included as additional parameters in the state vector and computed during the 4D-Var minimization, and so updated every assimilation cycle. It is noted that an adaptive bias correction within the analysis, such as VarBC, is potentially vulnerable to aliasing time-varying systematic errors in the short-range forecast background into erroneous drifting corrections of the observations. This can be avoided by anchoring the VarBC system to observations that present negligible to very small biases against independent observations and thus can be assimilated without bias correction. For ozone and in all the experiments considered here, the ozone VarBC is anchored to the SBUV/2 ozone observations as advised by Dragani (2009) and for the 2008 experiments also to two IR/O3 channels, one from IASI (channel 1585) and one from AIRS (channel 1088), as indicated by the Dragani and McNally (2013) study. Furthermore, the work from Dragani (2013) showed that the MIPAS observations can be useful in anchoring the ozone VarBC and provide better quality ozone analyses when they are assimilated uncorrected than those obtained after correction. Thus, this dataset was not bias corrected during the assimilation.

The remaining nadir products were all assimilated after applying a small bias correction. Figures 5a and 5b show the mean bias correction applied to the CCI GOME-2 NPO3 and two CCI TCO3 products (SCIAMACHY and GOME-2), respectively. In both cases, it is clear that the applied bias corrections generally represent small changes to the observations themselves.

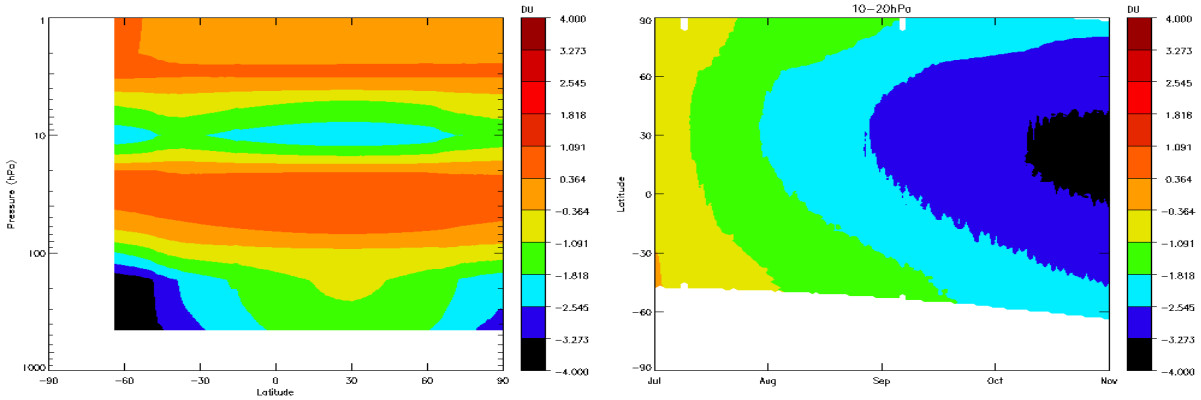

Figure 5a: Vertical cross-section (left) and hovmoeller plot (right) for the 10-20 hPa layer of the bias correction applied to GOME-2 NPO3 products in the DAS. Data are in DU.

Figure 5a shows the vertical cross-section view (left hand side) and the temporal evolution (right hand side) in the layer between 10 and 20 hPa (region of the ozone maximum) of the inferred correction. In the region of the atmosphere between 5 and 100 hPa, the mean bias correction applied to the GOME-2 NPO3 product is within ±4% of the observation values, rising up to +20% between 1 and 5 hPa and decreasing to -20% in the upper troposphere (not shown). The right panel of figure 5a shows a small progressive increase in the bias correction (also noted at other levels) that may suggest that the bias correction itself is not yet fully stabilized after four months reaching corrections as large as about 8% of the observation values in the tropics.

A similar behavior is seen in the total column products, though the corrections are particularly small and in the region of 0.05% of the observation value (figure 5b).

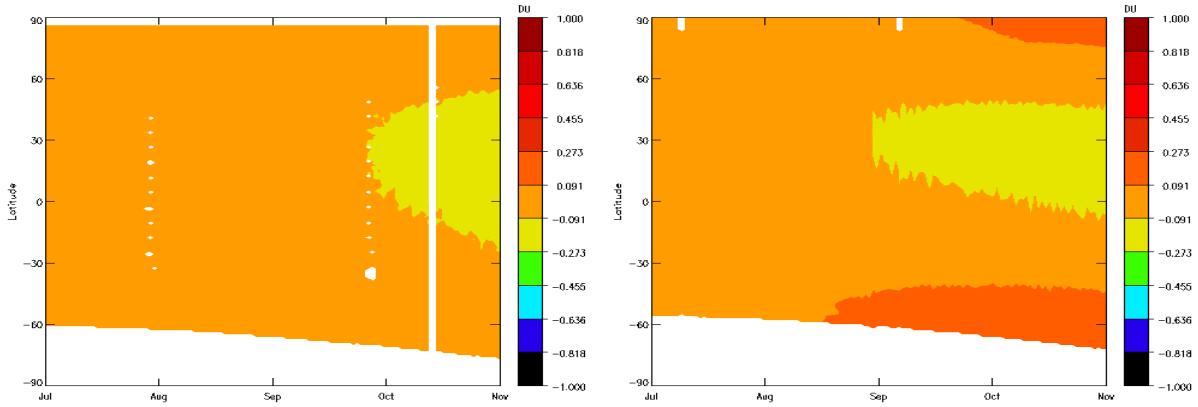

Figure 5b: Hovmoeller plot of the bias correction applied to SCIAMACHY TCO3 (left) and GOME-2 TCO3 (right) products in the DAS. Data are in DU.

3.2.3 Impact on the ozone analyses and results of the Round-Robin exercises

The results from the assessment of adding the O3-CCI products were evaluated for each instrument against independent observations. Ozone profiles from the Microwave Limb Sounder (MLS; Froidevaux *et al*, 2008) and ozone sondes retrieved from the World Ozone and Ultraviolet Radiation Data Centre (WOUDC) were used as independent ozone references for the stratosphere and troposphere/lower stratosphere, respectively.

The comparisons with MLS data will be displayed as the vertical cross-section of a quantity Δ defined as follows:

$$\Delta = \mathrm{STAT}\left(\mathrm{MLS} - \mathrm{Analyses}^{(\mathrm{Exp/PERT})} \right) - \mathrm{STAT}\left(\mathrm{MLS} - \mathrm{Analyses}^{(\mathrm{Exp/CTRL})} \right) \quad (1)$$

where STAT() can be either the mean or the standard deviation. For either statistics:

Δ { **>0. ➔ Negative impact** as Exp/CTRL fits MLS better than Exp/PERT.

<0. ➔ Positive impact as Exp/PERT fits MLS better than Exp/CTRL.

The comparisons with the ozone sondes are instead shown in terms of RMSE, i.e. RMS profiles of the sonde minus collocated analysis differences, thus the smaller the RMSE is the better is the fit of the analyses to the sondes. The ozone analyses are spatially collocated with the independent observations with a maximum of 3 hour time lag. The statistics in all cases are computed for the period August-October 2008.

Figure 6a shows the impact of assimilating three GOME-2 products on the quality of the ozone analyses in terms of their fit to the MLS ozone profiles as expressed by equation (1) both in terms of mean (top panels) and standard deviations (bottom panel). The three GOME-2 products are: the O3M SAF GOME-2 TCO3 (panels a); the CCI GOME-2 TCO3 (panels b); the CCI GOME-2 NPO3 (panels c).

The results of the GOME-2 TCO3 RR exercise summarised in the comparison of panels a) and b) of figure 6a show a clear improvement in the ozone analyses in the middle stratosphere for the experiment assimilating the CCI product compared to the control in terms of both the mean and the standard deviations of the Δ diagnostics. It is pointed out that the impact of assimilating the O3M SAF GOME-2 TCO3 product is negligible as is apparent from the values shown in panels a) of figure 6a.

Comparisons between panels b) and c) of figure 6a clearly show that between the two CCI GOME-2 products, the positive impact of assimilating the NPO3 dataset is far greater than that for TCO3 (see section 3.2.5).

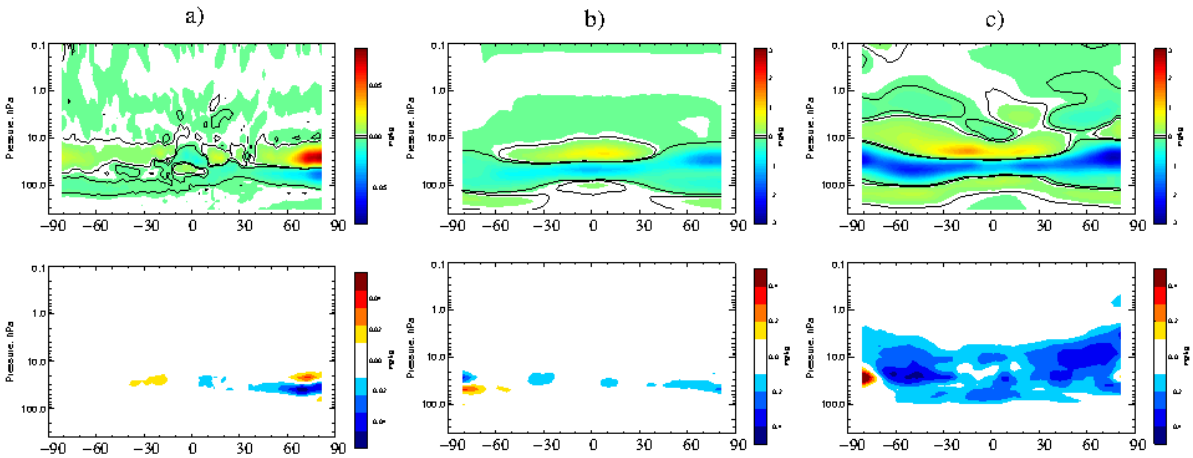

Figure 6a: ***Top panels:*** *Zonal means of the changes in the mean of differences between MLS retrievals and collocated analyses of ozone mixing ratio for the assimilation of three different GOME-2 products each compared to the same Exp/CTRL for Aug-Oct 2008. Panel a) refers to the O3M SAF GOME-2 TCO3, panel b) refers to the CCI GOME-2 TCO3product; panel c) refers to the CCI GOME-2 NPO3 product. Positive (red) values indicate an increase in the mean in the Control and thus a worst fit to MLS ozone profiles. Data are in parts per billion (ppmm).* ***Bottom panels:*** *As a), but for the standard deviation of differences. Please note the different colour scale for panels a) compared with panels b) and c).*

RR assimilation exercises were also performed for the SCIAMACHY and OMI TCO3, as detailed in table 2. For the former instrument, the impact on the quality of the ozone analyses produced by the CCI dataset was slightly more positive than that of the KNMI retrievals. For the latter instrument, the RR results are presented in figure 6b. They show that all products lead to a small degradation compared to the control in the tropical mid-stratosphere between 20-30 hPa while improving to some extent the extra-tropical stratospheric analyses. Of them, the KNMI product seems to be one that, whilst exhibiting a similar level of degradation of the other two in the tropics, also produces the largest positive impact in the extra-tropics, especially in the southern hemisphere.

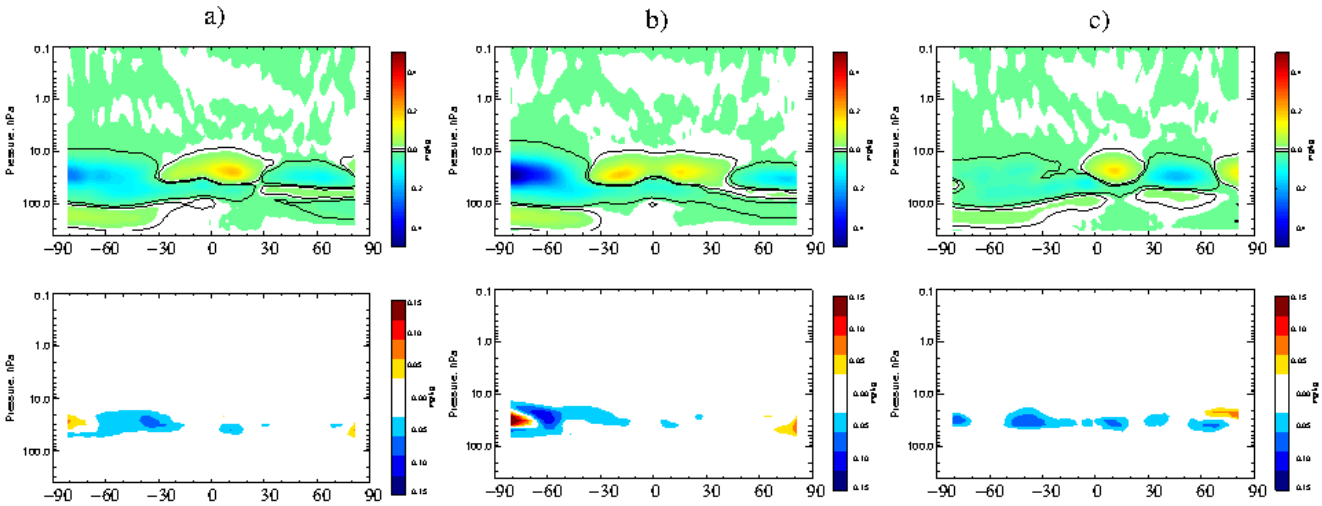

Figure 6b: Like in fig 6a but for three different OMI TCO3. Panel a) refers to the CCI OMI, panel b) refers to the KNMI OMI-DOAS product; panel c) refers to the NASA OMI-TOMS product.

The final RR exercise was performed for the two MIPAS reprocessed LPO3 products. Comparisons with the MLS ozone profiles generally show a large positive impact on the stratospheric ozone analyses of both products although in the case of the CCI dataset the improvement is greater than for the official ESA product (not shown). This is also confirmed by the comparisons with the WOUDC sondes shown in figure 6c. Although both MIPAS products substantially improve the agreement with the ozone sondes at most vertical levels and latitudinal bands compared with Exp/CTRL, the CCI dataset is the one that systematically shows the smaller RMSE. It is also noted that at high latitudes in the SH (where the ozone analyses are partly affected by the lack of UV data during the winter months and by the ozone hole in spring) the official ESA retrievals degrade the fit to the ozone sondes at all tropospheric levels. In contrast, the CCI product still leads to a marginal improvement. It is also noted that improvements are also found in the lower troposphere where limb instruments lack visibility. This aspect is discussed further in section 3.2.6.

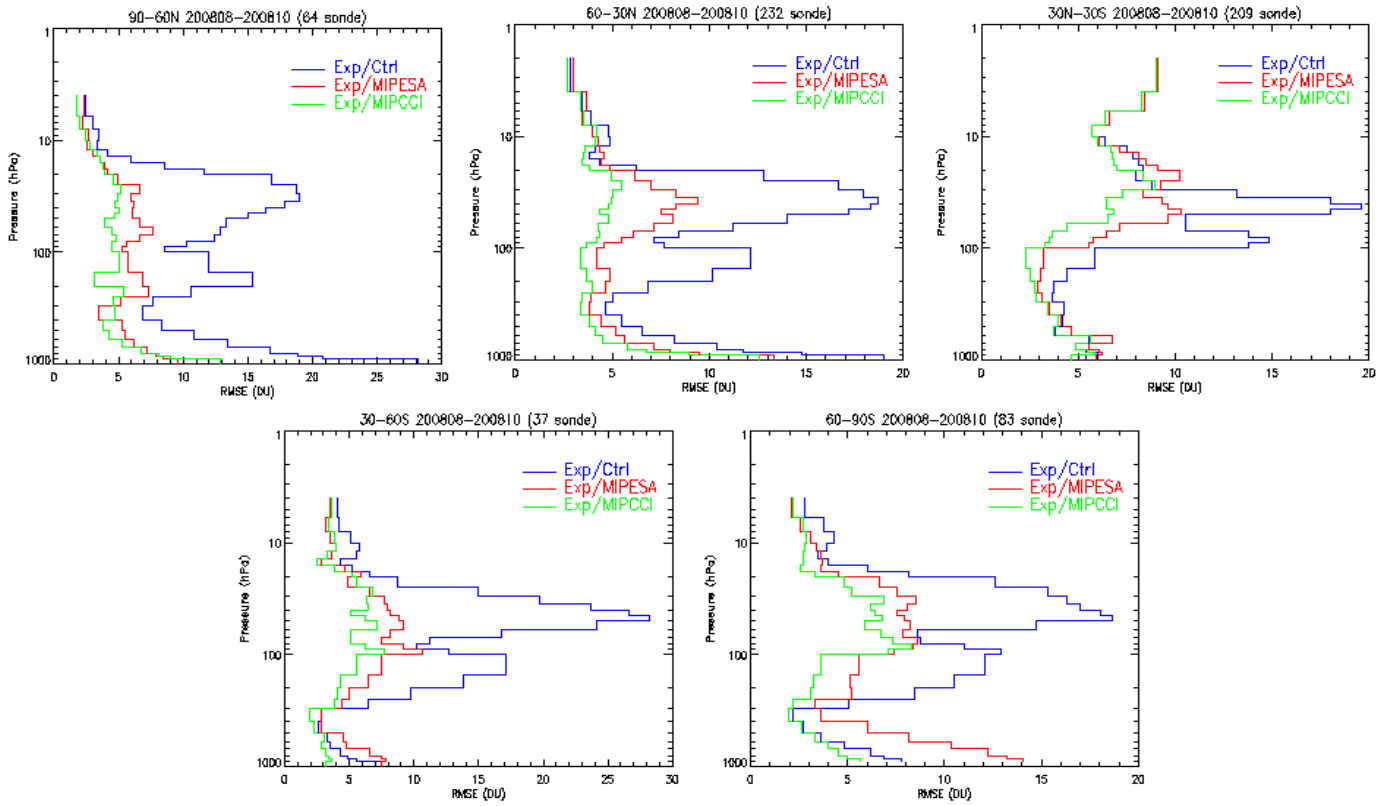

Figure 6c: RMS fit of the mean ozone analyses from three experiments and ozone sondes averaged over five latitudinal bands. The comparisons were computed by averaging over Aug - Oct 2008. The three analyses were taken from Exp/CTRL (blue lines), and two Exp/PERT assimilating also the reprocessed MIPAS LPO3 from ESA (red lines) and CCI (green lines). The number of ascents included in the average can be found in the title of each panel. Data are in DU.

3.2.4 Consistency with other variables

Ozone in the IFS is only loosely related to other variables. This is a precautionary measure to limit a potentially negative impact on the rest of the system. For that reason, most of the ozone products assessed in this study had little impact on the other variables or on the usage of other observations except in the case of the assimilation of the GOME-2 NPO3. It was found that the assimilation of the GOME-2 NPO3 could improve the fit to the ozone-sensitive infrared radiances (IR/O3) measured by the AIRS sensor and assimilated in both *Exp/CTRL* and *Exp/PERT* experiments (figure 7a). This is achieved after filtering out a small amount (up to 1%) of AIRS data in *Exp/PERT*. The improved fit to observations indicates increased internal consistency in the information provided by different observations.

The improved usage of IR/O3 triggered by the assimilation of the GOME-2 NPO3 is in turn most likely responsible to further affect the system by improving its forecasts skills. This improvement is most evident in a reduction of the RMS forecast error of the geopotential height for which statistical significant changes are found at most level from the middle

troposphere up to the middle stratosphere in the tropics (figure 7b). Some improvements were also found in the RMS of the temperature forecast errors, albeit not statistically significant.

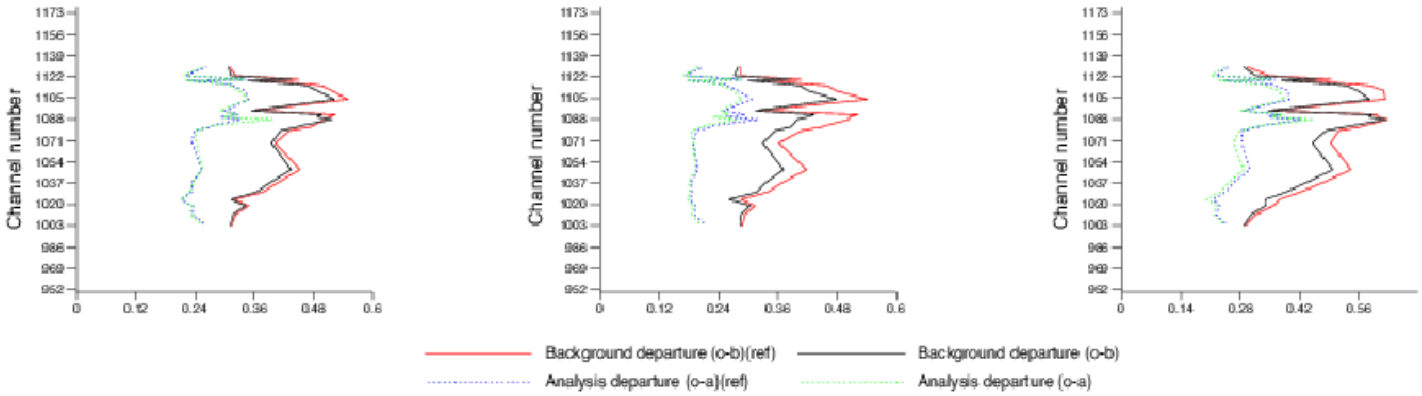

Figure 7a: Standard deviations of first-guess (solid lines) and analysis (dashed lines) departures from the used ozone sensitive IR channels measured by the AQUA AIRS sensor for Exp/CTRL (solid red and dashed blue) and Exp/PERT that assimilated the GOME-2 NPO3 (solid black and dashed green). The average period is Aug-Oct 2008 period. The left panel refers to the NH extra-tropics, the middle panel refers to the tropical region, and the right panel shows the result for the SH extra-tropics.

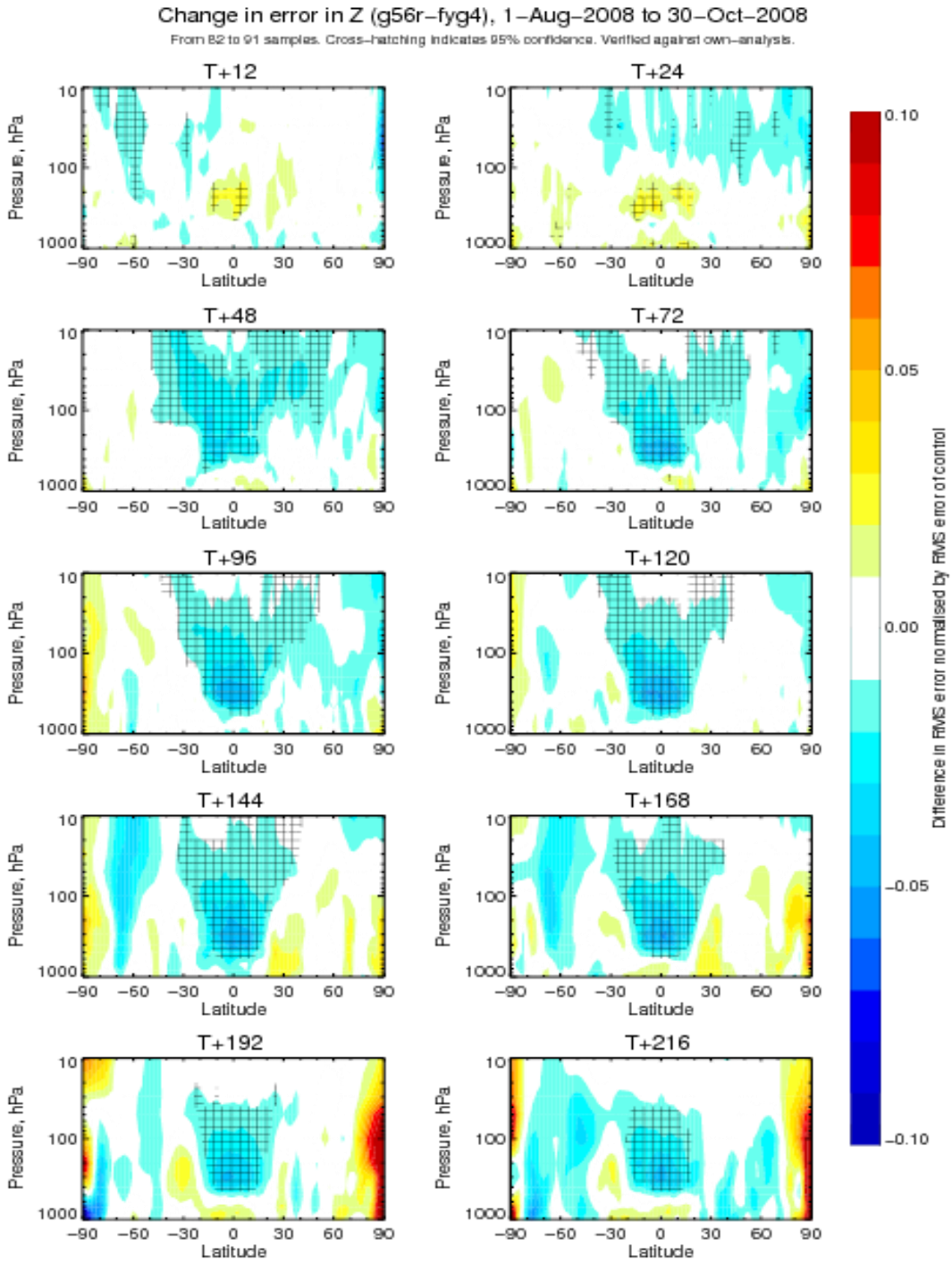

Figure 7b: Vertical cross-sections of the normalised difference in the RMS forecast error of the geopotential height between Exp/PERT obtained from the assimilation of GOME-2 NPO3 and Exp/CTRL. Each panel refers to a given forecast time spanning from 12 hours to day 9. The average period is Aug-Oct 2008 period. Hatched areas indicate areas where the scores have a statistical significance of 95%. Blue (negative) areas indicate where Exp/PERT has lower RMS errors (thus better scores) than Exp/CTRL.

3.2.5 User requirements: impact of vertical resolution

Comparisons of the impact of the assimilation of the total column ozone and nadir ozone profiles from the GOME-2 sensor show that in the stratosphere the improvement led by the assimilation of the ozone profiles on the ozone analyses is greater than that of the total column ozone (panels b) and c) in figure 6a). The improvement is apparent in both the mean and standard deviations. Panels b) and c) in figure 6a also show that the assimilation of the total column ozone degrades the fit of the analyses to MLS in the tropical stratosphere between 10 and 20 hPa where the ozone mixing ratio peaks (top left panel).

Similar results were found when comparing the impact on the ozone analyses of assimilating either the TCO3 product or the NPO3 product retrieved from the ERS-2 GOME measurements.

3.2.6 User requirements: impact of viewing geometry

Comparisons of the impact of the assimilation of nadir ozone profiles from GOME-2 with limb ozone profiles from MIPAS show that in the stratosphere and upper troposphere (down to about 400hPa) the improvement led by the assimilation of the limb observations on the ozone analyses is greater than that of the nadir profiles (figure 7c). The contrary applies below 400hPa, as confirmed by the comparisons with ozone sondes (e.g. figure 7d for the mid-latitudes in the northern hemisphere). It is interesting to notice, that in this region the assimilation of MIPAS LPO3 still improves the ozone analyses compared to the control experiment, even though the vertical coverage of a limb sounder can span down to about 400hPa only. This positive result is a consequence of exploiting the synergy between the LPO3 and the total column product that was assimilated in all experiments. By improving the stratospheric ozone concentration, the synergistic assimilation of the LPO3 and TCO3 products provides an indirect constraint on the ozone analyses at levels where the limb sounder are essentially blind.

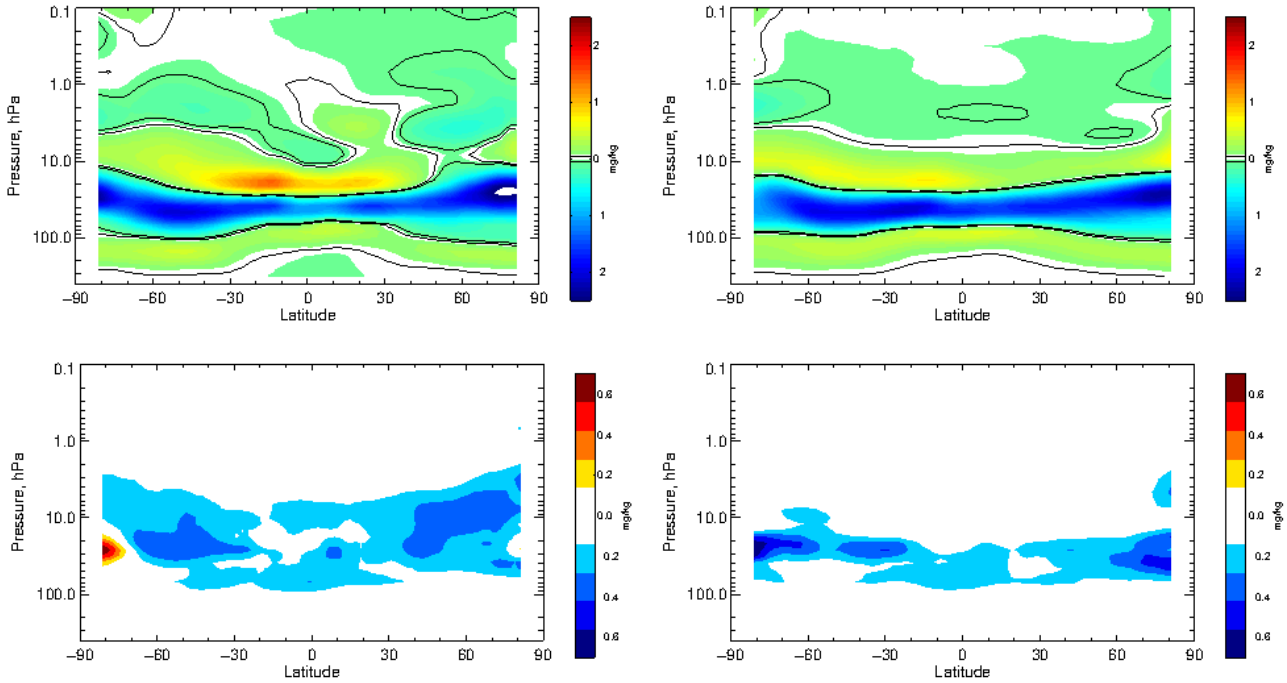

Figure 7c: For GOME-2 NPO3 (left) and for MIPAS LPO3 (right).

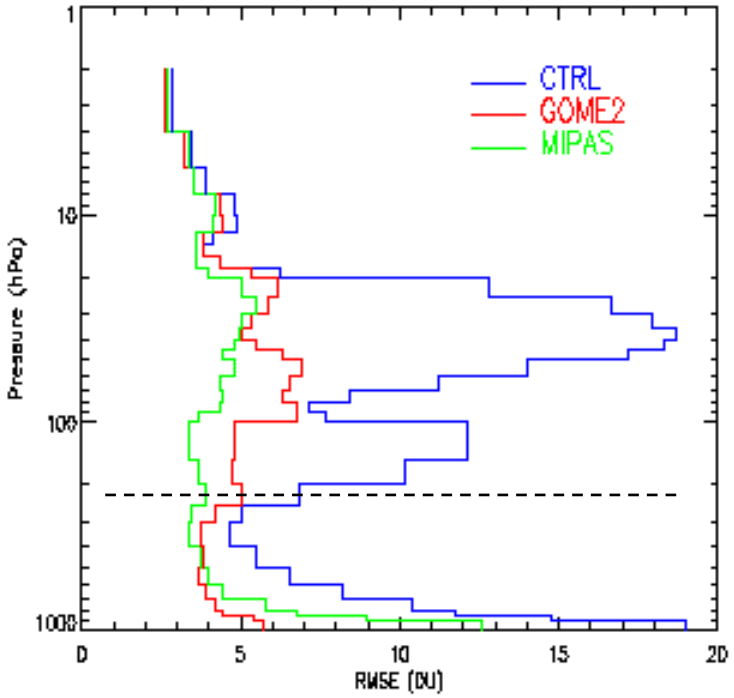

Figure 7d: RMS fit of difference between ozone sonde and ozone analysis averaged over the mid latitudes in the NH for the period Aug-Oct 2008 and it is based on a total of 232 ozone sondes. The ozone analyses are for the Exp/CTRL (blue line), and two perturbation experiments using GOME-2 NPO3 (red line) and MIPAS LPO3 (green line). The dashed line indicates the 400hPa pressure levels.

3.3 Integrated assessment of CCI terrestrial ECVs impact in the MPI-ESM [WP3.4]

Aim

WP3.4 includes an integrated assessment of the terrestrial ECV variables available in the CCI with a joint analysis of the ECVs land cover, fire, soil moisture, and greenhouse gases (GHG). The ECVs were used to optimize uncertain parameters in the MPI-M ESM fire model process formulations using an optimum estimate framework, to make use of the uncertainty information provided with the ESA CCI datasets. The overarching questions to be addressed were:

- Are the four CCI data-sets consistent with each other and with model data so that modelled and observations data can be used directly for model validation and data assimilation?
- How can CCI data records be used to improve fire emission modelling in an earth system model?
- Do simulated carbon emissions improve using CCI datasets?

Summary of Results

SPITFIRE-JSBACH simulations were performed for the time period 1850 to 2010 in which burned area and fire carbon emissions are interactively simulated. Simulations were run with the standard model setup as described in detail in Lasslop et al., 2014. In addition, simulations were peformed with a modified representation of the Nesterov-Index in SPITFIRE following Groisman et al. 2007. The modified version served as a first test case to use ESA CCI data in the evaluation of the SPITFIRE-JSBACH model. Simulated, FIRE_CCI burned area (MERIS and MERGED) as well as burned area reported in GFEDv3/GFEDv4 based on MODIS (Gilgio et al., 2006, Giglio et al., 2010) for the time period 2006-2008 are compared in figure 8.

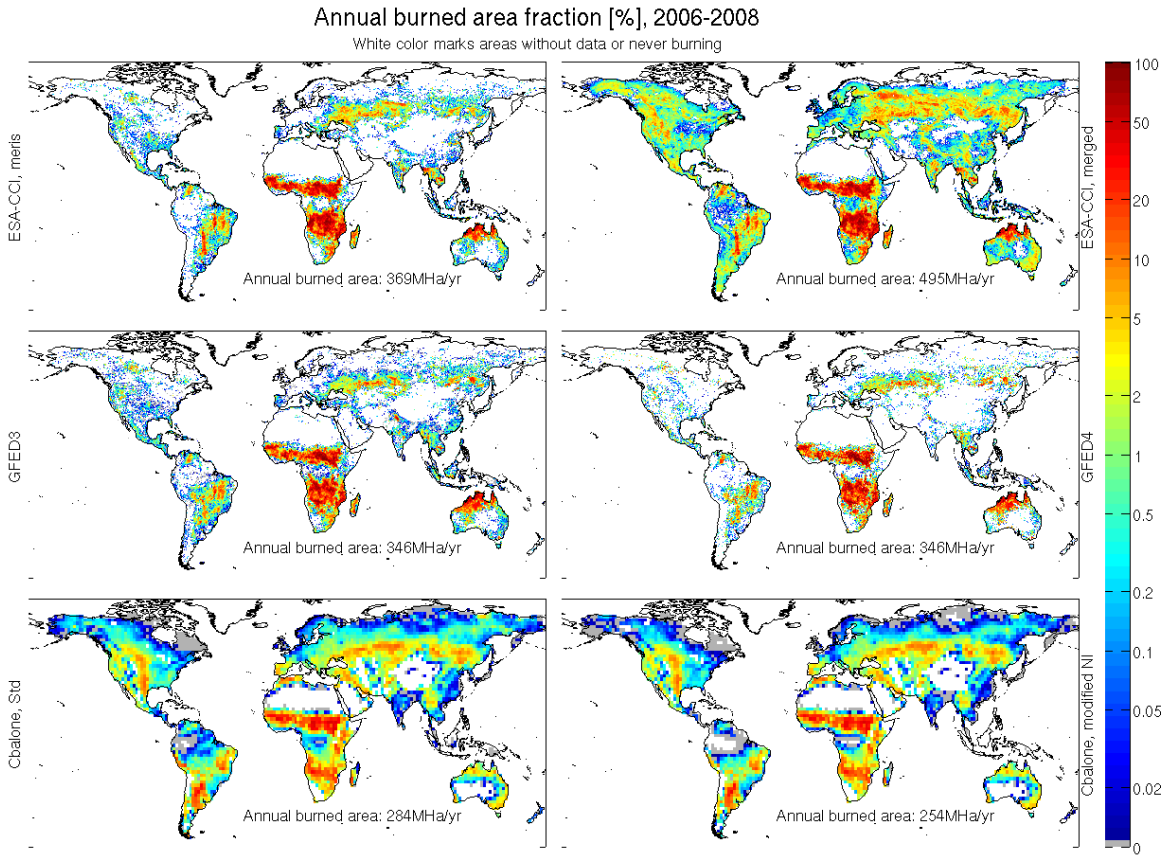

Figure 8: Burned area averaged for the years 2006-2008. FIRE_CCI MERIS and MERGED (upper row), GFEDv3 and GFEDv4 (middle row), SPITFIRE-JSBACH standard and modified (lower row).

Contrasting the burned area with soil moisture reported from CCI_SM (figure 9), we find a distinct relationship between burned area and soil moisture with low burned area for low soil moisture (fuel limitation) and low burned areas for high soil moisture (moisture limitation).

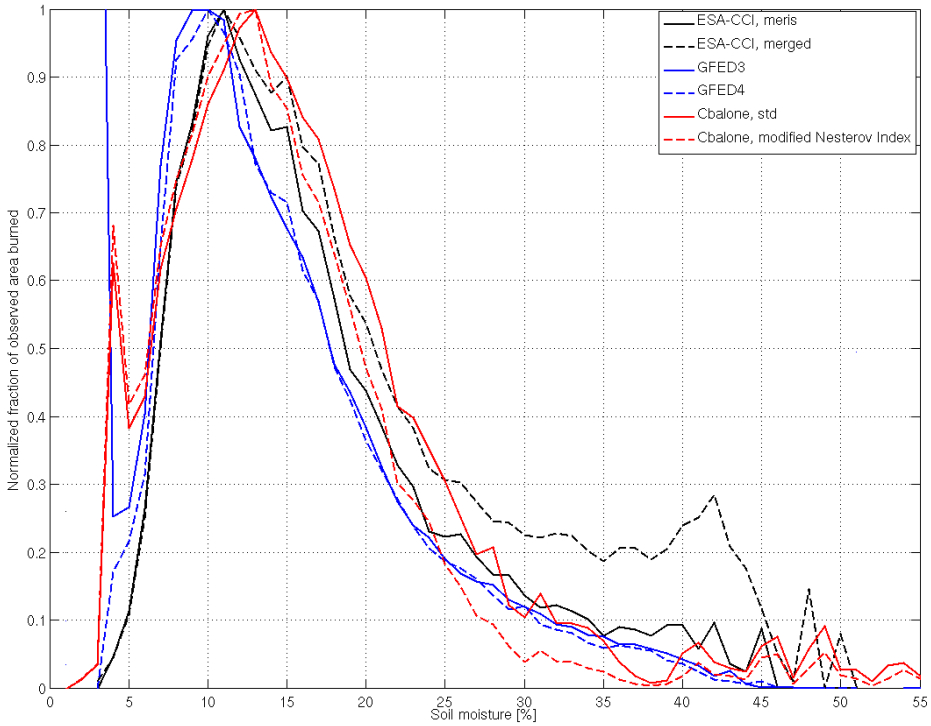

Figure 9: ESA CCI Soil Moisture compared with the fraction of observed burned area with the peak normalized to one. Burned area data is taken from the CCI Fire MERIS and MERGED product, as well as from GFEDv3/v4. Simulated data is shown for JSBACH-SPITFIRE in its standard version (Cbalone, std) and in the modified version JSBACH-SPITFIRE (Cbalone, modified Nesterov Index).

The comparison shows that all products have a very similar distribution with the exception of the CCI MERGED product, for which substantial burned areas are reported in regions with soil moistures exceeding 25%. The CCI-MERIS product peaks at a higher soil moisture compared to GFED products and the distribution is wider. Both versions of JSBACH-SPITFIRE peak at a too high soil moisture and the distribution is too wide.

In a first step we identified two parameters (conversion soil moisture to fuel moisture and ignition rate) in SPITFIRE-JSBACH that are not well constrained by observations, which we systematically varied over a reasonable parameter space to optimize width and peak position of the soil moisture / burned area relationship. JSBACH-SPITFIRE was optimized to run a large number of experiments with varying parameter settings in a reasonable amount of time. Figure 10 shows the deviations in peak position and distribution width for 70 experiments with CCI-MERIS as reference.

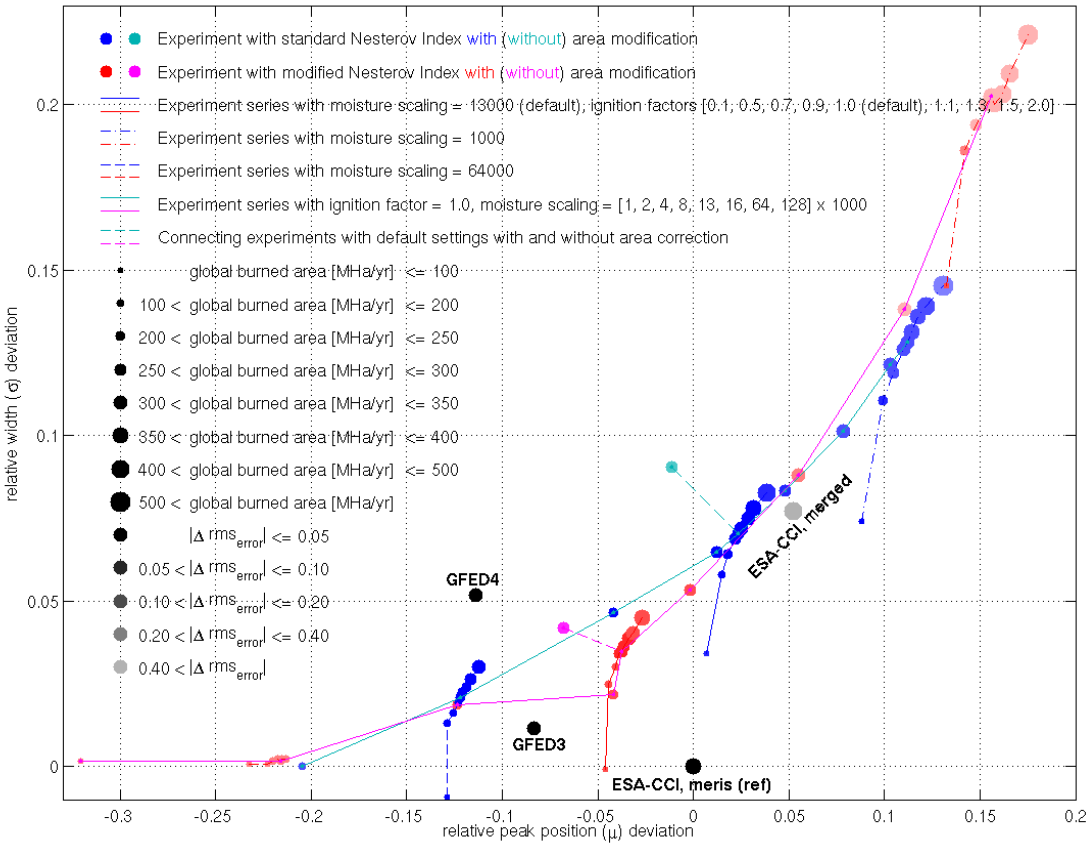

Figure 10: Relative difference in peak position and width of the burned area – soil moisture relationship for 70 experiments performed with JSBACH-SPITFIREv1/v2 compared to GFEDv3/v4, CCI MERGED and CCI MERIS (reference).

Overall, the analysis revealed that lower fuel moisture improves the peak position, while lower ignition rates improve the width of the distribution. The improvements are however small, i.e. default values perform already reasonable well. Other less well constrained parameters in the fire model are being tested for their significance in the burned area - soil moisture relationship, for which the analysis will be separated into different land cover types.

Quality relevant outcomes

In WP3.4, only the gridded FIRE_CCI products were used. The FIRE_CCI gridded products from phase I were only available for a 3 year period (2006-2008), which limited their applicability for climate studies. To test the functional relationships, such as the relationship between burned area and soil moisture, global data coverage was available, reducing the dependency on having a long time series. Further assessment for fire model development will require categorization by land cover type to optimize land cover dependent parameters, which will benefit from a longer time series.

A first assessment showed that the CCI-MERGED product reports unrealistically high burned fraction for regions with soil moistures exceeding 25%. The CCI-MERIS product was therefore selected as the reference. The CCI-MERIS product shows a very similar distribution

of soil moisture dependency compared with the MODIS based GFEDv3/GFEDv4 product, which was applied in previous studies. These findings agree with the analysis of the FIRE CCI team reported in the Product Validation Report II and the Climate Assessment Report. The temporal stability of the product was not assessed due to the limited time period covered by the global product.

3.4 Cross assessment of clouds, water vapour, aerosols, ozone, GHG, SST, radiation and soil moisture impact on global climate variability and trends [WP_O3.4]

Aim

The ability of climate models to capture large-scale and regional-scale climate variability is important to assess as well as mean climate features. Studying patterns of climate variability and correlations of different Essential Climate Variables (ECVs) in observations and models are useful for the understanding of processes and for model evaluation. The aim of this WP is to make an integrated assessment of ECVs from CCI and other observations studying climate variability by investigating statistical relationships between co-varying variables and evaluate the same processes in global climate models, such as ENSO, IOD and NAO. The uncertainty information for the CCI data sets will be used when comparing to other observational data sets and associated model-generated variability. The general scientific questions are:

- How are the observed ECVs related and what is the robustness of associated mechanisms across different observational data sets and climate model simulations?
- Can the models capture the relations between ECVs and the variability seen in observations?
- How do different representations of sea surface and sea ice impact on simulated variability and teleconnections (WP04.2 ESA CCI SST & SI)?
- How do the results depend on the horizontal resolution of EC-Earth in capturing climate variability and teleconnection skills?

Summary of Results

The work so far has involved obtaining observational data, CCI phase 1 (SST and clouds) and other (OLR, precipitation) data, reformatting and reading the data into the ESMVal analysis tool. Diagnostics were installed to calculate the correlation between CCI ENSO index and modelled precipitation and SST at different (medium and low) resolutions. For example, figure 11(a-c) shows observed and simulated correlations between precipitation and SST for TRMM and GPCP over relatively short (6 - 11 year) time periods. A longer correlation period of 30-100 years would be preferred. Figure 11(d) shows a measure of ENSO simulation performance for specific features (amplitude, horizontal structure, spectrum and seasonality) and feedbacks (atmospherics feedback, heat) in terms of the normalized errors for each selected metric and the ENSO and Feedback (FB) scores. Lower score values correspond to better performance in representing ENSO and its atmospheric feedbacks.

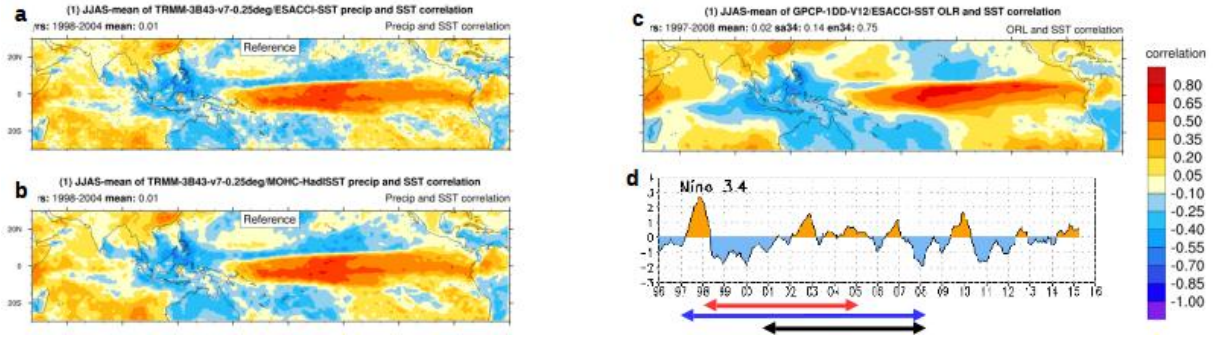

Figure 11a: Observed and simulated correlation between precipitation and SST for 1998-2004 a. TRMM precipitation and CCI SST, b. TRMM precipitation and Hadley SST: and for 1997-2008 c. GPCP precipitation and CCI SST and d) El Nino3.4 Index.

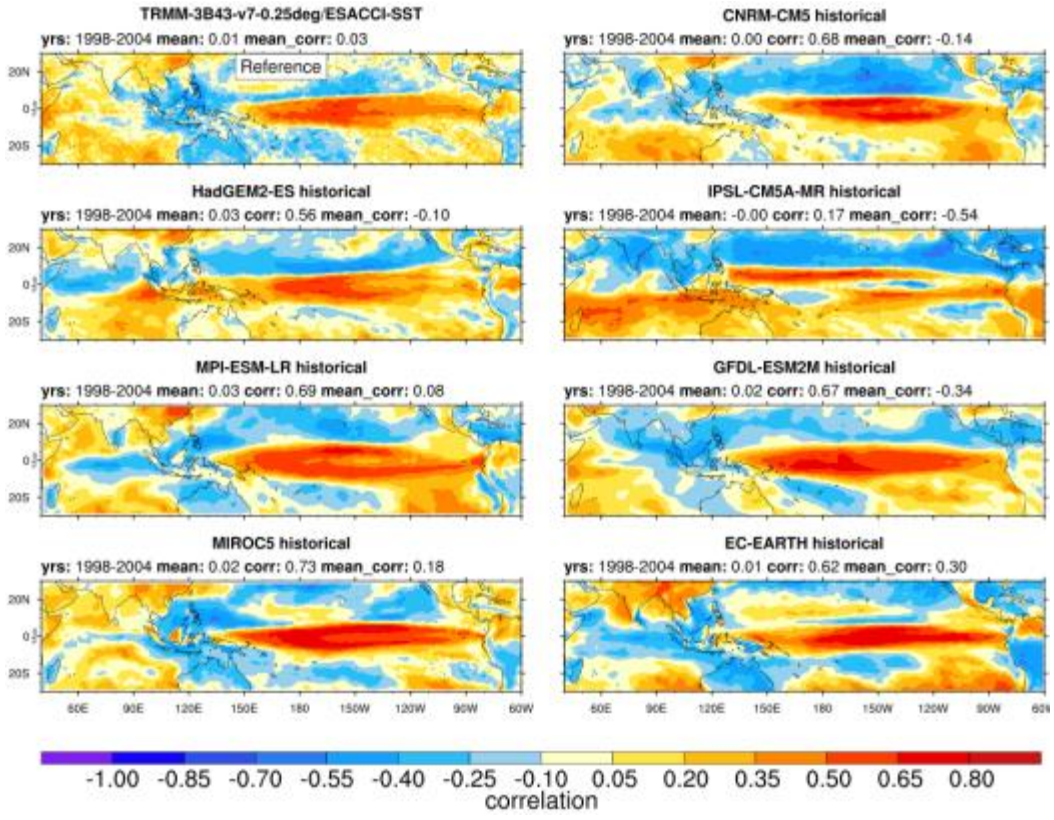

Figure 11b: Correlation between precipitation and SST for observations TRMM precipitation and ESA CCI SST (top right panel) and for CMIP5 models AMIP runs precipitation SST for 1998-2004.

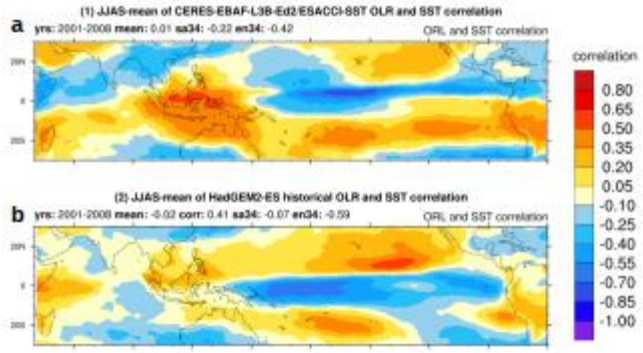

Figure 11c: Correlation between GPCP precipitation and ESA CCI SST, CERES EBAF OPLR and SST for 2001-2008 (and CLARA-A1 high clouds and SST index).

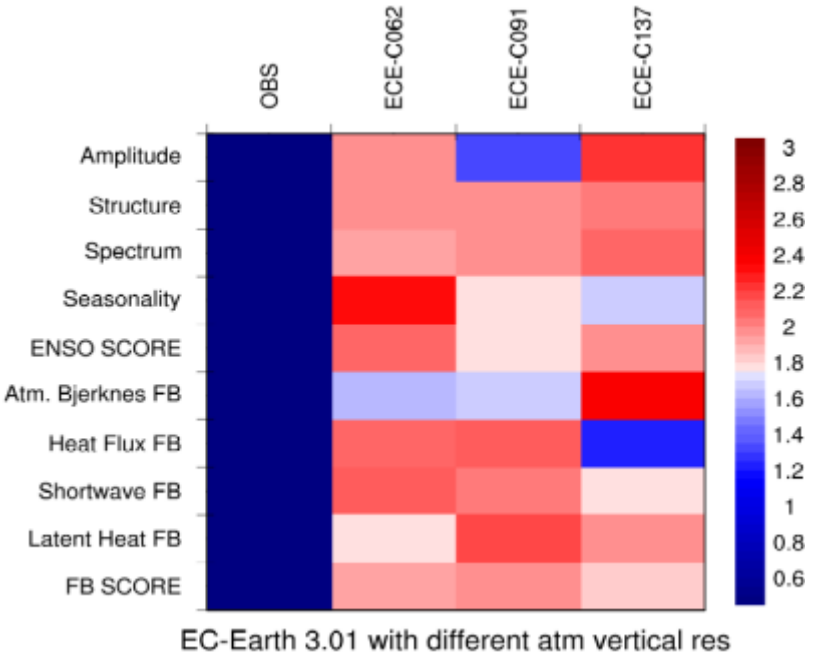

Figure 11d: ENSO simulation performances for specific features (amplitude, horizontal structure, spectrum and seasonality) and feedbacks (atmospherics feedback, heat).

3.5 Improved process understanding from Arctic and Antarctic cross ECV assessment [WP3.6]

ESA Sea Ice CCI sea ice concentration and thickness data products

Within the framework of the CMUG initiative we evaluated the quality of sea-ice concentration and sea-ice thickness datasets compiled by the ESA Sea Ice CCI (SICCI) team. For this purpose we assimilated these datasets into the Max Planck Institute Earth System Model (MPI-ESM; Stevens et al., 2013). In order to evaluate the SICCI ice concentration dataset we assimilated only SICCI ice concentration data into the model, and compared the performance of the simulated sea ice behaviour with identical experiments where ice concentration data from the National Snow and Ice Data Center (NSIDC) was assimilated. To evaluate the quality of the SICCI ice thickness dataset, we assimilated both SICCI ice concentration and thickness data into the model, and compared the simulated sea ice volume to other observational datasets as well as to the ice volume derived from the experiment where only ice concentration was assimilated.

The assimilation technique we apply is Newtonian relaxation (or "nudging"), and besides sea ice also atmospheric and oceanic observations are assimilated into the model. In the atmosphere, vorticity, divergence, temperature and surface pressure data provided by ERA-Interim reanalyses (Dee et al., 2011) are assimilated, while ocean temperature and salinity are nudged with ORA-S4 reanalysis data (Balmaseda et al., 2013). Relaxation times applied when data was assimilated into the model vary from 1 day for atmospheric nudging to 10 days for ocean nudging, and 20 days for nudging of sea ice. When only sea ice concentration is assimilated into the model, sea ice thickness is updated proportionally to sea ice concentration updates (Tietsche et al., 2013).

Results of our performance analysis for both SICCI sea ice concentration and thickness datasets are given below.

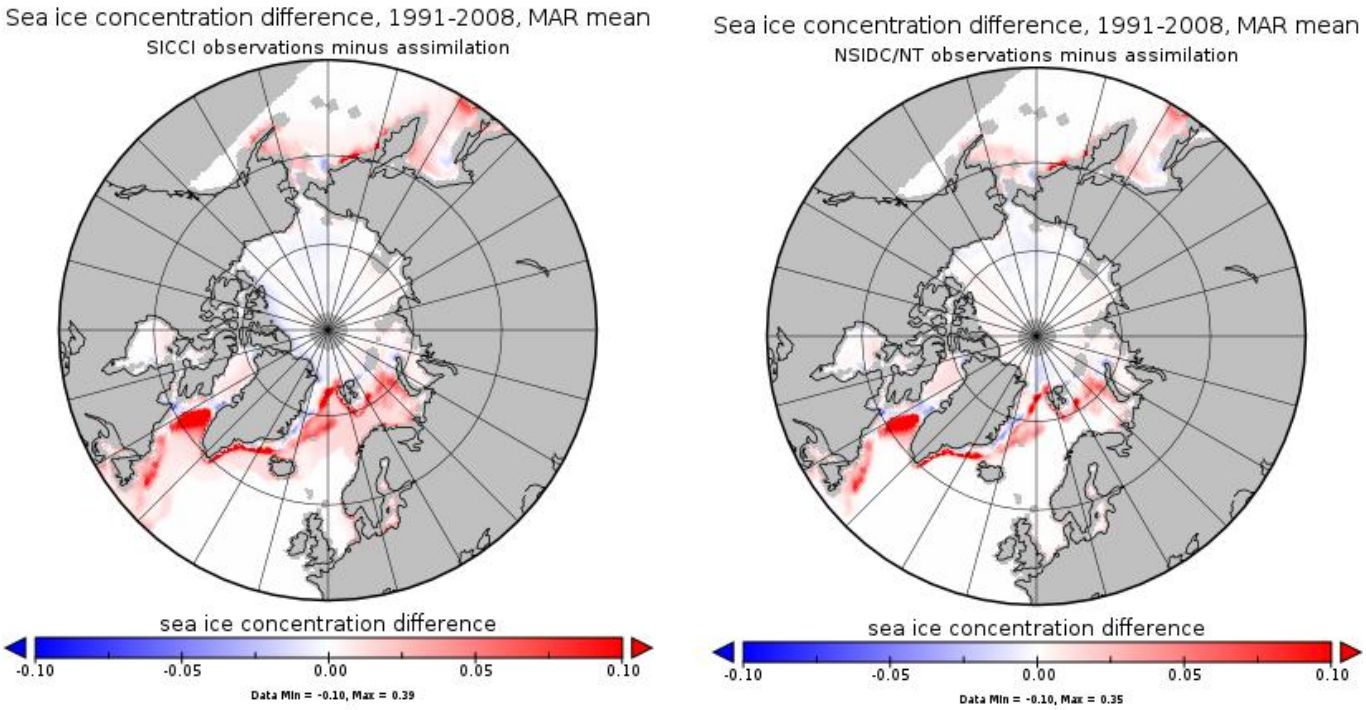

Figure 12: Sea ice concentration differences between observations and the associated assimilation runs are presented for SICCI (left) and NSIDC/NASA-Team (right) data products. March-mean values over the period 1991 to 2008 are shown.

3.5.1 SICCI sea ice concentration dataset (version 1.1, daily data, 1991-2008)

A comparison of SICCI and NSIDC sea ice concentration products shows that the Arctic sea ice area computed from SICCI data lies between NASA-Team (Cavalieri et al., 1984) and Bootstrap (Comiso, 1995) datasets from NSIDC. While NASA-Team data shows lower Arctic sea ice area than SICCI, the Arctic sea ice area derived from Bootstrap data is larger than for SICCI. The difference between NASA-Team and Bootstrap products lies in the selection of tie points for brightness temperatures representing “open water” and “fully ice-covered” grid boxes. From the different setting of tie points it follows that in the NASA-Team dataset, melt ponds appear as open water, while the missing sea-ice underneath melt ponds is compensated for in an ad-hoc manner in the Bootstrap product. From computed Arctic sea-ice areas we infer that the SICCI algorithm gives intermediate ice concentrations in the Arctic. This result also holds for simulated Arctic sea-ice area in assimilation experiments with the different ice concentration datasets.

The Antarctic sea ice area derived from both the SICCI ice concentration dataset and the assimilation run performed with SICCI ice concentrations shows that in the Antarctic the SICCI product resembles the NSIDC Bootstrap product, while the NASA-Team product shows about 10% less sea ice area.

A regional evaluation of the correspondence of the assimilated sea ice data product with the model physics indicates, however, a clear difference between SICCI and NSIDC data

products. In many regions, especially in the Norwegian and Labrador Sea, low ice concentrations (< 3%) are obtained by the SICCI algorithm in grid boxes where observed sea surface temperatures as well as NSIDC ice concentration products indicate ice-free waters (see figure 12). These spurious ice concentrations turn out to be due to the lack of a weather filter in the SICCI algorithm. In NSIDC ice concentration products these low ice concentrations, which originate from the contribution of clouds to brightness temperatures recorded by the satellite, are removed by a weather filter. However, since it is not feasible to objectively distinguish between the origins of possible brightness temperature sources, weather filters are likely to filter out also contributions of actual sea ice. Thus, although not using a weather filter introduces spurious ice concentrations in the open ocean, it provides a more objective view on the satellite data, since no actual ice concentrations are removed and it is left to the user to discard spurious low ice concentrations over open waters, if intended.

The regional investigation of the assimilation performance also showed that a notable amount of sea ice in the marginal ice zone melts directly after assimilation into the model. This turns out to be due to inconsistencies between assimilated sea ice concentration products and the ORA-S4 reanalysis product, which was used to nudge ocean temperatures (see figure 13). In the uppermost ocean layer extending from the sea surface to 12m depth, ORA-S4 reanalyses show temperatures of up to 5°C above freezing in several regions where both SICCI and NSIDC ice concentration products indicate ice concentrations above 5%. In a model grid box the temperature of the uppermost ocean layer needs to be at freezing point to allow even for small amounts of sea ice to exist. Thus, assimilated sea ice cannot persist if the heat content in a certain ocean model grid box plus the sum of heat contributions from the assimilated sea surface temperature and the assimilated sea ice adds up to an ocean surface temperature above freezing.

The regional inconsistencies between assimilated ocean temperature and sea ice concentration datasets originate most likely from the ORA-S4 ocean reanalysis product. The model system which was used to compile ORA-S4 did not contain a dynamical sea-ice model, and in the prescribed sea ice concentration dataset all ice concentrations below 20% were set to zero. This is likely to cause inconsistencies as found in the marginal ice zone (see figure 13), which we obtained for both SICCI and NSIDC assimilation runs in a similar pattern. Assimilating observational data for sea surface temperatures, such as the upcoming SST CCI dataset, might reduce the amount of sea ice melted directly after assimilation due to inconsistencies between sea ice and ocean temperature data.

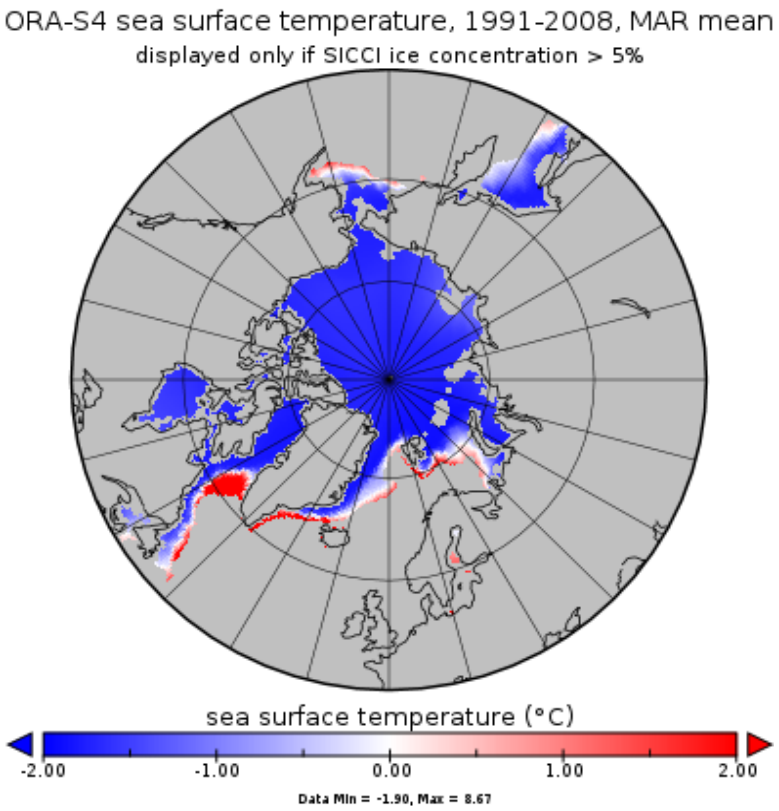

Figure 13: ORA-S4 ocean temperature in the uppermost ocean layer (surface to 12m depth) is shown. Values are displayed only in grid boxes where SICCI ice concentration is above 5%.

We consider the SICCI sea ice concentration data product as adequate for use in climate modelling, and of comparable quality as NSIDC data products. A major advantage of the SICCI product with respect to other datasets is its error characteristics. The different types of uncertainties provided with the dataset allow for more accurate studies, e.g., on the evaluation of model physics.

3.5.2 SICCI sea ice thickness dataset (version 0.9, Arctic-only, monthly data for October to March, 2003-2008)

A comparison of the SICCI ice thickness product with other data products derived from observational time series reveals a substantial positive bias in SICCI data. When besides sea ice concentration data also SICCI ice thickness data is assimilated into the model, the March-mean Arctic sea ice volume exceeds the ice volume derived from the assimilation run where only ice concentration is nudged by almost 100% (see figure 14). A side effect of assimilating high SICCI ice thicknesses into the model is that almost no assimilated sea ice in the marginal ice zone is lost directly after assimilation due to sea surface temperatures above freezing (see section on SICCI ice concentration data). The additional cooling of the system due to the positive bias in assimilated ice thicknesses prevents assimilated sea ice from being melted.

However, we find the positive bias in the SICCI sea ice thickness dataset to be too large to allow for the data product to be of adequate quality for climate modelling studies. Error characteristics were not provided with the SICCI ice thickness data product.

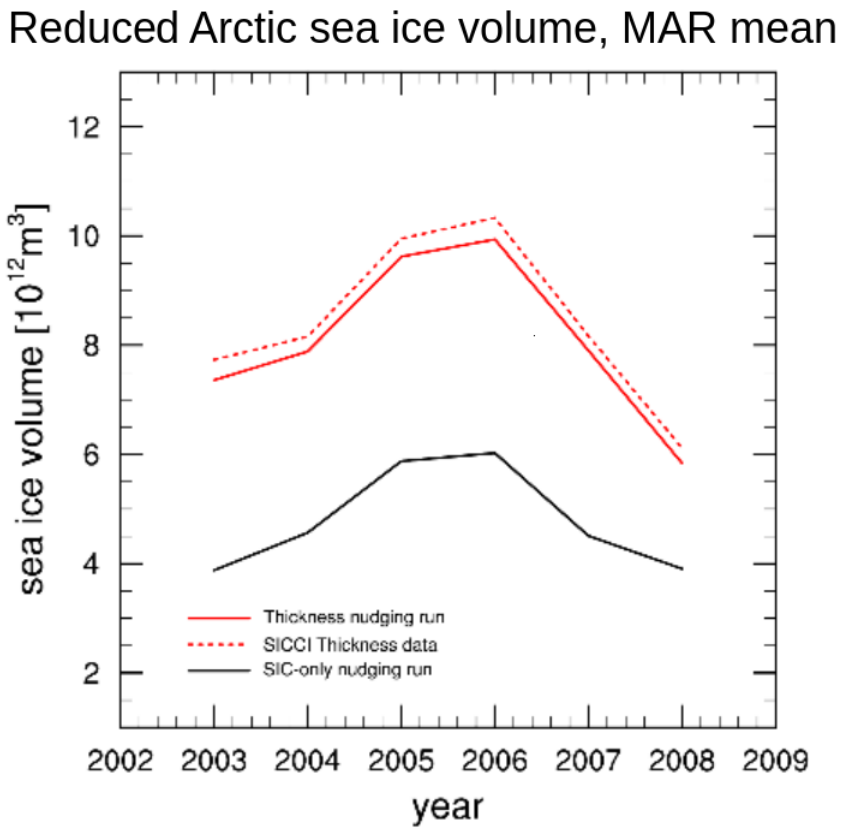

Figure 14: March-mean reduced Arctic sea ice volume over 2003-2008, as derived from SICCI ice thickness data (red dotted line), the combined SICCI ice thickness/concentration assimilation run (red solid line), as well as the SICCI ice concentration-only assimilation run (black line), is shown. The term "reduced" is introduced here, since only grid boxes, where the SICCI ice thickness dataset contains non-missing non-zero values, are considered.

3.6 Cross-Assessment of Aerosols, Cloud and Radiation CCI ECVs [WP3.7]

Aim

The aim of this work package is to complement the work of the Aerosol CCI Climate Research Group by providing a cross-assessment in the ESA CCI ECVs and in the CMIP5 climate models. We also aim at providing an improved process understanding by performing additional, more-detailed studies with the global aerosol model EMAC-MADE. The following scientific questions shall be addressed:

- What is the interrelation between different aerosols, cloud and radiation ECVs to CCI data and Earth System Models?
- How do the CMIP5 models perform in comparison to a more detailed aerosol global model (EMACMADE) in the representation of processes related to aerosol-radiation and aerosol-clouds interactions?

Summary of Results

We accessed the first release of aerosol data from ESA-CCI. It consisted of a long-term climate data record based on data from two platforms: ERS2-ATSR2 (covering the period 1996-2003) and ENVISAT (2002-2012). The satellite data have been processed by the Aerosol CCI team using three different algorithms from different groups. After validation with ground-based observations, the CCI team recommended using the University of Swansea (SU) algorithm.

The data were provided as Level 3 daily fields and includes the following variables: aerosol optical depth (AOD) at five wavelengths, Angstrom exponent 555/659 and 555/865, fine-mode AOD, absorbing AOD and dust AOD, surface reflectance at four wavelengths, cloud fraction, land-area fraction and other auxiliary information about the satellite position (solar and satellite zenith angle, relative azimuth angle). All variables are accompanied by uncertainty information and/or standard deviation. For our analysis, we calculated monthly mean time series, considering only complete years (January to December). For that reason, the data for the years 1996 and 2012 had to be excluded since they do not completely cover 12 months.

Given the overlap between the two dataset used to construct the long-term record, we first analysed the differences in the overlap period. As shown in the figure 15, such differences are small. Therefore combining the two dataset in a single data record has not been an issue in this work package.

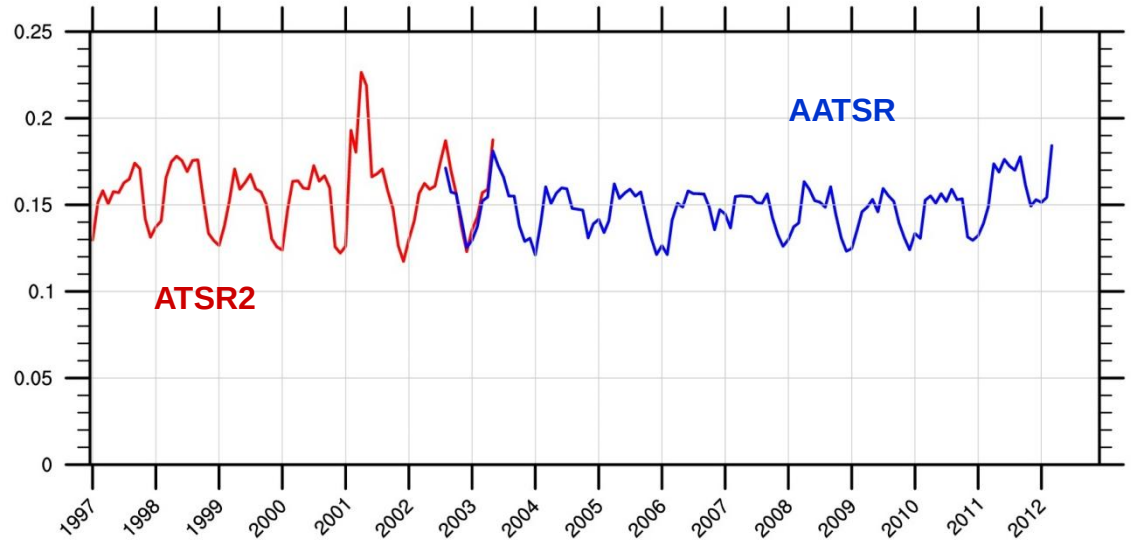

Figure 15: monthly-mean time series of aerosol optical depth at 550 nm from the two dataset of the aerosol long-term data record.

Using the ESMValTool, which is being developed as part of this project, we first compared the new aerosol-CCI product against AERONET. This was not meant to be a thorough validation of the aerosol-CCI product, but rather a simple comparison to understand how the new aerosol-CCI product compares to existing data sets. AERONET is a well-established global network of ground stations measuring AOD and related quantities for several decades. AERONET is widely accepted as a reference data set for validating AOD measured by satellites.

The result of this comparison is shown in figure 16. We found an overall good agreement between ESA-CCI and AERONET. An overestimate of AOD can be seen in some stations (especially in the Sahara, Arabia Peninsula, and South America). The agreement was also good for the marine stations, where the ground measurements are quite limited and the satellite product represent a valuable addition for the evaluation of model results.

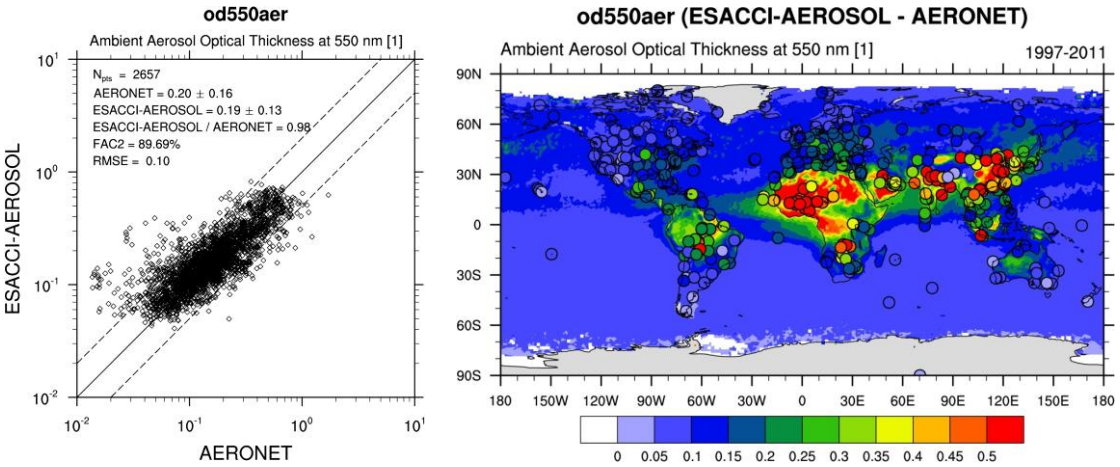

Figure 16: comparison of AOD at 550 nm (od550aer) between aerosol-CCI satellite data and the AERONET global network. The left panel shows a scatter plot with the relevant statistics, the right panel shows the satellite data as a contour map and the station measurements as circles, using the same color coding.

The aerosol-CCI product was used for evaluating AOD in the CMIP5 models with the diagnostic routines implemented in the ESMValTool. The tool currently includes data from MISR and MODIS. Figure 17 shows the AOD time series over the ocean for the period 1850-2015, for the CMIP5 models in comparison to MODIS and aerosol-CCI. All models simulate an increasing AOD trend starting around 1950. Some models (BNU-ESM, MRI-CGCM3 and Nor-ESM1-M) also show distinct AOD peaks in correspondence of the major volcanic emissions, e.g. El Chicon (1982) and Pinatubo (1991). The models simulate quite a wide range of AOD, between 0.05 and 0.20 in 2010, which deviates significantly from the observed values of MODIS and ESACCI-AEROSOL. A significant difference also exists between the two satellite datasets (about 0.05), which reveals the existence of observational uncertainties.

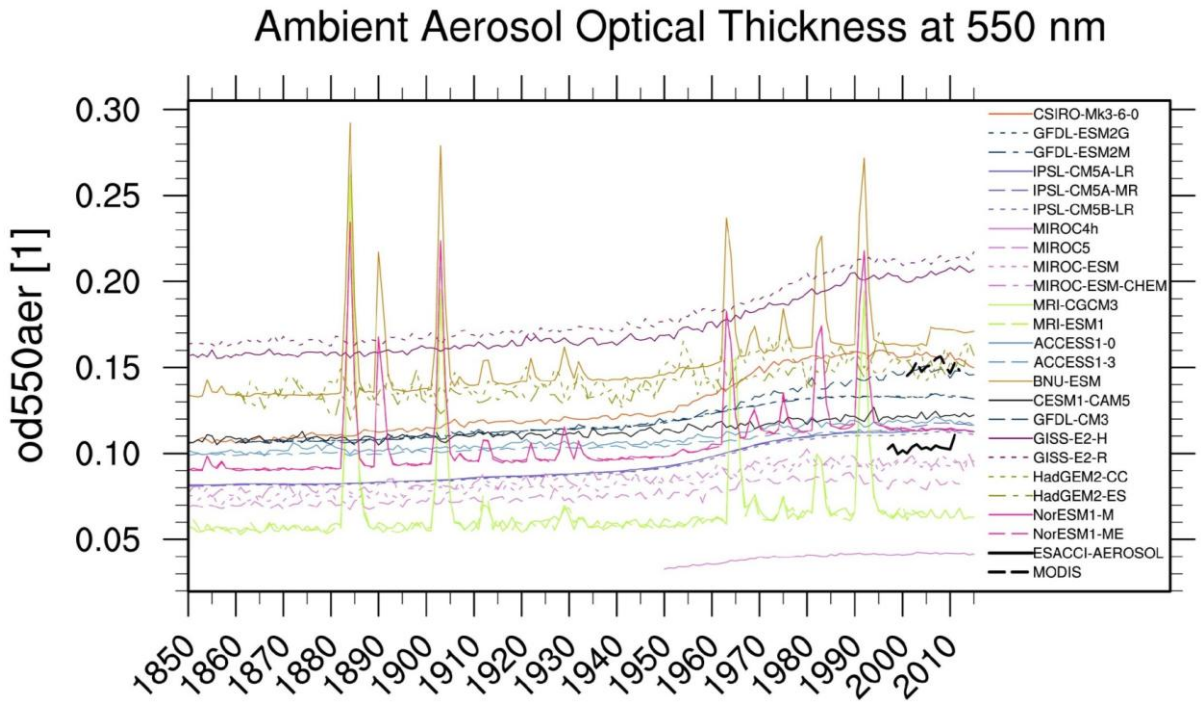

Figure 17: Time series of global oceanic mean aerosol optical depth (AOD) from individual CMIP5 models' historical (1850–2005) and RCP4.5 (2006–2010) simulations, compared with MODIS and aerosol-CCI satellite data. The figure is similar to Figure 9.29 in Flato et al. (2013).

Quality relevant outcomes

The analysed product has good temporal and spatial coverage and is well suited for climate modelling evaluation studies. The temporal coverage, defined here as the number of days with available data in each month of the data record (figure 18, left panel), is above 80% for most of the months. No significant differences in the temporal coverage were found between the two platforms. Spatial coverage is about 43% on average (figure 18, right panel). A significant improvement can be seen in the AATSR data due to a wider observing swath (48 versus 36%).

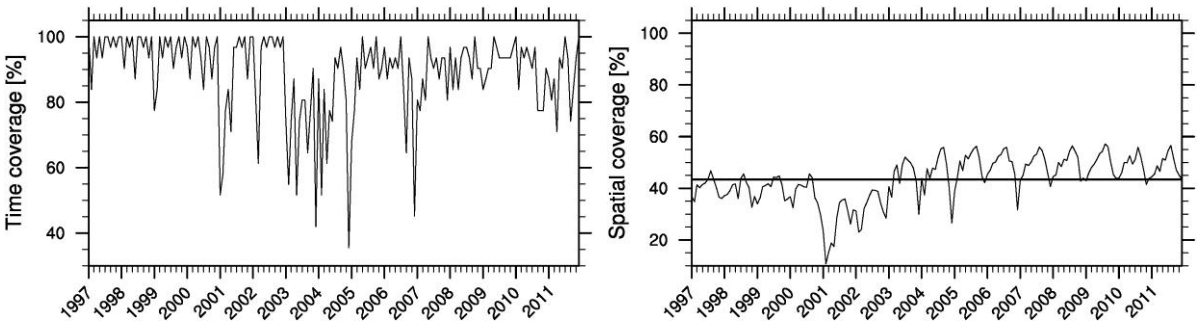

Figure 18: temporal (left) and spatial (right) coverage of the CCI aerosol product along the analysed time period. Values are calculated on a monthly-mean basis.

3.7 Cross assessments of clouds, water vapour, radiation, soil moisture for regional climate models [WP3.8]

Aim

The aim of this experiment was to make an integrated assessment of ECVs related to clouds, and soil moisture as well as water vapour and top of atmosphere (TOA) radiation, to assess their consistency for African and South American monsoon and European rainfall as simulated by regional climate models. The assessment includes an estimation of the uncertainties provided. It will address the following scientific questions:

- How do the CORDEX regional climate models simulate cloudiness and soil moisture for the West African/ South American (and Europe) regions?
- Investigate moisture related feedbacks which are important in the African and South American monsoon development. This involves local feedback mechanisms, lagged regional correlations in time and space and large scale forcing.
- Identify key processes in regional climate models affecting the simulated WAM/ SAMS that can lead to improvements in representation of the WAM/SAMS in climate simulations.
- Are observed soil moisture and extreme precipitation relationships captured by CORDEX simulations at different horizontal resolutions?

Summary of Results

The initial work of WP3.8 included the validation of surface soil moisture simulated by two Regional Climate Models (RCMs) utilizing the ESA CCI soil moisture remote sensing product, from now on only referred to as ESA (Liu et al., 2012, 2011; Wagner et al., 2012). Simulations were performed using two different RCM systems, the Rossby Centre Regional Climate model (RCA4) and a climate version of the meso-scale modelling system HARMONIE (HCLIM).

Climate Models

RCA4 is the model version used for the CORDEX (Coordinated Regional Climate Down-scaling Experiment) downscaling with RCA (Strandberg et al., 2014). The land-surface scheme of RCA (Samuelsson et al., 2014) divides the soil into three layers with respect to soil moisture and divides a grid box into two surface tiles, forest and open land, depending on land-use information. In this WP the top layer soil moisture was validated, represented by the upper 7.2 cm of the soil, of the open-land tile.

HARMONIE represents a suite of physical parametrization packages that are developed to be applicable to different resolutions. For this study we used results from a simulation based on the ALARO package (Lindstedt et al., 2015). The land-surface scheme of HARMONIE, SURFEX (Masson et al., 2013), also represents a suite of physical parametrization packages. For this study the force-restore soil option was used which divides the soil into three layers with respect to soil moisture. Also, the land was treated as one single tile with no sub-division

with respect to different land use. For this report, the top layer soil moisture was validated, represented by the upper 1 cm of the soil.

Experimental setup

For RCA we used the CORDEX domain over Africa at 50 km horizontal resolution (see figure 19). The simulation covers 1990 to 1994 with one year of spin-up time prior to this. The analysis for this study covers the period 1990-1994. For HCLIM we used a European domain with 16 km horizontal resolution (Lindstedt et al., 2015) (see figure 20). The simulation covers the period 1998 to 2007 with four months of spin-up time prior to this. The analysis for this study covers the period 2003-2007. Both simulations use ERA-Interim (ERA-I (Dee and co-authors, 2011)) at the lateral boundaries and for sea surface temperature (SST) every six hours.

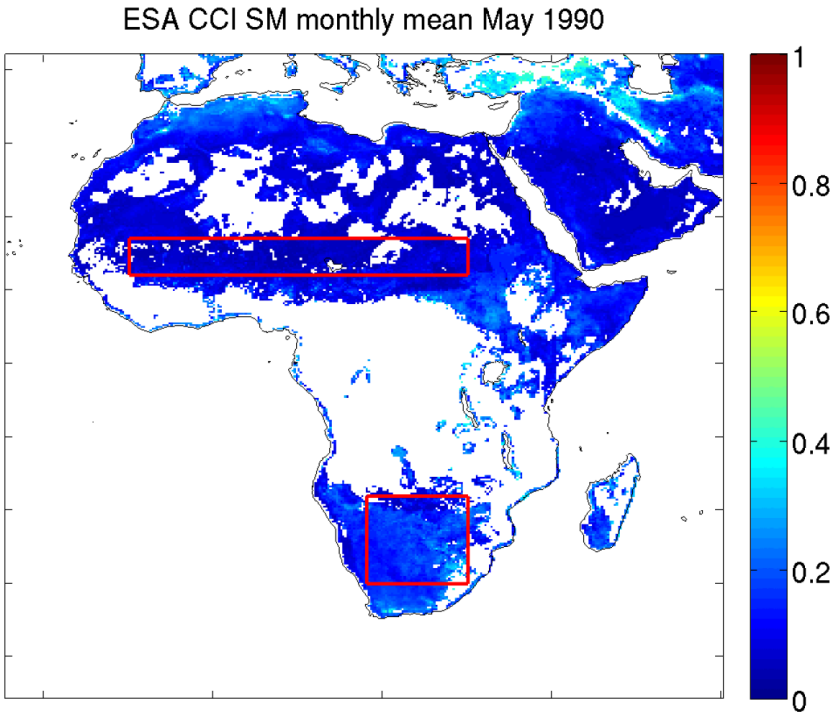

Figure 19: An example showing the ESA monthly mean soil moisture (m^3 m^{-3}) for the month of May 1990 over Africa.

Method of Analysis

The 2D (longitude/latitude) daily values of RCM soil moisture were interpolated to the ESA grid. A daily mask represented by the grid boxes in ESA which have valid SSM values was applied to the corresponding RCM SSM of the interpolated 2D fields. Thus, daily RCM SSM fields were created which have the same patterns of valid values as the ESA product. From these daily values monthly mean values were created for RCM and ESA SSM, respectively. An analysis of area averaged SSM was applied to three different regions, Sahel and Southern Africa, for the Africa domain and the Mediterranean for the Europe domain. Finally anomalies of SSM values were presented by simply removing the five year mean value from each area averaged time series.

To illustrate the effect of the daily mask the results based on non-masked RCA SSM are presented for the Africa regions. Also, to illustrate how the total column soil moisture in RCA relates to the SSM, the total soil moisture is included in the Africa results.

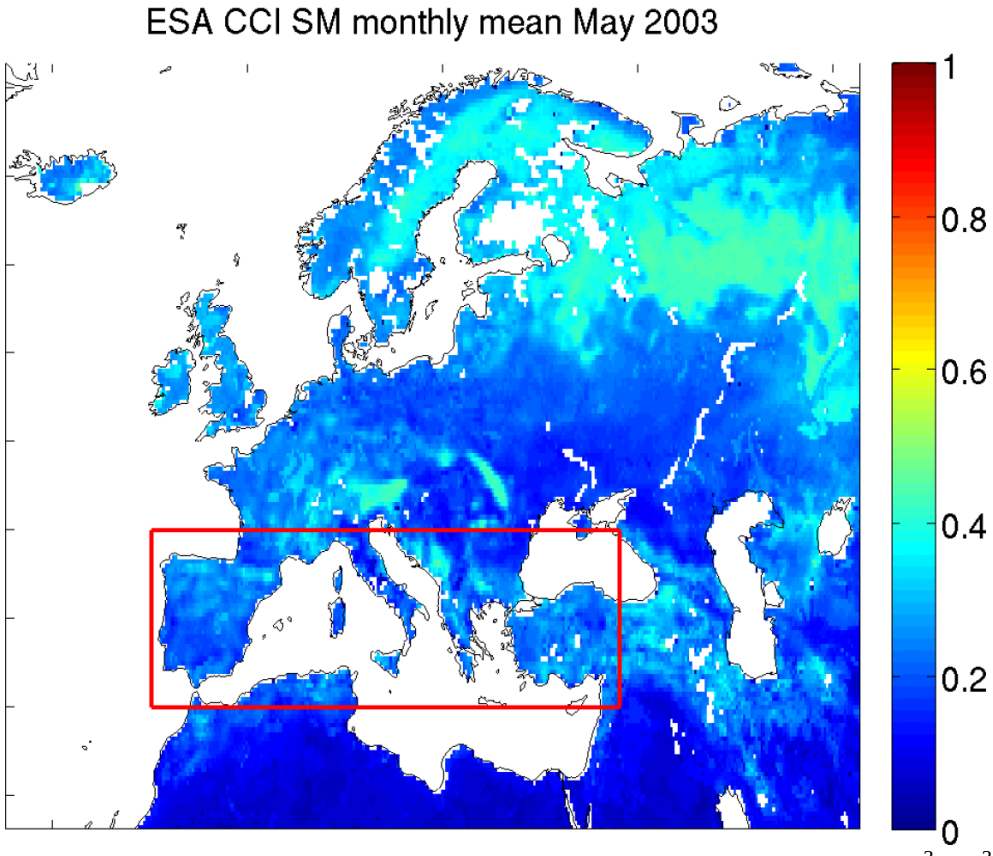

Figure 20: An example showing the ESA monthly mean soil moisture (m^3 m^{-3}) for the month of May 2003 over Europe.

RCA over Africa

For the Sahel region the RCA absolute SMM is close to the upper uncertainty limit of the ESA SSM, defined as plus one standard deviation above the ESA SSM (figure 21). This may indicate a wet bias in the RCA SSM. Assuming that SSM anomaly can still be analysed we see that the ESA SSM shows higher peak values than RCA SSM. The reason may be that RCA SSM represents a more thick soil layer than ESA but it may also be caused by less precipitation in RCA and/or more evapotranspiration in RCA during the rainy period. The RCA SSM climbs earlier and reaches a plateau at the beginning of each rainy season. The faster climbing is a known feature of RCA and is caused by a too quickly northward propagation of the West-African Monsoon system in RCA. Further analysis also including one or more observational precipitation products is needed to gain more understating of the model behaviour.

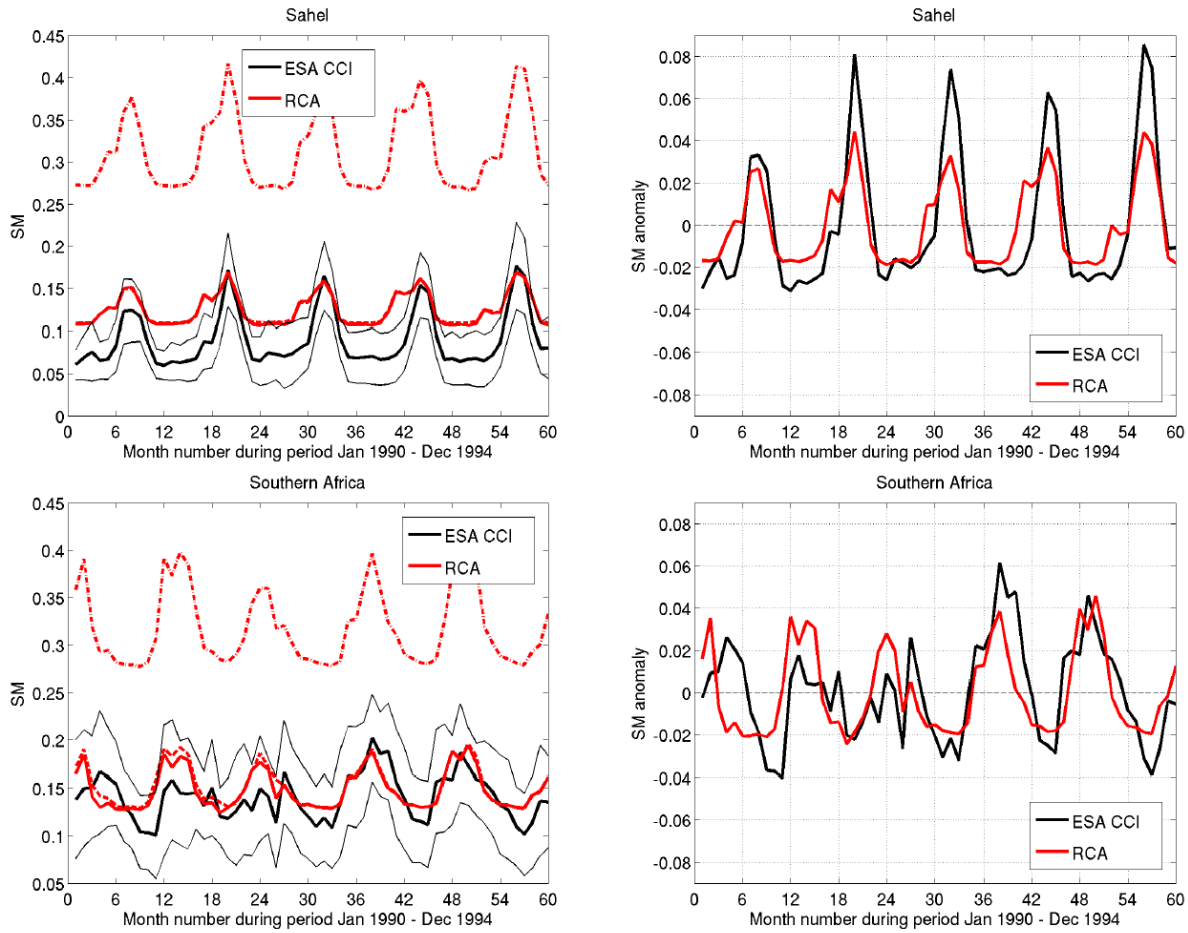

Figure 21: Top row shows results for Sahel and bottom row for Southern Africa regions respectively. Left column shows absolute soil moisture (m^3 m^{-3}) and right column soil moisture anomaly (m^3 m^{-3}). Red lines show RCA SSM results and black lines ESA SSM results. For the absolute soil moisture results three additional line types are shown; black thin lines show the soil moisture uncertainty (one standard deviation) for ESA, red dashed line shows RCA SSM for all grid points (i.e. no masking applied), and red dash-dotted line shows RCA total column soil moisture (m^3 m^{-3}).

For the Southern Africa region the absolute RCA SSM is closer to the corresponding ESASSM (figure 21). In the beginning of the period, looking at anomaly values, the model and the observations seem to be out of phase. Considering that one year of spin-up is applied prior to the analysing period, a delay in RCA soil moisture time evolution does not seems to be a reasonable explanation for this. Again an analysis including precipitation observations are needed to further understand the relationships between modelled and observed SSM. Although correct, figure 21 shows that the masking procedure described in Section 3 does not have a big impact compared to the case if masking had been omitted, i.e. the solid and dashed red lines in left column of figure 21 are similar. Figure 21 also confirms that one cannot use ESA SSM to validate modelled total column soil moisture.

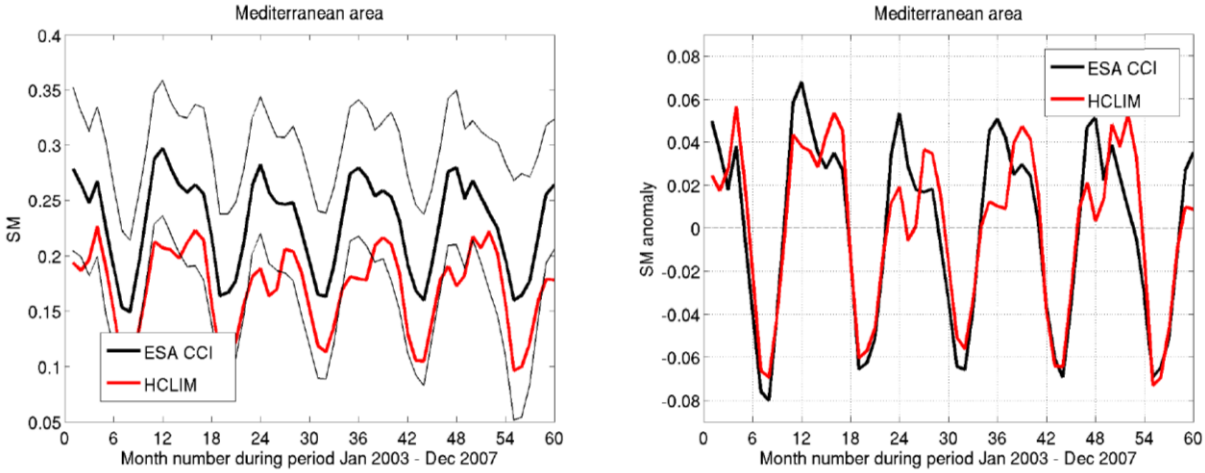

Figure 22: Results for the Mediterranean region. Left figure shows absolute soil moisture (m^3 m^{-3}) and right figure soil moisture anomaly (m^3 m^{-3}). Red lines show RCA SSM results and black lines ESA SSM results. Black thin lines in left figure show the soil moisture uncertainty (one standard deviation) for ESA.

HCLIM over Europe

The high resolution non-hydrostatic model HCLIM has been run over Europe where we have started to assess CCI soil moisture and clouds. According to figure 22 the HCLIM absolute SSM is close to the lower uncertainty limit of the ESA SSM. This may indicate a general dry bias in HCLIM. Again as for RCA, assuming that the SSM anomaly can still be analysed we see that modelled and observed SSM variability show in general good correspondence. For HCLIM the SSM represents a shallower layer than for RCA which may be one reason for a larger amplitude in simulated SSM over the Mediterranean compared with the Sahel. However, the ESA SSM shows a peak value each December while the simulated SSM peaks later during the spring. An analysis of precipitation is recommended to explain this.

We have included CCI Cloud phase 1 three year data in the regional climate model analysis tool as seen in figure 23, where the summer time, June, July and August (2007-2009) CCI cloudiness is compared to HCLIM, ERA-Interim and CLARA-A1 (CM-SAF AVHRR) data. The CCI cloud cover is similar to the other satellite observations and the models as expected in a first comparison. The Cloud-CCI team will provide 30 years of data autumn 2015 then this analysis will be extended.

We note that the CCI cloud cover is larger over sea than for CLARA-A1 and the models, the cloud mask used in CCI and thresholds for land and sea needs to be checked. The line noted for ESA-CCI clouds over the North Atlantic is due to empty scan lines in the AVHRR orbits, which were accidently set to zero. The empty scan lines occurred in the beginning and end of the orbits most commonly over the North Atlantic, according to the Cloud-CCI team. It has been corrected for the phase 2 data. We suggest that this type of known issues for any of the ECVs should be listed on the web-page where the data can be downloaded.

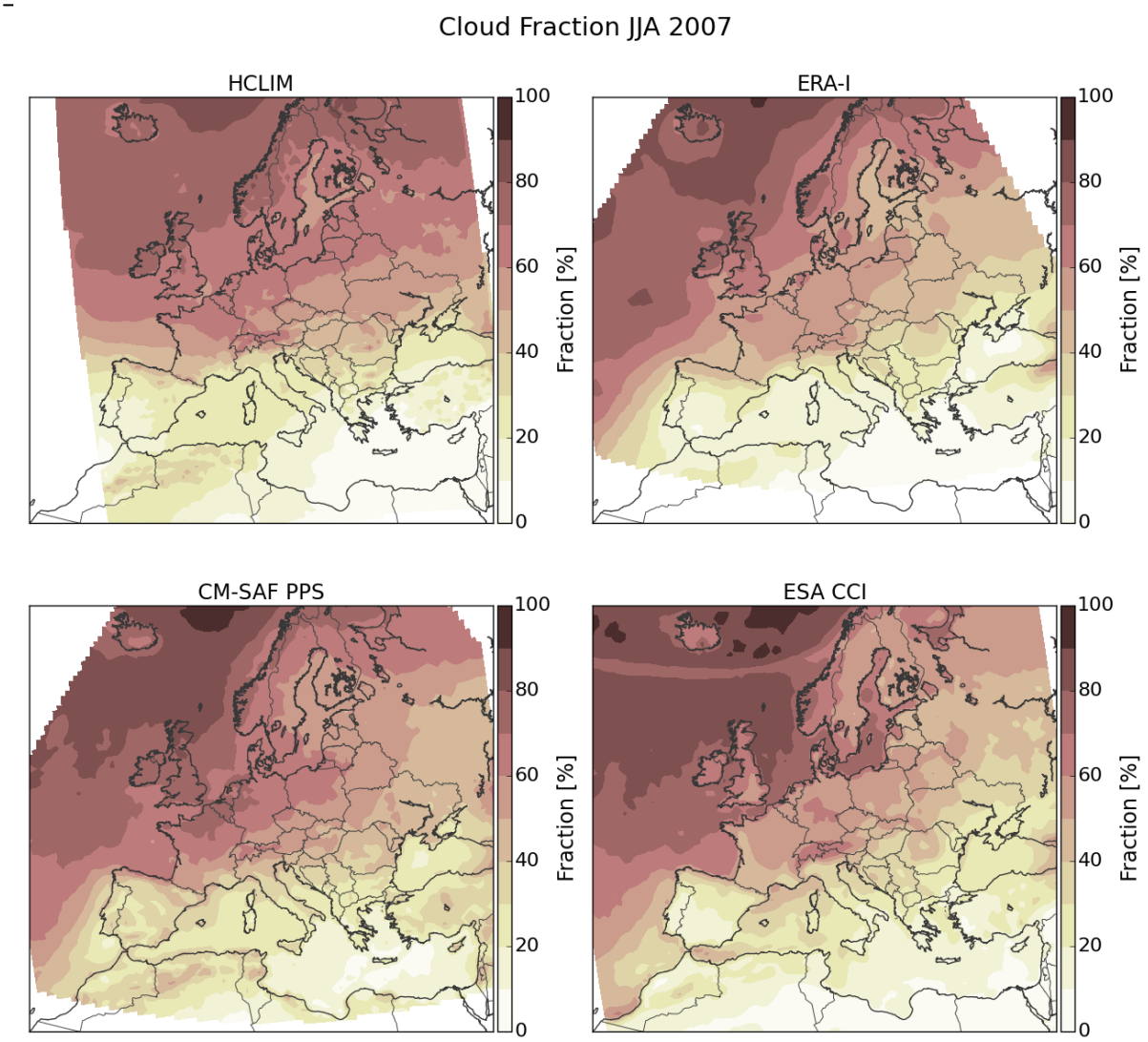

Figure 23: Cloudiness in a. H-CLIM (top left panel), in b. ERA-interim (top right panel), in c. CLARA-A1 observations (bottom left) and for d. Cloud-CCI NOAA18 observations (bottom right).

Quality relevant outcomes

We found from these preliminary results assessing CCI SM and cloud cover that both variables are of "climate quality" although the limited time period of Cloud CCI phase 1 does not allow any detailed studies. Listed below are some recommendations for individual variables and some general thoughts on observed versus modelled soil moisture.

Cloud-CCI

The data were downloaded from http://www.esa-cloud-cci.org/?q=data_access. Some observations are listed below:

- Any bugs and known issues, such as the line in cloud cover data (figure 23d), should be communicated to the users (e.g. listed where the data is available) for all ECVs.

- The simulator and simplistic simulator (compare only day time, spatial sampling etc.) that are being developed in cloud CCI will be very useful and should be available via the download data site.
- The cloud mask land/sea and snow should be checked, it appears as the land/sea cloudiness contrast is too high in cloud-CCI data.

SM-CCI

The Frequently Asked Questions on the SM website (http://www.esa-soilmoisture-cci.org/node/136) was very useful. It is recommended that a FAQ page be set up for all CCI ECVs, and any bugs can be listed under known issues/errors. The following points should be added to the SM FAQ to avoid misuse under 'Do', Don't' or 'Data usage in models'.

- Do not compare (or take care when comparing) your model total SM directly with these products, the satellite observes the top ~2cm" (figure 21).
- Any model data should be masked ("simplistic simulator approach") when compared to the observations. This is indirectly implied in the spatial and temporal availability SM FAQ's. It was less important in this study (figure 21) but for other regions and time periods the differences can be much larger. Any user comparing with model data should strongly be recommended to do mask the model data.
- It would be useful to have a presentation similar to that presented at the CMUG 5th integration meeting available at the FAQ link or somewhere else at the website.

General thoughts on satellite and model soil moisture comparisons

The ESA SSM usually represents a very shallow layer corresponding to the top two centimeters of the soil, but the observed depth depends on the soil moisture content (deeper for drier soils). It is not easy to characterize this top soil layer but in many regions it is some combination of active or dormant vegetation mixed by some dead vegetation material mixed with mineral soil. In the model, depending on the exact parameterization applied, the top SSM layer may be purely mineral soil or some weighted value between mineral soil, soil carbon and vegetation material.

As stated on ESA Web page "the statistical comparison metrics like root-mean-square-difference and bias based on our combined dataset are scientifically not meaningful. However, the CCI SM products can be used as a reference for computing correlation statistics or the unbiased root-mean-square-difference". This would support the anomaly analysis of SSM in this report although the absolute simulated SSM values are sometimes at the uncertainty limit of the ESA SSM. The most important soil moisture in models is represented by the layer occupied by roots since this is the soil moisture limiting the transpiration. Methods do exist which can be used to integrate ESA SSM in time to reach a soil moisture representing a thicker layer but assumptions, sometimes difficult to control, are needed for such methods. ESA SSM can be nudged or assimilated in a land-surface model to compile a deep soil moisture product but such a product will always be model dependent and must be used carefully when compared to other models. A soil moisture product representing the degree of saturation rather than volumetric soil moisture would limit, or even exclude, any model dependence. We argue that such a product is preferable. The SM team at the CMUG 5th integration meeting informed that such products are planned to be made, we support that work.

3.8 Assessment of ESA CCI glacier, land cover and sea level data for hydrological modelling of the Arctic Ocean drainage basin [WP3.9]

Aim

The aim of this study is to assess the use of the CCI glacier, land cover, and sea level data in hydrological modelling of the Arctic Ocean drainage basin. The main underlying question is if the use of CCI Glacier and Land cover can improve simulated river runoff to the Arctic Ocean? The current assessment is focused on the usefulness of the data as input for model parameterization compared to pre-cursor datasets, as well as on the 'climate quality' of the products in terms of understanding long term trends and seasonal variation in the Arctic hydrological system. The following scientific questions are addressed:

- Can the use of CCI Glacier data improve hydrological modelling and the simulated river runoff to the Arctic Ocean?
- Is there a relation between changes in observed land cover and simulated and observed river runoff?
- Are the sea level and runoff observations correlated?

Data requirements for the Pan-Arctic hydrological model Arctic-HYPE

A pan-arctic application of the hydrological model HYPE (Hydrological Predictions for the Environment) developed by SMHI (e.g. Lindström et al., 2010; Arheimer et al., 2012) is used in the analysis. The model is based on a semi-distributed multi-basin approach, with each river basin divided into sub-basins, and each such sub-basin divided into a set of soil-type/land-cover classes. The model simulates processes including for instance accumulation and melt of snow and glaciers, evapotranspiration, surface runoff, and drainage from individual soil layers, routing in lakes and rivers, and accumulated water discharge through the mouth of each sub-basin.

The following spatial data are normally used for a setup of the HYPE model for a particular domain (current data used for Arctic-HYPE in brackets):

- Gridded elevation data for routing and sub-basin delineation (Hydro1K)
- Discharge station locations for routing and sub-basin delineation (GRDC)
- Gridded land cover and soil data for derivation of soil and land use classes (ESA GlobCover 2004-2006, and HWSD, respectively)
- Outlines of major lakes and dams (GLWD).
- Information on irrigated areas and crops (GMIA and MIRCA2000, respectively).

The model is forced by time-series of daily average air temperature (mean, min and max) and precipitation (WFDEI) and has been calibrated/evaluated with data on river discharge (GRDC), snow (ESA GlobSnow/Former Soviet union snow course data), evaporation (FluxNet), and glacier mass balance (WGMS).

The Arctic-HYPE model covers the land area draining into the Arctic Ocean (excluding Greenland) and covers 23 million km^2, divided into 32599 sub-basins with an average size of 715 km^2 (see further on http://hypeweb.smhi.se).

Summary of Results

CCI Glacier

- CCI Glacier data (Randolph Glacier Inventory, RGI v4.0) was found to be very useful for evaluating and improving the setup of the glacier sub-model in the Arctic-HYPE model:
    - RGIv4 glacier outlines was used for calculating total glacier area within the sub-basins of the hydrological model, and compared to glacier area estimated from CCI Land Cover and the pre-cursor data set ESA GlobCover 2004-2006.
    - RGIv4 glacier outlines could be further used for improving sub-basin delineation following the glacier outlines.
    - RGIv4 includes additional information that will be further used to improve the glacier sub-model: mean, maximum and minimum elevation, slope and length.
- Glacier area estimated from the class "permanent snow and ice" from CCI Land cover and Glob cover was found to largely overestimate the glacier area derived from CCI Glacier data (figure 24; table 3).

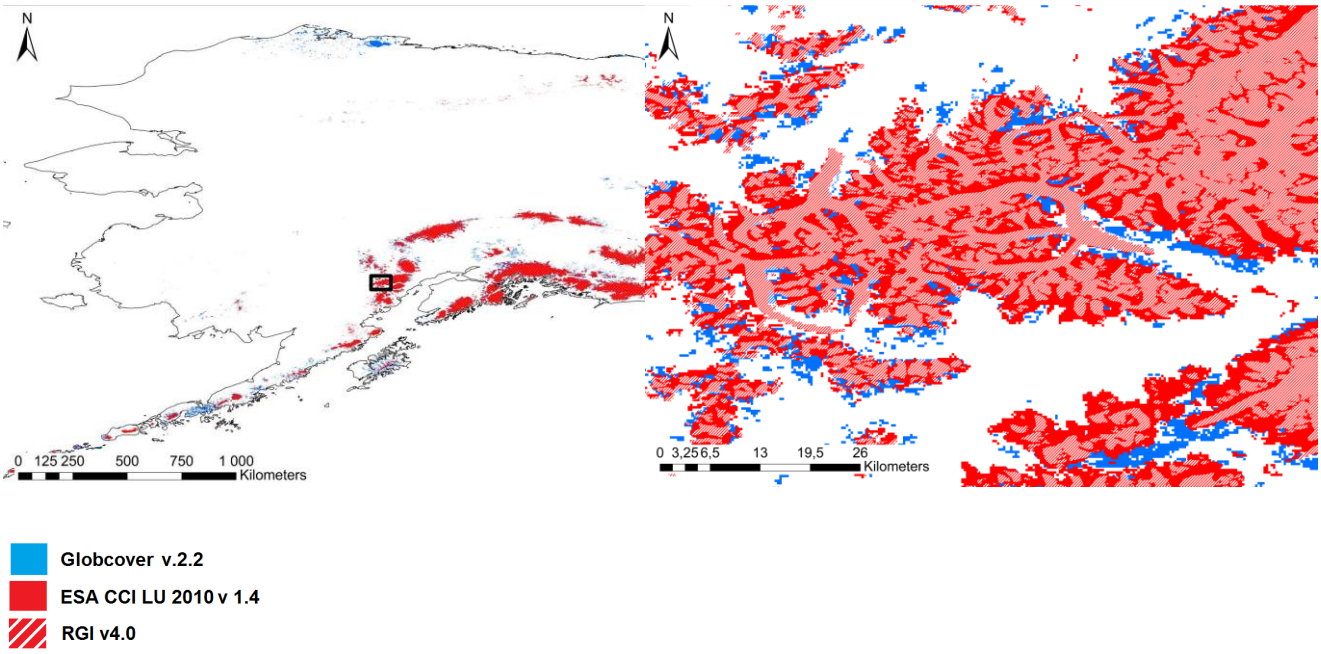

Figure 24: Comparison of glacier area in Alaska derived from CCI land cover and ESA GlobCover 2004-2006 (permanent snow and ice) and the glacier outlines from CCI Glacier (RGIv4).

RGI region	RGI glacier area (km2)	RGI glacier area (fraction of total model area)	Glacier area based on CCI Land cover (fraction of RGI area)	Glacier area based on GlobCover (fraction of RGI area)
01 Alaska	1232	0.007	1.359	1.569
02 Western Canada/US	315	0.001	**3.152**	**17.114**
03 Arctic Canada North	104074	0.291	**1.272**	**2.4**
04 Arctic Canada South	41303	0.036	**1.607**	**2.647**
06 Iceland	11060	0.109	**1.009**	**2.079**
07 Svalbard	32342	0.542	1.185	1.65
08 Scandinavia	1805	0.006	1.56	1.311
09 Russian Arctic	50756	0.346	**1.198**	**2.286**
10 North Asia	759	0	**2.039**	**8.599**
Total	243646	0.014	1.315	2.424

Table 3: Glacier area in the Arctic-HYPE model per RGI region, comparing data from CCI glacier (RGIv4) and estimations based on the land cover class "permanent snow and ice" from CCI land cover and GlobCover 2004-2006.

CCI Land cover

CCI land cover was compared to the precursor data GlobCover 2004-2006 with regard to differences in land cover distribution. The "climate quality" of the information in the land cover time series (2000, 2005, 2010) was of special interest, since the on-going changes in the Arctic regions (mainly climate related) are expected to be expressed for instance in the distribution of vegetation, surface water, and snow and ice.

Preliminary results to date:

- More surface water in CCI Land cover compared to the pre-cursor GlobCover 2004-2006):
  - CCI Land cover was found to include more surface water (about 6-20% more), which might be important for understanding Arctic hydrology (figure 25) dominated by large rivers and a large number of small and large lakes. Impact in the model still to be analyzed.

- The fraction of deciduous needle leaf trees (larches?) was reduced in the latest epoch (2008-2012) compared to previous periods in eastern Siberia.
  - Field observations suggest that this might be due to increasing precipitation during the period.
  - This will affect the 'climate quality' of the land cover time-series data.
  - Analysis of relation to observed and simulated river discharge still to be analyzed.
- The class "water bodies" is constant throughout the three epochs and water bodies are not included in the seasonal products.

- From a "climate quality" perspective, it would be interesting to get information on the trends and seasonal variation in the spatial distribution of surface water. Variation in small water bodies is a relevant ECV related to permafrost melting, which is of highest interest in the Arctic region.

- The difference between the CCI glacier area and the area with "permanent snow and ice" is much improved in the CCI land cover data compared to the GlobCover data, which apparently is based on data from only one complete melting period. However, CCI land cover data for "permanent snow and ice" still overestimates glacier area with up to more than 30%, as discussed above.

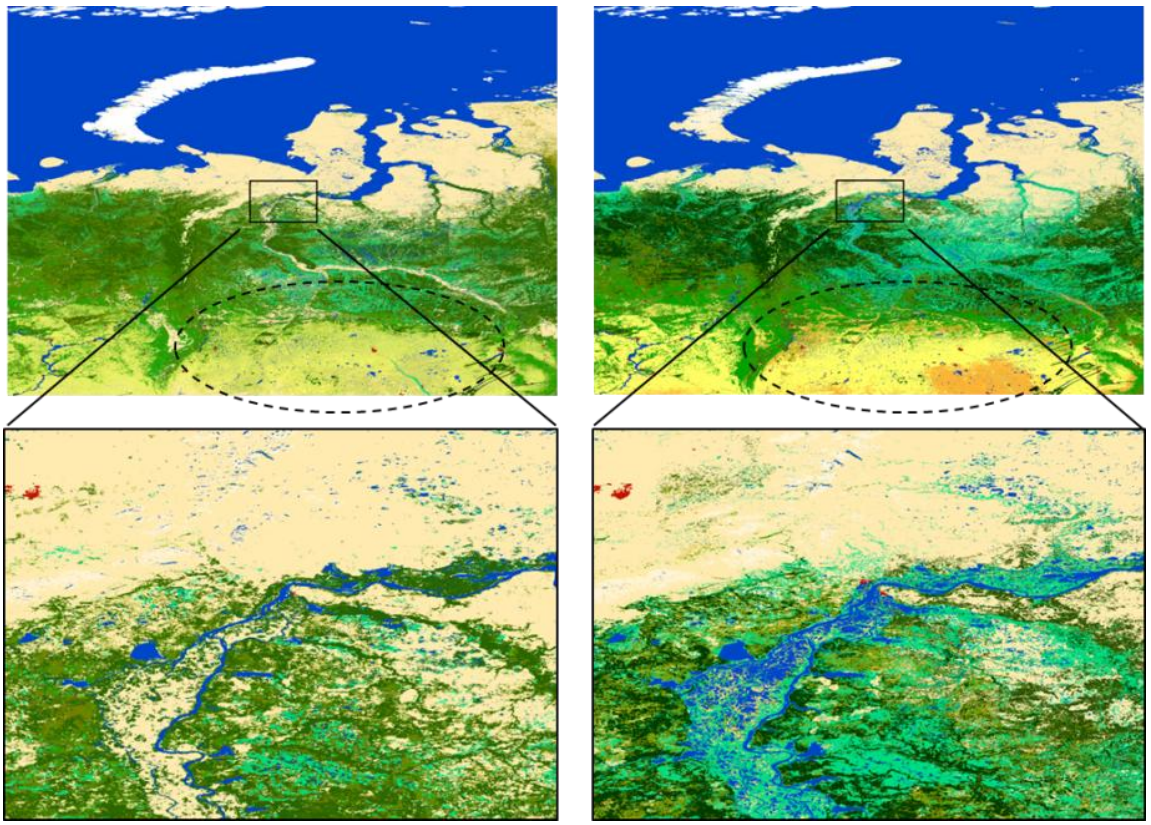

Figure 25: Land cover data from the area around the Ob River showing a clear increase in surface water area from Left: GlobCover to Right: CCI land cover.

Quality relevant outcomes

- Disagreement between CCI Glacier and CCI Land cover:
  - The CCI Land cover class "permanent snow and ice" is larger than the glacier area derived from the glacier outlines in CCI Glacier - in some regions the more than 30% too large (figure 24; table 3).
  - The CCI Land cover documentation reveals that the CCI Glacier outlines have been used to assign "permanent snow and ice" to all land cover pixels within the outlines – however, areas outside of the CCI Glacier outlines classified as

"permanent snow and ice" have not been reset to "unclassified" or any other land cover class.
    - Discussions with Science Leaders from CCI Glacier and Land cover confirmed this situation, and it was suggested to include a sub-class under "permanent snow and ice" separating pixels under ice and other snow pixels.
- No ice thickness in CCI Glacier data (RGIv4):
    - Glacier thickness is not included in RGIv4 even though estimates of each glacier exist based on modelling and observations (Farinotti & Huss, 2012).
    - The model estimates can be requested from the CCI Glacier team on request. However this information is not clear in the CCI Glacier documentation.
- No temporal information in CCI Glacier (RGIv4):
    - The information in RGIv4 is only a snapshot in time representing the most recent available data. Information needed for initialization, calibration and evaluation of glacier models for long-term hydrological or climate model simulations are missing. Such information has to be compiled by the user from other sources, for instance from the other activities linked to CCI Glacier.

3.9 Cross-assessment of CCI-ECVs over the Mediterranean domain [WP3.10]

The activity within the context of this Work Package is in the continuity of the Météo-France activity in the context of CMUG Phase 1. Its main objective is to evaluate the performances (mean climate, variability and trends) of the Med-CORDEX regional climate system models over the Mediterranean domain with a sub-set of atmosphere, marine and surface CCI-ECVs. The first scientific question to address is the following: are the state of the art RCSMs able to reproduce observed Mediterranean climate trends and variability over the last decades?

During CMUG Phase 1, the SSH simulated by the so-called RCSM4 coupled regional climate model (Sevault et al., 2009) developed at CNRM and applied in the Med-CORDEX international simulation exercise, was confronted with the CCI Sea Level ECV and its precursor over the 1993-2010 period (see Phase 1 deliverable 3.1). Some results of this confrontation have been recently published in the scientific literature as part of a presentation of the evaluation of the ocean component of the RCSM4 model (Sevault et al, 2014).

One main conclusion from this confrontation was that the CCI SSH is suitable for regional climate studies over the Mediterranean basin, even at a scale of a few tens of kilometres. The results of the model concerning trends of sea level change are encouraging. It also let some open questions concerning the way to facilitate the comparison between the modelled and observed sea levels. These questions come from the fact that climate models are not directly calculating the contributions to sea level changes that are due to mass changes implied by glaciers and ice sheet melting or by changes in continental water storage. In addition, in the specific case of regional climate models simulating the Mediterranean domain, the contribution to mass change in the Mediterranean Sea due to the mass flux at the Gibraltar Strait need also to be carefully taken into account.

Since the beginning of CMUG Phase 2, thanks to the development of a new version of the Mediterranean Sea model, and thanks to the availability of a new ocean reanalysis, it was possible to improve the comparison between the modelled and the satellite-derived SSH.

The operational ocean reanalysis system (ORAS4; Balmaseda et al., 2013) has been implemented at ECMWF and it spans the period 1958 to the present. This make this reanalysis suitable for MedCORDEX simulations since it can be used to constrain the oceanic component of a regional climate model in the Atlantic buffer zone over the ERA-Interim period (1980-2013). Contrary to the so-called COMBINE reanalysis previously used, ORAS4 assimilates satellite-derived SSH anomalies from the AVISO dataset (the precursor used in Phase 1). This is significant because it potentially accounts for for sea level changes due to mass changes in the simulated Mediterranean Sea level through the boundary condition applied in the Atlantic buffer zone (see Phase 1 deliverable 3.1). The results presented below confirm that this is indeed the case.

The new version of the Mediterranean Sea model is NEMOMED12, a regional version of NEMO v3.2 model simulating the free surface evolution associated to the convergence of the

oceanic current and to the fresh water flux at the ocean surface, as this was the case for NEMOMED8 used during Phase1. Compared to this last, the resolution is improved on the horizontal (1/12° versus 1/8°) and on the vertical (75 vertical levels versus 43). The model was integrated over the period 1980-2013 with an atmospheric forcing from ALDERA (a dynamical downscaling of ERA-Interim using the ALADIN-Climat regional climate model) and a relaxation toward ORAS4 in the Atlantic buffer zone of the model (3D for temperature and salinity, 2D for SSH). However, since ORAS4 underestimate the mean seasonal cycle of the SSH over the basin (see figure 26), it has been previously corrected in the Atlantic buffer zone in order to reproduce on average the mean annual cycle obtained from the CCI-ECV over the 1993-2010 period. This correction also applies before the satellite observing period.

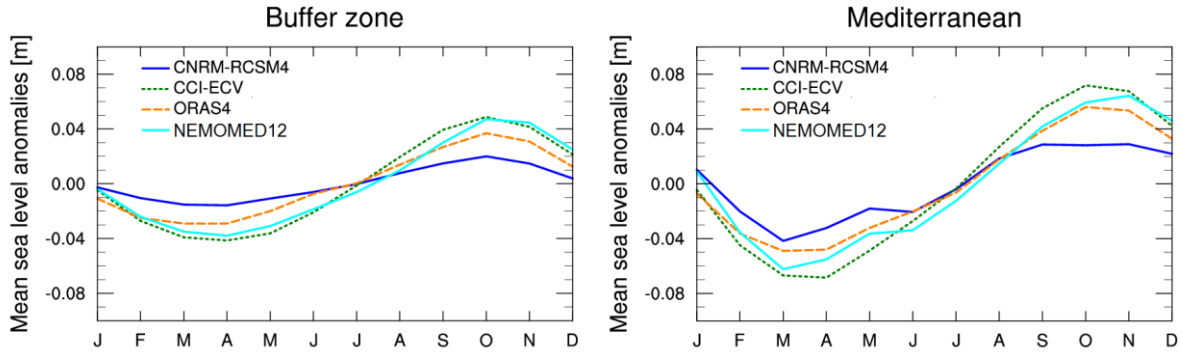

Figure 26: Seasonal cycle of mean sea level anomaly over the buffer zone (left) and over the Mediterranean Sea (right) for the CCI sea level (green dotted line), ORAS4 ocean reanalysis (orange dashed line), the coupled regional climate system model RCSM4 (dark blue line) and the Nemomed12 Mediterranean sea model (light blue line).

The results presented in figure 26 show that the NEMOMED12 model reproduces correctly the mean seasonal cycle from the CCI-ECV over the buffer zone, small differences coming from the fact that the relaxation coefficients toward the corrected ORAS4 are decreasing in the eastern part of this zone. But NEMOMED12 also reproduces fairly well the Mediterranean Sea mean sea level inferred from the CCI-ECV, and with a much better agreement than the RSCM4 free surface (in Phase 1 deliverable 3.1, RCSM4 sea level was presented after adding the thermosteric component of sea level inferred from the simulated temperature changes only over the basin to account for missing terms in the model equations).

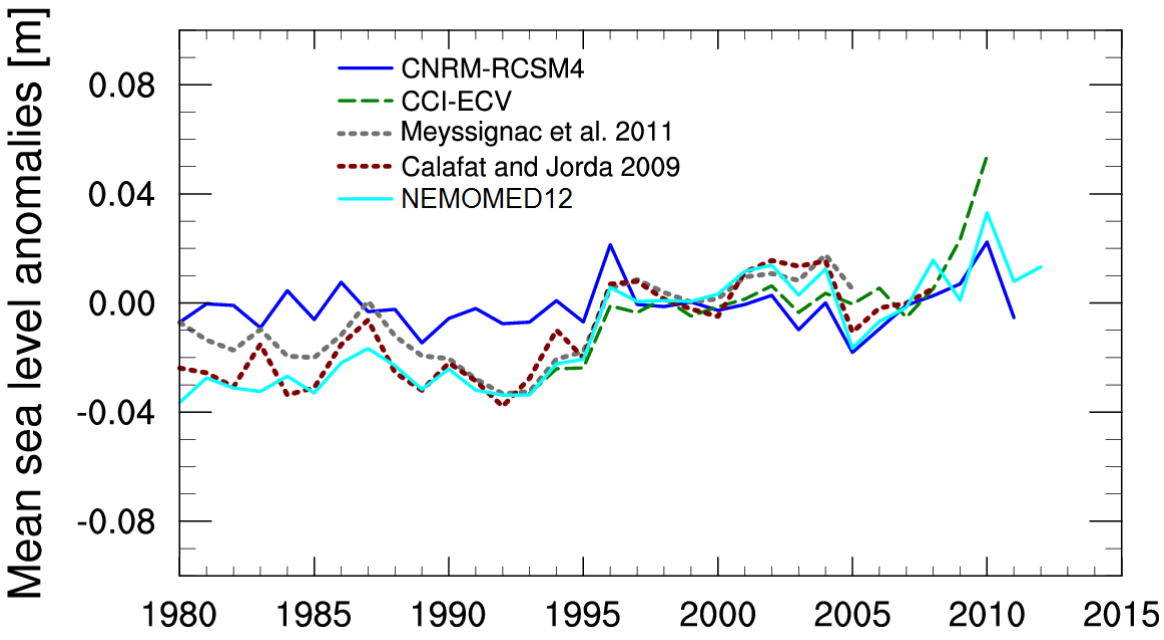

Figure 27: Time series of mean sea level anomalies averaged over the Mediterranean Sea over the period 1980-2013 for the CCI sea level (dashed green line), the tide gauge derived sea level reconstructions of Meyssignac et al. (dotted grey line) and Calafat and Jordà (dotted brown line), for the coupled regional climate system model RCSM4 (dark blue line) and the Nemomed12 Mediterranean sea model (light blue line).

The positive impact of the assimilation of satellite-derived sea level in the ocean reanalysis used to constrain the ocean model in the Atlantic is also illustrated in figure 27 showing the time series of mean sea level over the Mediterranean Sea. NEMOMED12 is indeed able to reproduce the sea level change over the period as observed from tide gauges and by the CCI-ECV. This also illustrates that the mean sea level change in the Mediterranean Sea mainly depends on the mass flux change at the Gibraltar Strait. Here again, without the thermosteric term contribution, the RCSM4 model has reduced performance due to the absence of SSH assimilation in the COMBINE reanalysis used to constrain the model in the Atlantic.

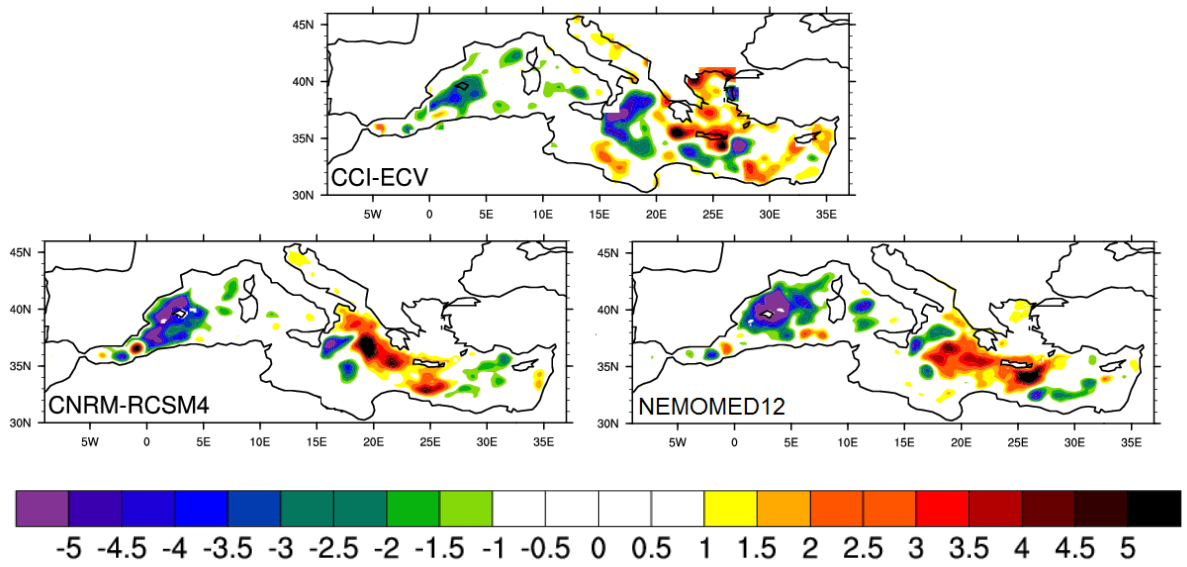

Figure 28: Trends in mm/year of Mediterranean sea surface height anomalies over the period 1993-2010 for the CCI Sea level (top), the coupled regional climate system model RCSM4 (bottom left) and the Nemomed12 Mediterranean Sea model (bottom right).

Simulated and observed sea level trends have been reproduced in figure 28 after removing the spatial and temporal averages of the SSH over the Mediterranean domain for the 18-year period (1993-2010). RCSM4 and Nemomed12 display very similar performances because the different boundary conditions have little impact on the spatial trend variability. This proves that this variability is not significantly affected by the coupling between the atmosphere and the Mediterranean Sea. In addition, the agreement shows that the uncertainty on local trends estimated to be 3mm/yr, might have been overestimated by the CCI Sea level team, because the signal of change, consistently simulated by the two models (RCSM4 and Nemod12), is the same order of magnitude as the error.

4. Summary of Results by ECV

4.1 Greenhouse Gases

CMUG analysis of these ECV data will be presented in the next version of this report.

4.2 Aerosols

This section summarises the results from [WP3.7] Cross-Assessment of Aerosols, Cloud and Radiation CCI ECVs.

We first compared the new aerosol-CCI product against AERONET. This was not meant to be a thorough validation of the aerosol-CCI product, but rather a simple comparison to understand how the new aerosol-CCI product compares to existing data sets. AERONET is a well-established global network of ground stations measuring AOD and related quantities for several decades. AERONET is widely accepted as a reference data set for validating AOD measured by satellites.

The results of this comparison are shown in figure 29. Overall a good agreement was found between ESA-CCI and AERONET. An overestimate of AOD can be seen in some stations (especially in the Sahara, Arabia Peninsula, and South America). The agreement is good also in the marine stations, where the ground measurements are quite limited and the satellite product represent a valuable addition for the evaluation of model results.

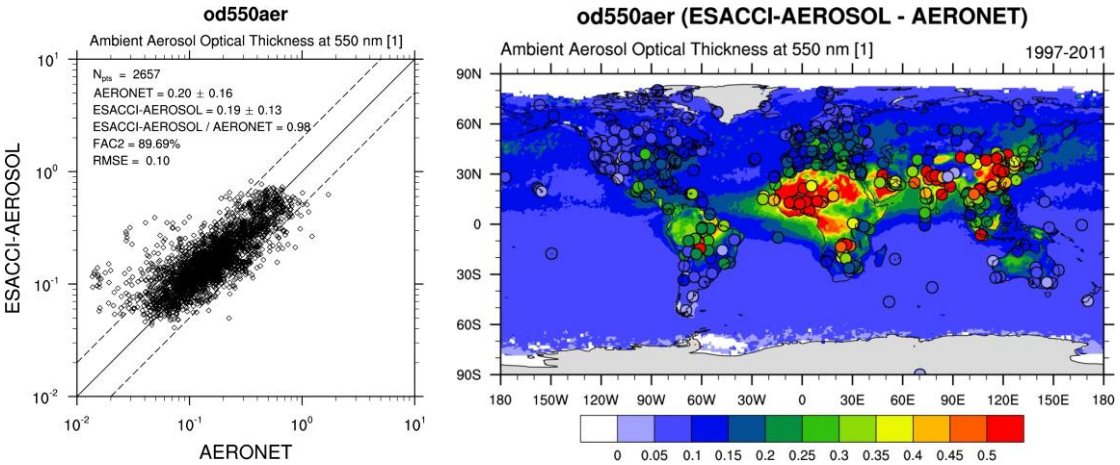

Figure 29: comparison of AOD at 550 nm (od550aer) between aerosol-CCI satellite data and the AERONET global network. The left panel shows a scatter plot with the relevant statistics, the right panel shows the satellite data as a contour map and the station measurements as circles, using the same color coding.

The aerosol-CCI product was used for evaluating AOD in the CMIP5 models with the diagnostic routines implemented in the ESMValTool. The tool currently includes data from MISR and MODIS. Figure 30 shows the AOD time series over the ocean for the period 1850-

2015, for the CMIP5 models in comparison to MODIS and Aerosol-CCI. All models simulate an increasing AOD trend starting around 1950. Some models (BNU-ESM, MRI-CGCM3 and Nor-ESM1-M) also show distinct AOD peaks in correspondence of the major volcanic emissions, e.g. El Chicon (1982) and Pinatubo (1991). The models simulate quite a wide range of AOD, between 0.05 and 0.20 in 2010, which deviates significantly from the observed values of MODIS and ESACCI-AEROSOL. A significant difference also exists between the two satellite datasets (about 0.05), which reveals the existence of observational uncertainties.

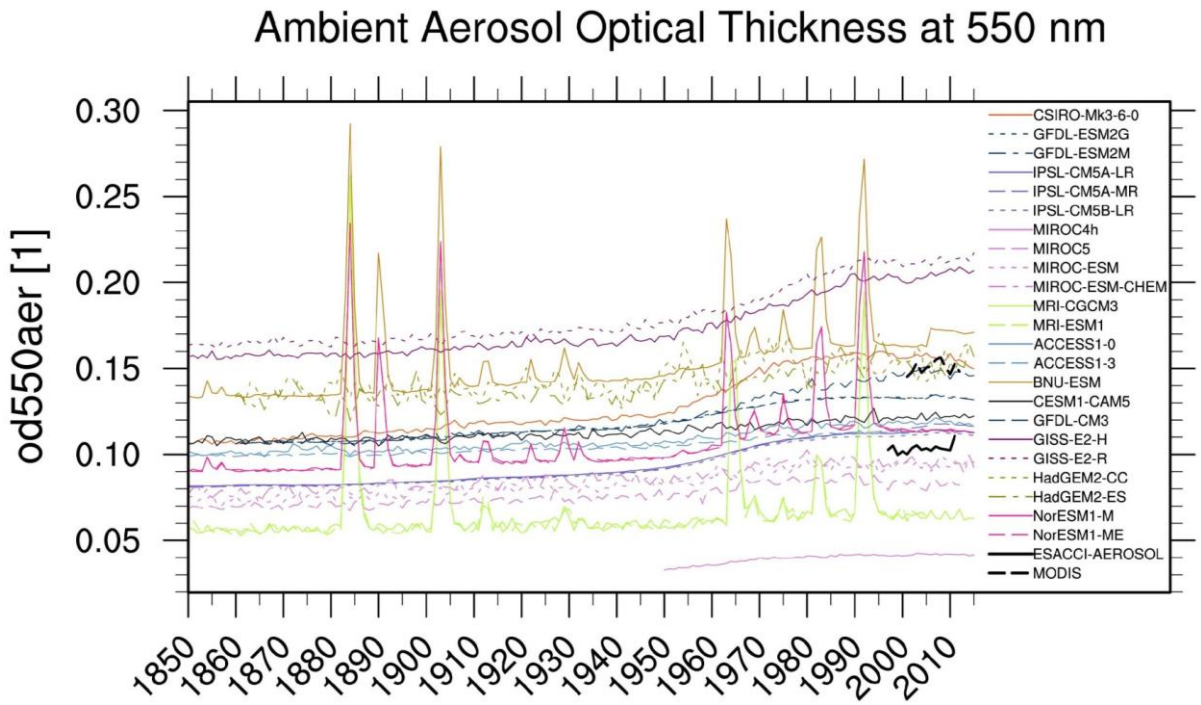

Figure 30: Time series of global oceanic mean aerosol optical depth (AOD) from individual CMIP5 models' historical (1850–2005) and RCP4.5 (2006–2010) simulations, compared with MODIS and aerosol-CCI satellite data. The figure is similar to Figure 9.29 in Flato et al. (2013).

The analysed product has good temporal and spatial coverage and is well suited for climate modelling evaluation studies. The temporal coverage, defined here as the number of days with available data in each month of the data record (figure 31, left panel), is above 80% for most of the months. No significant differences in the temporal coverage were found between the two platforms. Spatial coverage is about 43% on average (figure 31, right panel). A significant improvement can be seen in the AATSR data due to a wider observing swath (48 versus 36%).

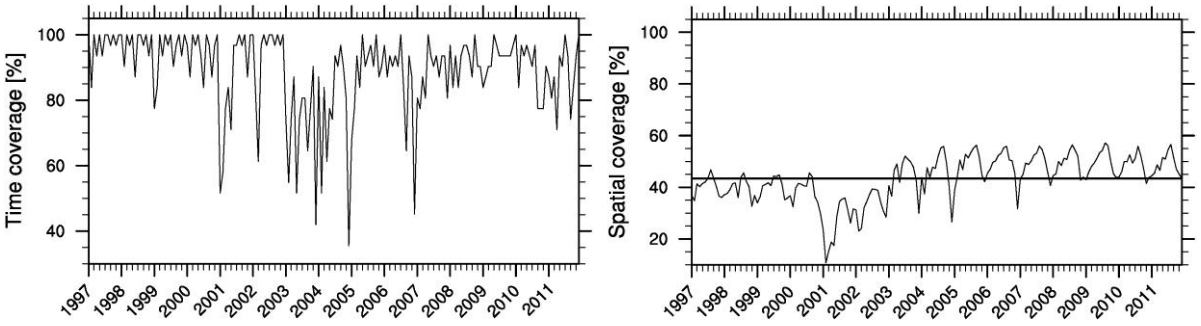

Figure 31: temporal (left) and spatial (right) coverage of the CCI aerosol product along the analysed time period. Values are calculated on a monthly-mean basis.

4.3 Ozone

This section summarises the results from [WP 3.2] Assimilation of several L2 ozone products in the ERA-Clim system.

The results so far from this study can be summarized as follows:

- The observation uncertainties generally well compare in structure with estimates obtained using the Desroziers method (Desroziers et al., 2005). The differences between estimated and provided uncertainties show up to 60% overestimation in the tropical mid stratosphere for GOME-2 NPO3 (this accounts for less than 4% of the observation values) and up to 100% underestimation in the tropics for the total columns (this difference is about 8% of the global mean total column ozone value).
- All the products exhibit negligible to very small biases.
- All assessed O3-CCI datasets lead to improved ozone analyses.
- Regarding the RR assimilation exercises, with the exception of OMI TCO3, the O3-CCI retrievals seem to better constrain the ozone analyses than retrievals obtained from the same radiances using alternative algorithms.
- The assimilation of the GOME-2 NPO3 show a clear improvement in the internal consistency of the data assimilation system in terms of better fit to the AIRS ozone-sensitive IR channels that in turn leads to statistically significant reduction (i.e. improvement) in the RMS of the geopotential forecast errors in the tropics.
- Assimilation User Requirements to Space Agencies and retrieval teams:
  - ❖ The comparison of the impact generated by the GOME-2 TCO3 and that of the GOME-2 NPO3 shows that the latter dataset can lead to a greater positive impact on the ozone analyses than the former.

The comparison of the impact generated by the GOME-2 NPO3 and that of the MIPAS LPO3 shows that thanks to its higher vertical resolution limb observations can lead to a greater positive impact in the stratosphere and upper troposphere than the nadir ozone profiles. This is not always the case in the lower troposphere. where, despite lacking visibility, the limb observations can still improve the ozone analyses compared to a control experiment if their synergy with other observations (in particular total column ozone products) can be exploited within the data assimilation system.Based on the discussed results and conclusions, the following O3-CCI products are recommended to be assimilated in the forthcoming ERA5 reanalysis: SCIAMACHY TCO3; GOME and GOME-2 NPO3; MIPAS LPO3.

4.4 Cloud

This section summarises the results from [WP3.8] Cross assessments of clouds, water vapour, radiation, soil moisture for regional climate models.

We have included CCI Cloud phase 1 three year data in the regional climate model analysis tool as seen in figure 32, where the summer time, June, July and August (2007-2009) CCI cloudiness is compared to HCLIM, ERA-Interim and CLARA-A1 (CM-SAF AVHRR) data. The CCI cloud cover is similar to the other satellite observations and the models as expected in a first comparison. The Cloud-CCI team will provide 30 years of data autumn 2015 then this analysis will be extended.

We note that the CCI cloud cover is larger over sea than for CLARA-A1 and the models, the cloud mask used in CCI and thresholds for land and sea needs to be checked. The line noted for ESA-CCI clouds over the North Atlantic is due to empty scan lines in the AVHRR orbits, that were accidently set to zero. The empty scan lines occurred in the beginning and end of the orbits most commonly over the North Atlantic, according to the Cloud-CCI team. It has been corrected for the phase 2 data. We suggest these type of known issues for any of the ECV's should be listed on the web-page where the data can be downloaded.

We found from these preliminary results assessing CCI SM and cloud cover that both variables are of "climate quality" although the limited time period of Cloud CCI phase 1 does not allow any detailed studies. Listed below are some recommendations for individual variables and some general thoughts on observed compared with modelled soil moisture.

Data were downloaded from http://www.esa-cloud-cci.org/?q=data_access where it was easily accessed.

- We recommend that any known bugs, such as the line in cloud cover data (figure 32d) data, should be communicated to the users (e.g. listed where the data is available). This is true for all ECV's, any known issues, bugs should be listed.
- The simulator and simplistic simulator (which compare only day time, spatial sampling etc.) that are being developed in cloud CCI will be very useful and should be available via the download data site.
- The cloud mask land/sea and snow should be checked, it appears that the land/sea cloudiness contrast is too high in cloud-CCI data.

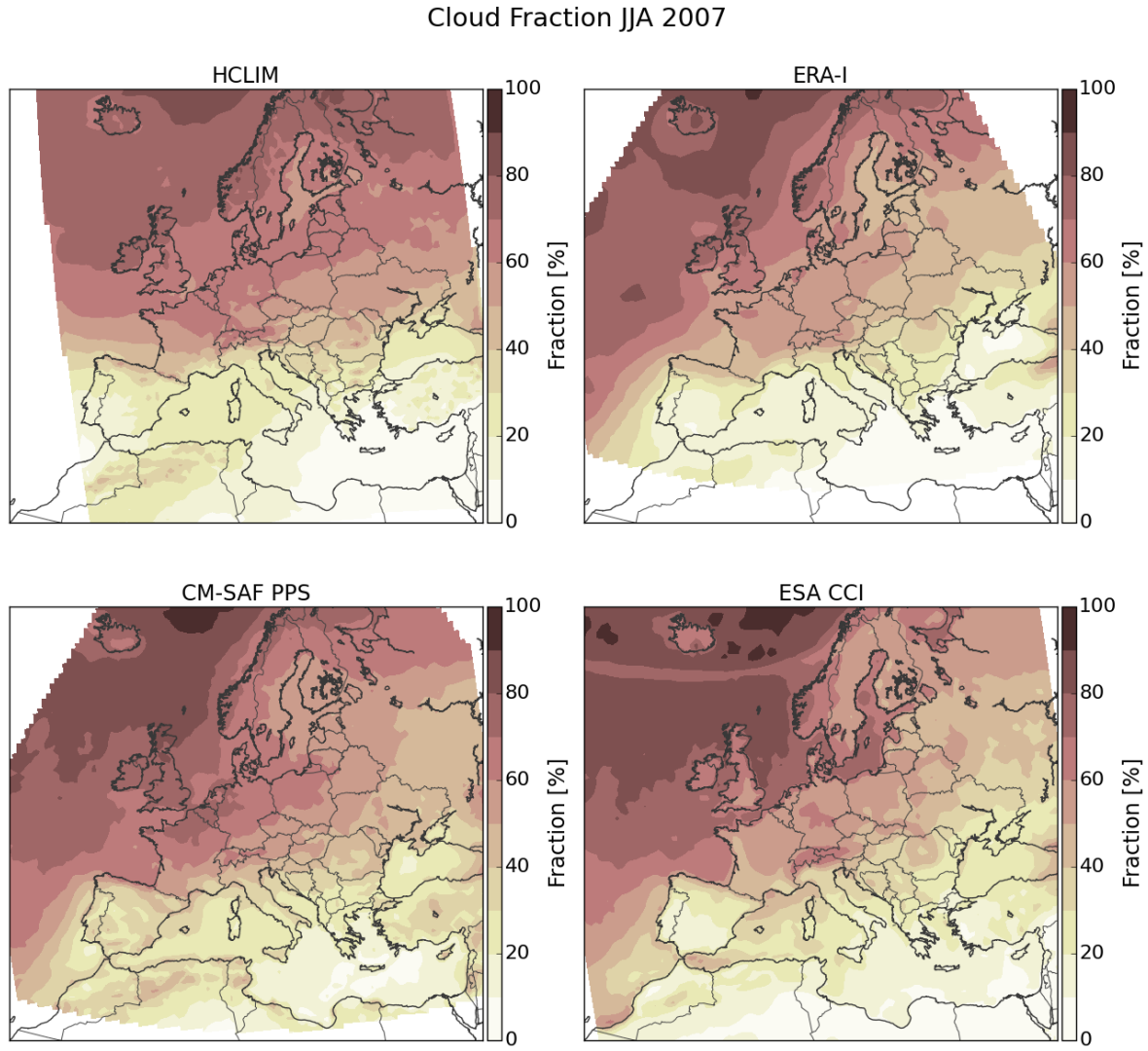

Figure 32: Cloudiness in a. H-CLIM (top left panel), in b. ERA-interim (top right panel), in c. CLARA-A1 observations (bottom left) and for d. Cloud-CCI NOAA18 observations (bottom right).

4.5 Sea Surface Temperature

CMUG analysis of these ECV data will be presented in the next version of this report.

4.6 Sea Surface Height

This section summarises the results from [WP3.10] Cross-assessment of CCI-ECVs over the Mediterranean domain.

Results presented in figure 33 on Phase 1 CCI SSH data show that the NEMOMED12 model reproduces correctly the mean seasonal cycle from the CCI-ECV over the buffer zone, small differences coming from the fact that the relaxation coefficients toward the corrected ORAS4 are decreasing in the eastern part of this zone. But NEMOMED12 also reproduces fairly well the Mediterranean Sea mean sea level inferred from the CCI-ECV, and with a much better agreement than the RSCM4 free surface.

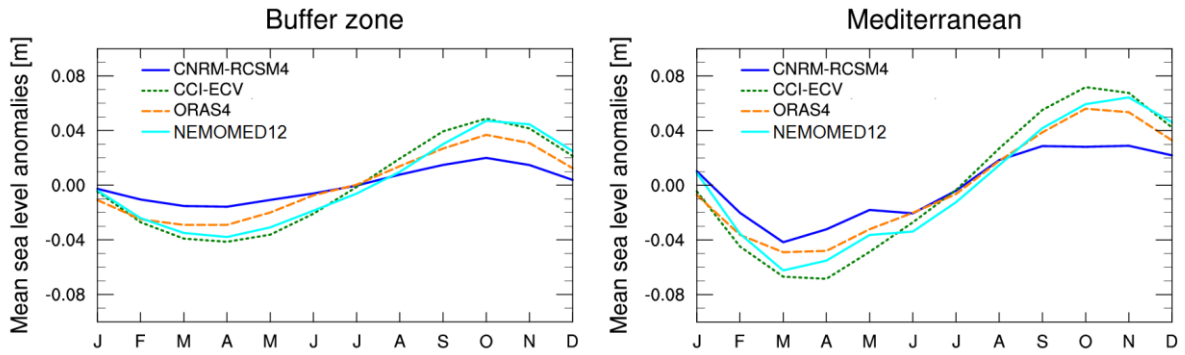

Figure 33: Seasonal cycle of mean sea level anomaly over the buffer zone (left) and over the Mediterranean Sea (right) for the CCI sea level (green dotted line), ORAS4 ocean reanalysis (orange dashed line), the coupled regional climate system model RCSM4 (dark blue line) and the Nemomed12 Mediterranean sea model (light blue line).

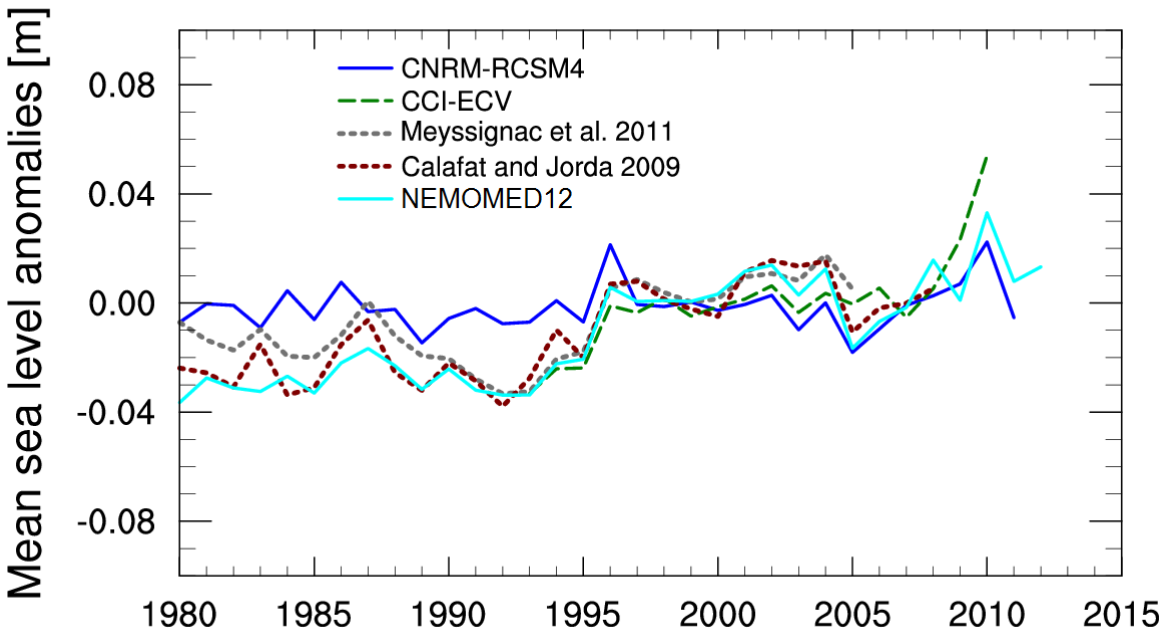

Figure 34: Time series of mean sea level anomalies averaged over the Mediterranean Sea over the period 1980-2013 for the CCI sea level (dashed green line), the tide gauge derived sea level reconstructions of Meyssignac et al. (dotted grey line) and Calafat and Jordà (dotted brown line), for the coupled regional climate system model RCSM4 (dark blue line) and the Nemomed12 Mediterranean sea model (light blue line).

The positive impact of the assimilation of satellite-derived sea level in the ocean reanalysis used to constrain the ocean model in the Atlantic is also illustrated in figure 34 showing the time series of mean sea level over the Mediterranean Sea. NEMOMED12 is indeed able to reproduce the sea level change over the period as observed from tide gauges and by the CCI-ECV. This also illustrates that the mean sea level change in the Mediterranean Sea mainly depends on the mass flux change at the Gibraltar Strait. Here again, without the thermosteric term contribution, the RCSM4 model has reduced performance due to the absence of SSH assimilation in the COMBINE reanalysis used to constrain the model in the Atlantic.

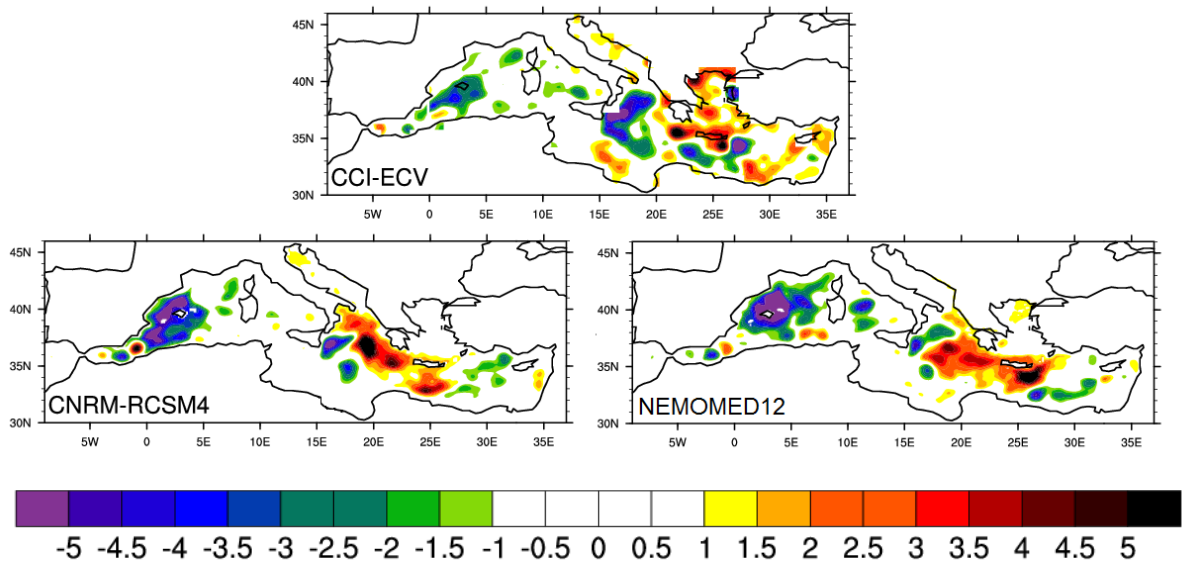

Figure 35: Trends in mm/year of Mediterranean sea surface height anomalies over the period 1993-2010 for the CCI Sea level (top), the coupled regional climate system model RCSM4 (bottom left) and the Nemomed12 Mediterranean Sea model (bottom right).

We have reproduced in figure 35 the simulated and observed sea level trends after removing the spatial and temporal averages of the SSH over the Mediterranean domain for the 18-year period (1993-2010). RCSM4 and Nemomed12 display very similar performance because the different boundary conditions have little impact on the spatial trend variability. This also proves that this variability is not significantly affected by the coupling between the atmosphere and the Mediterranean Sea. In addition, this agreement shows that the uncertainty on local trends estimated to be 3mm/yr, might have been overestimated by the CCI Sea level team, because the signal of change, consistently simulated by the two models (RCSM4 and Nemod12), has the same order of magnitude as this error.

4.7 Ocean Colour

This section summarises the results from [WP3.1] Assessment of Marine ECVs in FOAM Ocean Model.

The OC-CCI products were found to be of sufficient quality for data assimilation purposes, and of at least equal quality to the GlobColour. Assimilating OC-CCI chlorophyll data improved the model's representation of sea surface chlorophyll compared with both satellite data sets, and also a range of independent in situ observations. An example of this is shown in figure 36, which plots a time series of sea surface chlorophyll from all three model runs at the Hawaii Ocean Time Series (HOT) site in the North Pacific, along with in situ observations. The assimilation results in a much better match for both the magnitude and seasonality of the observations. It is also able to produce a reanalysis which is stable with time whilst displaying inter-annual variability.

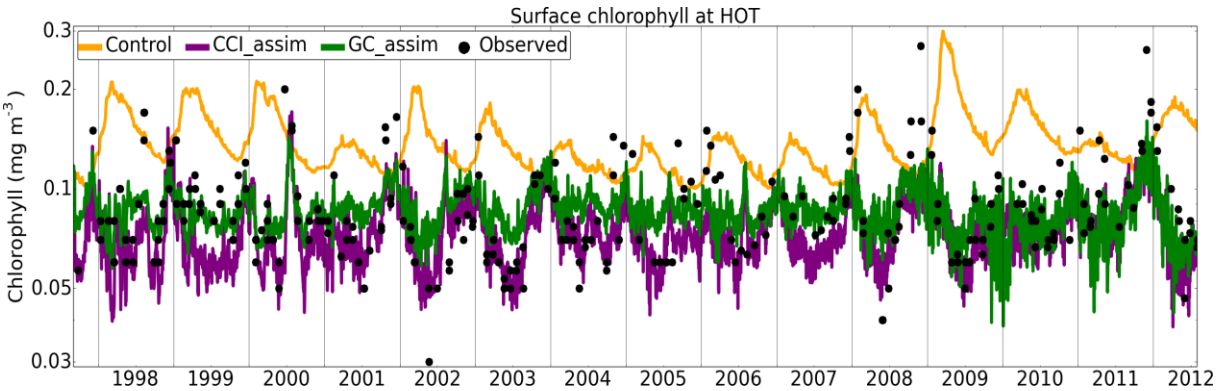

Figure 36: Time series of modelled and observed chlorophyll concentration in the surface 10 m at the HOT site. Observations have been obtained from http://hahana.soest.hawaii.edu/hot.

The largest impact of the assimilation was on sea surface chlorophyll, but an improved representation of chlorophyll was also found throughout the water column. Corresponding changes were found in phytoplankton and zooplankton biomass, although limited observational data are available for validation. Changes to nutrient concentrations were small, and largely neutral compared with observations. This is an important result, as some studies have found a degradation of nutrients due to chlorophyll assimilation.

Validation has also focused on the impact of the assimilation on the model carbon cycle, as this is of particular relevance for climate studies. Validation has been performed against surface fugacity of carbon dioxide (fCO_2) observations from the SOCAT V2 database (Bakker et al., 2014). Overall, the effect of the chlorophyll assimilation was small compared with the magnitude of model biases. In part, this is because there are large physical controls on the carbon cycle. The impact on these of additionally assimilating physical ECVs will be assessed as part of forthcoming Phase 2 activities. In regions of strong biological activity, the chlorophyll assimilation was found to have a beneficial impact on carbon variables, an example of which is shown in Figure 37. In some areas, the assimilation was found to improve representation of the biological component of the carbon cycle, but overall degrades fCO_2 compared with observations due to compensating errors in the physical component of the carbon cycle. Again, the impact in these cases of combined assimilation of all marine ECVs will be assessed later in Phase 2.

Technical issues with the OC-CCI V1 products have already been reported on during Phase 1. OC-CCI V2 products have recently been released (although the release was not directly communicated to CMUG researchers), and testing will be performed to see if previous issues have been resolved. An initial reading of the Product User Guide suggests that the documentation has been improved, particularly regarding use of the uncertainty estimates.

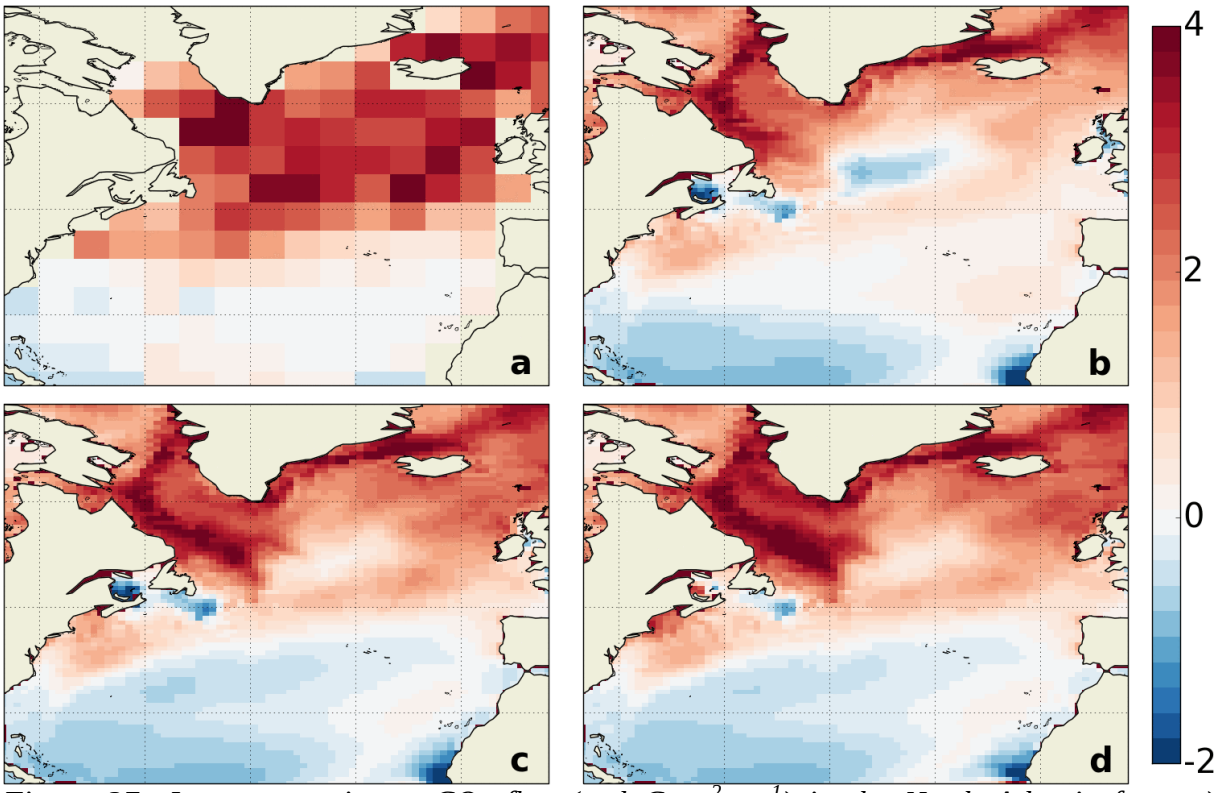

Figure 37: June mean air-sea CO_2 flux (mol C m^{-2} yr^{-1}) in the North Atlantic from a) climatology of Takahashi et al. (2009), b) FOAM-HadOCC control, c) reanalysis assimilating GlobColour data, d) reanalysis assimilating OC-CCI data. Positive values represent a flux into the ocean. The reduction in spurious outgassing in the centre of the domain in c) and d) compared with b) is due to the assimilation reducing the chlorophyll bias in this area.

A comparison between the OC-CCI V1 and GlobColour observation products has been performed to assess their stability and spatial coverage, building on that reported on at the end of Phase 1. GlobColour has greater spatial coverage prior to 2002, as it uses an older NASA SeaWiFS processing which discards fewer data points. Between 2002 and 2012, OC-CCI has greater coverage as more use is made of MERIS data. This is of particular benefit to the assimilation in certain regions, such as the Mauritanian upwelling region and the Arabian Sea during the Asian monsoon period, which were poorly covered by GlobColour. There is a lack of *in situ* observations with which to validate the results in these areas, but the model fields when assimilating OC-CCI data are in line with qualitative expectations. The global mean and spatial standard deviation of the OC-CCI chlorophyll products are also more stable with time than GlobColour, although a marked reduction in variability is noted when MERIS is introduced in 2002. This seems to suggest that the different sensors are not fully inter-calibrated. Such features are less clear in the reanalysis fields, as to some extent the model acts to smooth these out, and overall very similar results are obtained whether OC-CCI or GlobColour products are assimilated.

In the current line of work, the uncertainty estimates have been used to assign observation errors during the quality control stage, but not as part of the assimilation. The latter requires a development to the data assimilation scheme, which is expected to be included for future Phase 2 activities, allowing the uncertainty estimates to be assessed in this context. As part of

the quality control, the only issue found was that not every observation had a corresponding uncertainty, as reported during Phase 1, which led to these observations being automatically rejected. This is a known issue which the OC-CCI team is aware of. Some use has been made of the uncertainties in a validation context, although a lack of documentation for the V1 products meant their appropriate usage was not entirely clear. As noted above, this appears to have been much improved for the V2 release, which should allow more, and improved, use of these uncertainties.

Assessment of the seasonal and inter-annual variability of the reanalyses has also been performed, including the impact of the data assimilation on this variability, as an assessment of the applicability of the end product to climate monitoring activities. As mentioned above, the assimilation has a beneficial impact on the variability of model chlorophyll, and has also been found to impact phenological indicators, for instance the start dates of the North Atlantic spring bloom.

The effect of the assimilation on the carbon cycle variability is more subtle, with it impacting the magnitude more than the variability of the air-sea CO_2 flux. Nonetheless, the model is able to capture observed variability relating to climate drivers such as the El Niño Southern Oscillation (ENSO), the North Atlantic Oscillation and the Atlantic Meridional Overturning Circulation. An example is shown in figure 38, which plots time series of the Tropical Pacific mean air-sea CO_2 flux, along with the multivariate ENSO index. Anomalies are seen corresponding to El Niño and La Niña events, related to changes in upwelling.

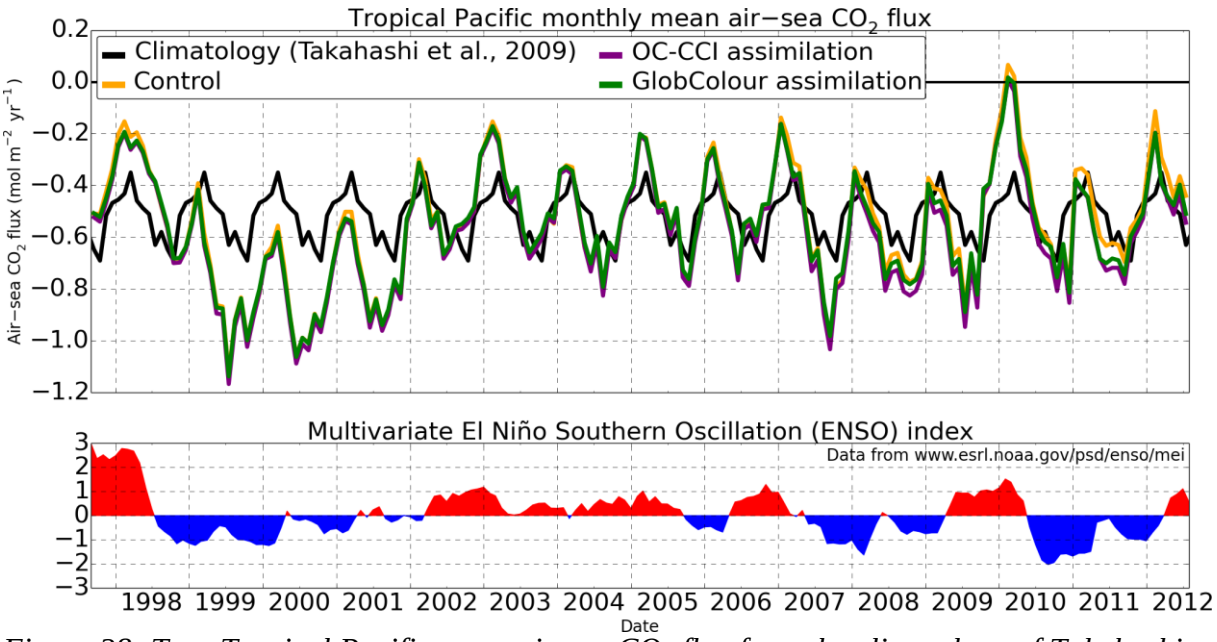

Figure 38: Top: Tropical Pacific mean air-sea CO_2 flux from the climatology of Takahashi et al. (2009) repeating in black, and each model run (coloured lines, as labeled). Bottom: multivariate ENSO index, as obtained from http://www.esrl.noaa.gov/psd/enso/mei.

4.8 Sea Ice

This section summarises the results from [WP3.6] Improved process understanding from Arctic and Antarctic cross ECV assessment.

4.8.1 SICCI sea ice concentration dataset (version 1.1, daily data, 1991-2008)

A comparison of SICCI and NSIDC sea ice concentration products shows that the Arctic sea ice area computed from SICCI data lies between NASA-Team (Cavalieri et al., 1984) and Bootstrap (Comiso, 1995) datasets from NSIDC. While NASA-Team data shows lower Arctic sea ice area than SICCI, the Arctic sea ice area derived from Bootstrap data is larger than for SICCI. The difference between NASA-Team and Bootstrap products lies in the selection of tie points for brightness temperatures representing "open water" and "fully ice-covered" grid boxes. From the different setting of tie points it follows that in the NASA-Team dataset, melt ponds appear as open water, while the missing sea-ice underneath melt ponds is compensated for in an ad-hoc manner in the Bootstrap product. From computed Arctic sea-ice areas we infer that the SICCI algorithm gives intermediate ice concentrations in the Arctic. This result also holds for simulated Arctic sea-ice area in assimilation experiments with the different ice concentration datasets.

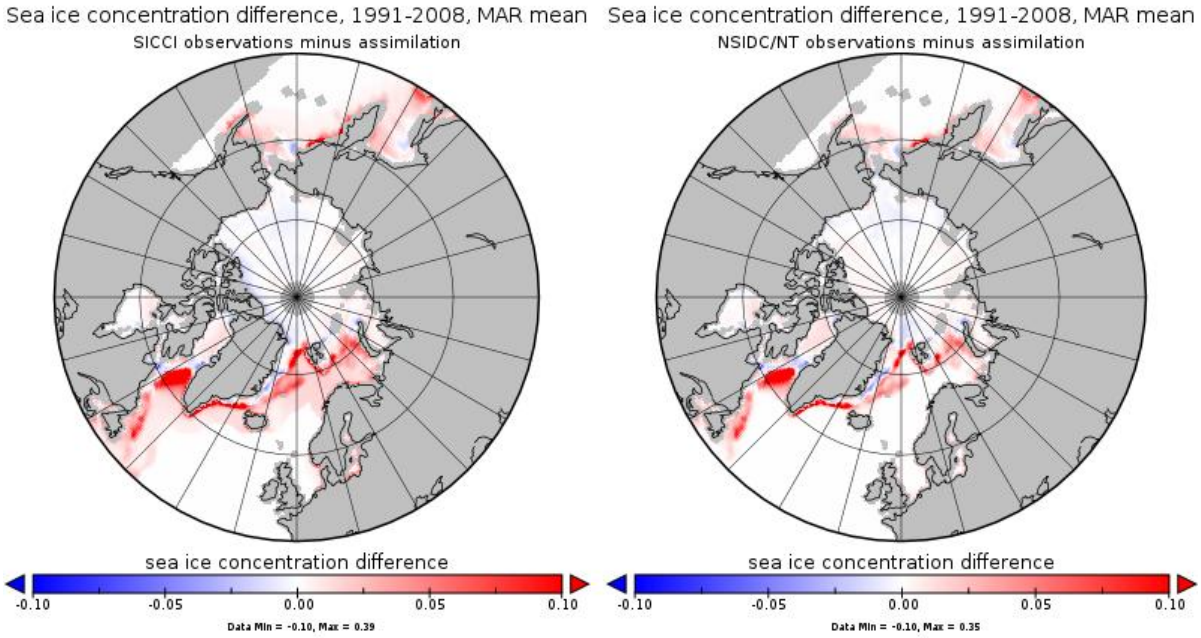

Figure 39: Sea ice concentration differences between observations and the associated assimilation runs are presented for SICCI (left) and NSIDC/NASA-Team (right) data products. March-mean values over the period 1991 to 2008 are shown.

The Antarctic sea ice area derived from both the SICCI ice concentration dataset and the assimilation run performed with SICCI ice concentrations shows that in the Antarctic the SICCI product resembles the NSIDC Bootstrap product, while the NASA-Team product shows about 10% less sea ice area.

A regional evaluation of the correspondence of the assimilated sea ice data product with the model physics indicates, however, a clear difference between SICCI and NSIDC data products. In many regions, especially in the Norwegian and Labrador Sea, low ice concentrations (< 3%) are obtained by the SICCI algorithm in grid boxes where observed sea surface temperatures as well as NSIDC ice concentration products indicate ice-free waters (see figure. 39). These spurious ice concentrations turn out to be due to the lack of a weather filter in the SICCI algorithm. In NSIDC ice concentration products these low ice concentrations, which originate from the contribution of clouds to brightness temperatures recorded by the satellite, are removed by a weather filter. However, since it is not feasible to objectively distinguish between the origins of possible brightness temperature sources, weather filters are likely to filter out also contributions of actual sea ice. Thus, although not using a weather filter introduces spurious ice concentrations in the open ocean, it provides a more objective view on the satellite data, since no actual ice concentrations are removed and it is left to the user to discard spurious low ice concentrations over open waters, if intended.

The regional investigation of the assimilation performance also showed that a notable amount of sea ice in the marginal ice zone melts directly after assimilation into the model. This turns out to be due to inconsistencies between assimilated sea ice concentration products and the ORA-S4 reanalysis product, which was used to nudge ocean temperatures (see figure 40). In the uppermost ocean layer extending from the sea surface to 12m depth, ORA-S4 reanalyses show temperatures of up to 5°C above freezing in several regions where both SICCI and NSIDC ice concentration products indicate ice concentrations above 5%. In a model grid box the temperature of the uppermost ocean layer needs to be at freezing point to allow even for small amounts of sea ice to exist. Thus, assimilated sea ice cannot persist if the heat content in a certain ocean model grid box plus the sum of heat contributions from the assimilated sea surface temperature and the assimilated sea ice adds up to an ocean surface temperature above freezing.

The regional inconsistencies between assimilated ocean temperature and sea ice concentration datasets originate most likely from the ORA-S4 ocean reanalysis product. The model system which was used to compile ORA-S4 did not contain a dynamical sea-ice model, and in the prescribed sea ice concentration dataset all ice concentrations below 20% were set to zero. This is likely to cause inconsistencies as found in the marginal ice zone (see figure 40), which we obtained for both SICCI and NSIDC assimilation runs in a similar pattern. Assimilating observational data for sea surface temperatures, such as the upcoming SST CCI dataset, might reduce the amount of sea ice melted directly after assimilation due to inconsistencies between sea ice and ocean temperature data.

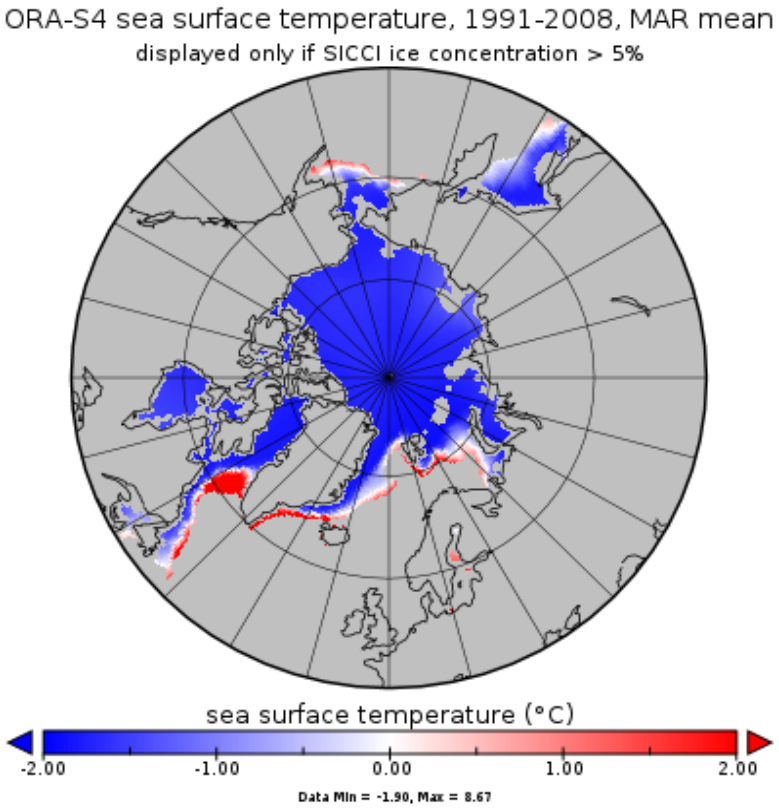

Figure 40: ORA-S4 ocean temperature in the uppermost ocean layer (surface to 12m depth) is shown. Values are displayed only in grid boxes where SICCI ice concentration is above 5%.

We consider the SICCI sea ice concentration data product as adequate for use in climate modelling, and of comparable quality as NSIDC data products. A major advantage of the SICCI product with respect to other datasets is its error characteristics. The different types of uncertainties provided with the dataset allow for more accurate studies, e.g., on the evaluation of model physics.

4.8.2 SICCI sea ice thickness dataset (version 0.9, Arctic-only, monthly data for October to March, 2003-2008)

A comparison of the SICCI ice thickness product with other data products derived from observational time series reveals a substantial positive bias in SICCI data. When besides sea ice concentration data also SICCI ice thickness data is assimilated into the model, the March-mean Arctic sea ice volume exceeds the ice volume derived from the assimilation run where only ice concentration is nudged by almost 100% (see figure 41). A side effect of assimilating high SICCI ice thicknesses into the model is that almost no assimilated sea ice in the marginal ice zone is lost directly after assimilation due to sea surface temperatures above freezing (see section on SICCI ice concentration data). The additional cooling of the system due to the positive bias in assimilated ice thicknesses prevents assimilated sea ice from being melted. However, we find the positive bias in the SICCI sea ice thickness dataset to be too large to allow for the data product to be of adequate quality for climate modelling studies. Error characteristics were not provided with the SICCI ice thickness data product.

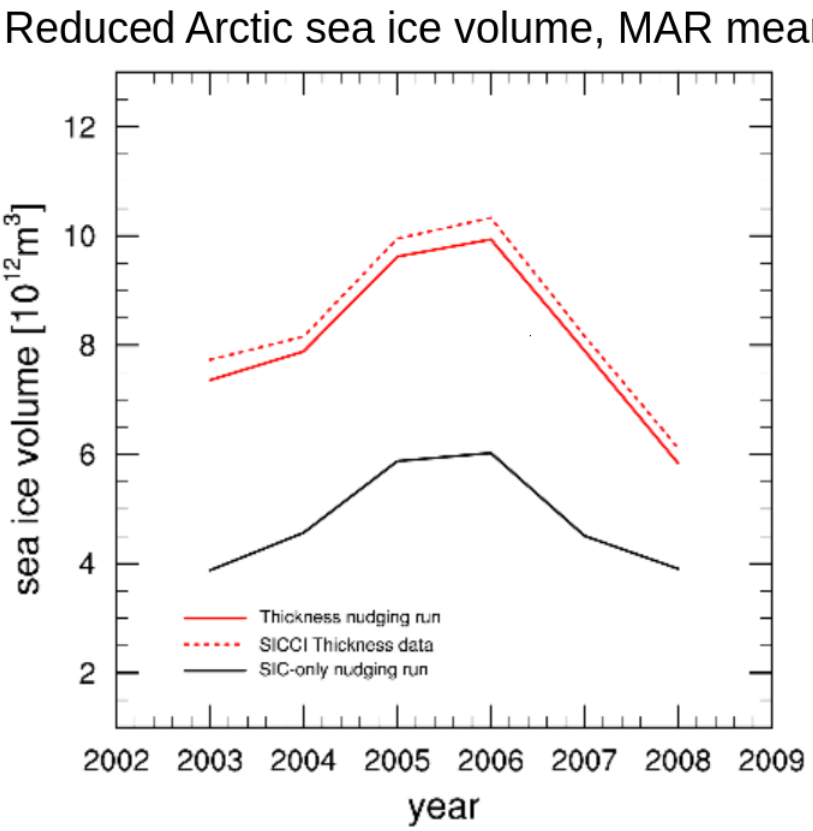

Figure 41: March-mean reduced Arctic sea ice volume over 2003-2008, as derived from SICCI ice thickness data (red dotted line), the combined SICCI ice thickness/concentration assimilation run (red solid line), as well as the SICCI ice concentration-only assimilation run (black line), is shown. The term "reduced" is introduced here, since only grid boxes, where the SICCI ice thickness dataset contains non-missing non-zero values, are considered.

4.9 Ice Sheets

No CMUG results are available for this report.

4.10 Soil Moisture

This section summarises the results from [WP3.4] Integrated assessment of CCI terrestrial ECVs impact in the MPI-ESM, and [WP3.8] Cross assessments of clouds, water vapour, radiation, soil moisture for regional climate models.

[WP3.4] Integrated assessment of CCI terrestrial ECVs impact in the MPI-ESM

Contrasting the burned area with soil moisture reported from CCI_SM (figure 42), we find a distinct relationship between burned area and soil moisture with low burned area for low soil moistures (fuel limitation) and low burned areas for high soil moistures (moisture limitations).

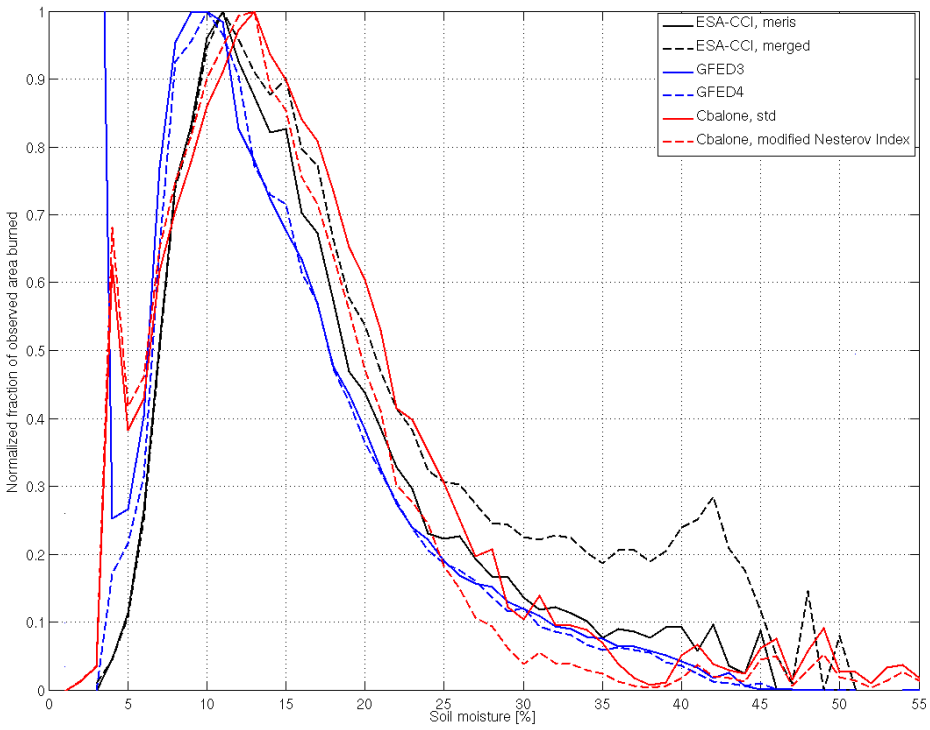

Figure 42: ESA CCI Soil Moisture against fraction of observed burned area with the peak normalized to one. Burned area data is taken from the CCI Fire MERIS and MERGED product, as well as from GFEDv3/v4. Simulated data is shown for JSBACH-SPITFIRE in its standard version (Cbalone, std) and in the modified version JSBACH-SPITFIRE (Cbalone, modified Nesterov Index).

The comparison shows that all products have a very similar distribution with the exception of the CCI MERGED product, for which substantial burned areas are reported in regions with soil moistures exceeding 25%. The CCI-MERIS product peaks at a higher soil moisture compared to GFED products and the distribution is wider. Both versions of JSBACH-SPITFIRE peak at a too high soil moisture and the distribution is too wide. In a first step we identified two parameters (conversion soil moisture to fuel moisture and ignition rate) in SPITFIRE-JSBACH that are not well constrained by observations, which we systematically

varied over a reasonable parameter space to optimize width and peak position of the soil moisture / burned area relationship. JSBACH-SPITFIRE was optimized to run a large number of experiments with varying parameter settings in a reasonable amount of time. Figure 43 shows the deviations in peak position and distribution width for 70 experiments with CCI-MERIS as reference.

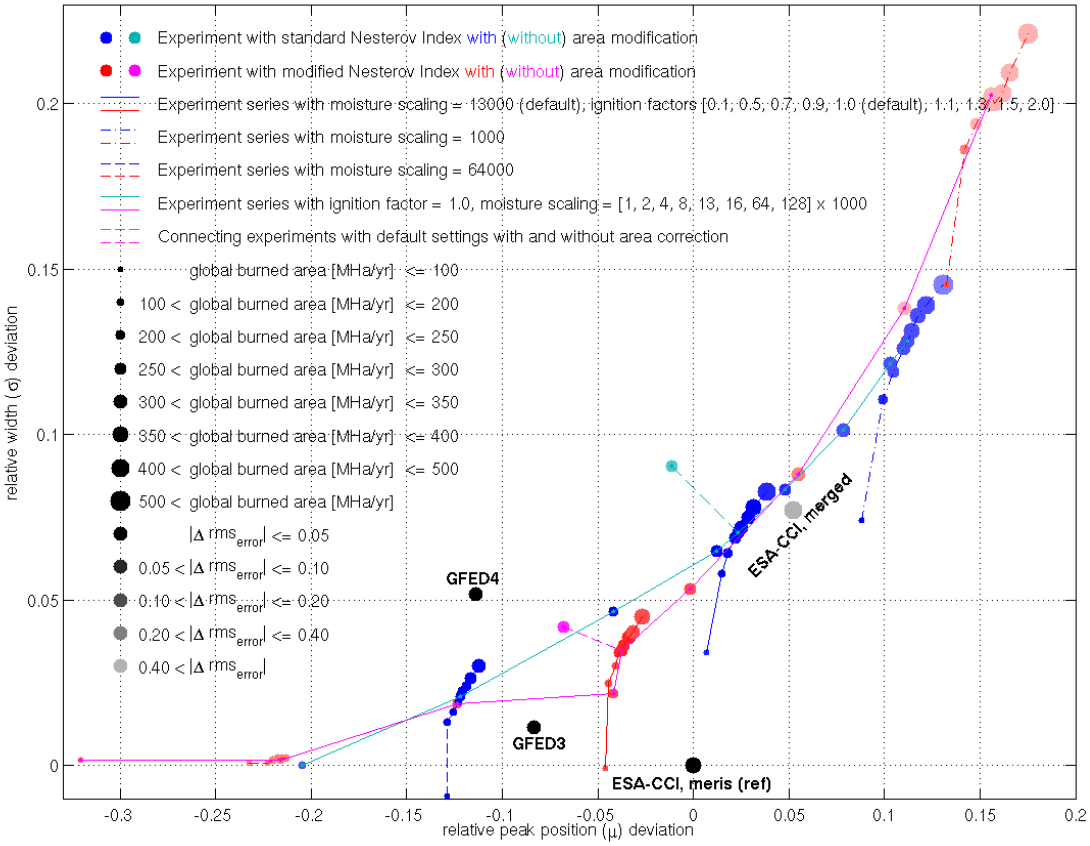

Figure 43: Relative difference in peak position and width of the burned area – soil moisture relationship for 70 experiments performed with JSBACH-SPITFIREv1/v2 compared to GFEDv3/v4, CCI MERGED and CCI MERIS (reference).

Overall, the analysis revealed that lower fuel moisture improves the peak position, while lower ignition rates improve the width of the distribution. The improvements are however small, i.e. default values perform already reasonable well. Other less well-constrained parameters in the fire model are being tested for their significance in the burned area - soil moisture relationship, for which the analysis will be separated into different land cover types.

[WP3.8] Cross assessments of clouds, water vapour, radiation, soil moisture for regional climate models.

The initial work of this WP explains how we validate surface soil moisture simulated by two Regional Climate Models (RCMs) utilizing the ESA CCI soil moisture remote sensing product, from now on referred to as ESA (Liu et al., 2012, 2011; Wagner et al., 2012). Simulations were performed using two different RCM systems, the Rossby Centre Regional Climate model (RCA4) and a climate version of the meso-scale modelling system HARMONIE (HCLIM).

Climate Models
RCA4 is the model version used for the CORDEX (Coordinated Regional Climate Down-scaling Experiment) downscaling with RCA (Strandberg et al., 2014). The land-surface scheme of RCA (Samuelsson et al., 2014) divides the soil into three layers with respect to soil moisture and divides a grid box into two surface tiles, forest and open land, depending on land-use information. In this WP the top layer soil moisture was validated, represented by the upper 7.2 cm of the soil, of the open-land tile.

HARMONIE represents a suite of physical parameterization packages that are developed to be applicable to different resolutions. For this study we use results from a simulation based on the ALARO package (Lindstedt et al., 2015). The land-surface scheme of HARMONIE, SURFEX (Masson et al., 2013), also represents a suite of physical parameterization packages. For this study the force-restore soil option is used which divides the soil into three layers with respect to soil moisture. Also, the land is treated as one single tile with no sub-division with respect to different land use. In this report we validate the top soil moisture, represented by the upper 1 cm of the soil.

Experimental setup
For RCA we used the CORDEX domain over Africa at 50 km horizontal resolution (see figure 44). The simulation covers 1990 to 1994 with one year of spin-up time prior to this. The analysis for this study covers the period 1990-1994. For HCLIM we used a European domain with 16 km horizontal resolution (Lindstedt et al., 2015) (see figure 45). The simulation covers the period 1998 to 2007 with four months of spin-up time prior to this. The analysis for this study covers the period 2003-2007. Both simulations use ERA-Interim (ERA-I (Dee et al., 2011)) at the lateral boundaries and for sea surface temperature (SST) every six hours.

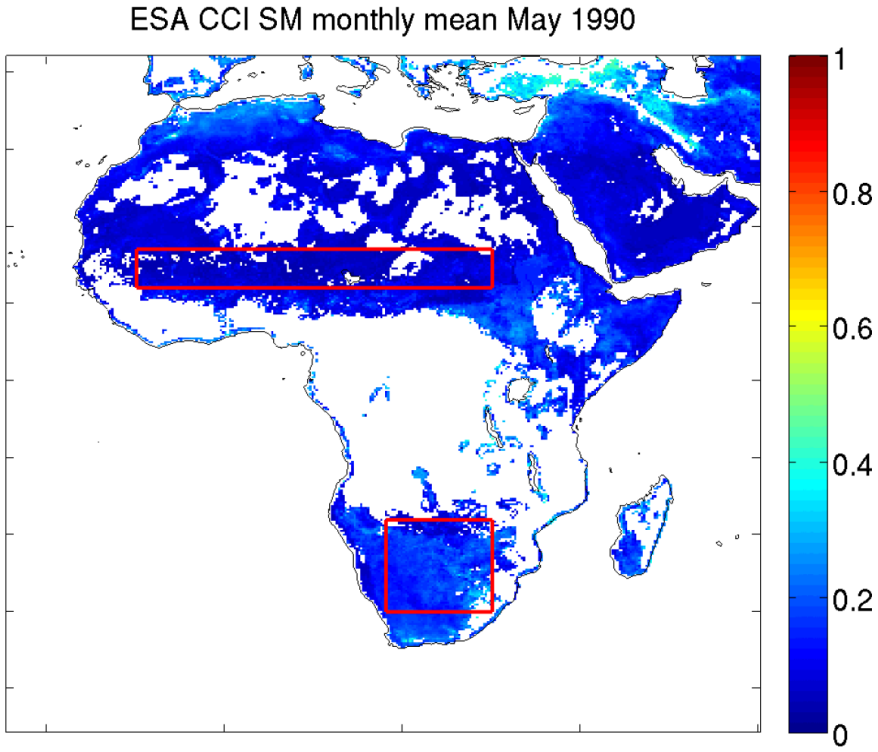

Figure 44: An example showing the ESA monthly mean soil moisture (m^3 m^{-3}) for the month of May 1990 over Africa.

The 2D (longitude/latitude) daily values of RCM soil moisture are interpolated to the ESA grid. A daily mask represented by the grid boxes in ESA which have valid SSM values is applied to the corresponding RCM SSM of the interpolated 2D fields. Thus, we create daily RCM SSM fields which have the same patterns of valid values as the ESA product. From these daily values we create monthly mean values for RCM and ESA SSM, respectively. An analysis of area averaged SSM is applied to three different regions, Sahel and Southern Africa, for the Africa domain and the Mediterranean for the Europe domain. Finally anomalies of SSM values are presented by simply removing the five year mean value from each area averaged time series.

To illustrate the effect of the daily mask, the results based on non-masked RCA SSM are presented for the Africa regions. To illustrate how the total column soil moisture in RCA relates to the SSM the total, soil moisture is included in the Africa results.

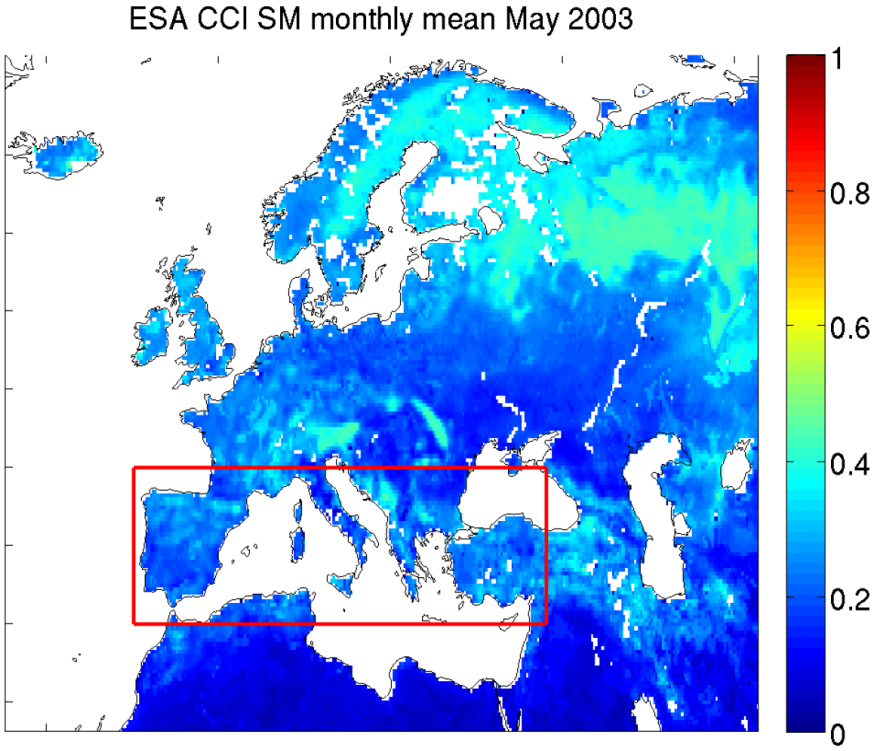

Figure 45: An example showing the ESA monthly mean soil moisture (m^3 m^{-3}) for the month of May 2003 over Europe.

For the Sahel region the RCA absolute SMM is close to the upper uncertainty limit of the ESA SSM, defined as plus one standard deviation above the ESA SSM (figure 46). This may indicate a wet bias in the RCA SSM. Assuming that SSM anomaly can still be analysed we see that the ESA SSM shows higher peak values than RCA SSM. The reason may be that RCA SSM represents a more thick soil layer than ESA but it may also be caused by less precipitation in RCA and/or more evapotranspiration in RCA during the rainy period. The RCA SSM climbs earlier and reaches a plateau at the beginning of each rainy season. The faster climbing is a known feature of RCA and is caused by a too quickly northward propagation of the West-African Monsoon system in RCA. Further analysis also including one or more observational precipitation products is needed to gain more understating of the model behaviour.

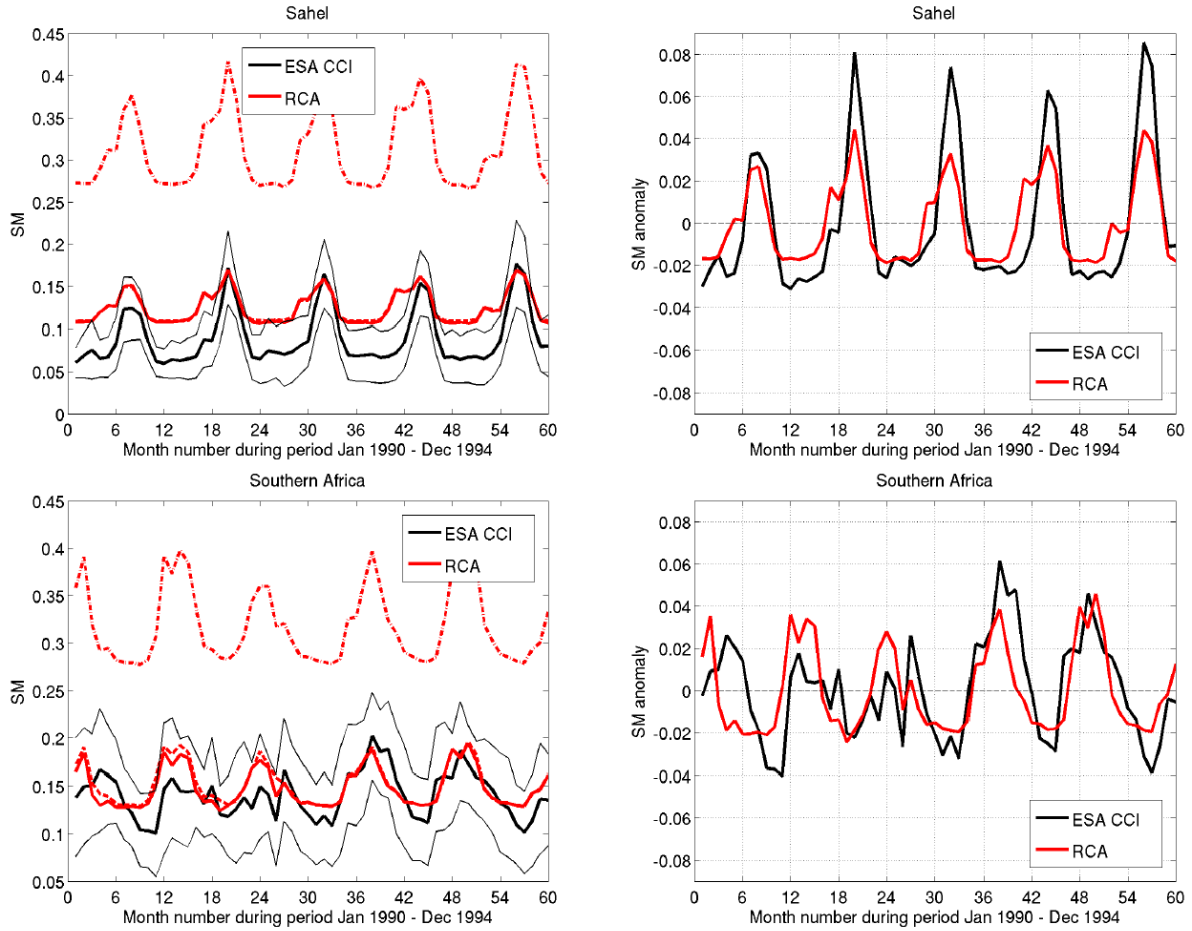

Figure 46: Top row shows results for Sahel and bottom row for Southern Africa regions respectively. Left column shows absolute soil moisture (m^3 m^{-3}) and right column soil moisture anomaly (m^3 m^{-3}). Red lines show RCA SSM results and black lines ESA SSM results. For the absolute soil moisture results three additional line types are shown; black thin lines show the soil moisture uncertainty (one standard deviation) for ESA, red dashed line shows RCA SSM for all grid points (i.e. no masking applied), and red dash-dotted line shows RCA total column soil moisture (m^3 m^{-3}).

For the Southern Africa region the absolute RCA SSM is closer to the corresponding ESASSM (figure 46). In the beginning of the period, looking at anomaly values, the model and the observations seem to be out of phase. Considering that one year of spin-up is applied prior to the analysing period, a delay in RCA soil moisture time evolution does not seem to be a reasonable explanation for this. Again an analysis including precipitation observations are needed to further understand the relationships between modelled and observed SSM. Although correct, figure 46 shows that the masking procedure described in Section 3 does not have a large impact compared to the case if masking had been omitted, i.e. the solid and dashed red lines in left column of figure 46 are similar. Figure 46 also confirms that one cannot use ESA SSM to validate modelled total column soil moisture.

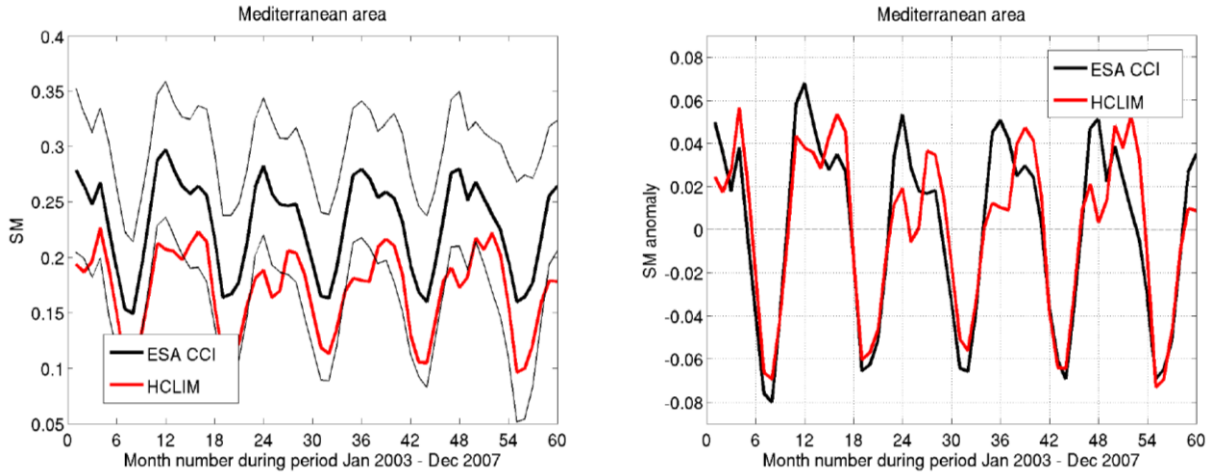

Figure 47: Results for the Mediterranean region. Left figure shows absolute soil moisture (m^3 m^{-3}) and right figure soil moisture anomaly (m^3 m^{-3}). Red lines show RCA SSM results and black lines ESA SSM results. Black thin lines in left figure show the soil moisture uncertainty (one standard deviation) for ESA.

The high resolution non-hydrostatic model HCLIM has been run over Europe where we have started to assess CCI soil moisture and clouds. According to figure 47 the HCLIM absolute SSM is close to the lower uncertainty limit of the ESA SSM. This may indicate a general dry bias in HCLIM. Again as for RCA, assuming that the SSM anomaly can still be analysed we see that modelled and observed SSM variability show in general good correspondence. For HCLIM the SSM represents a shallower layer than for RCA so this may be one reason for a larger amplitude in simulated SSM over the Mediterranean compared with the Sahel. However, the ESA SSM shows a peak value each December while the simulated SSM peaks later during the spring. An analysis of precipitation is recommended to explain this.

The Frequently Asked Questions on the SM website (http://www.esa-soilmoisture-cci.org/node/136) very useful. We recommend a FAQ page for all CCI ECVs, and any bugs can be listed under known issues/errors. The following points should be added to the SM FAQ to avoid misuse under 'Do', 'Don't' or 'Data usage in models'.

- Do not compare (or take care when comparing) your model total SM directly with these products, the satellite observes the top ~2cm. (figure 46).
- Any model data should be masked ("simplistic simulator approach") when compared to the observations. This is indirectly implied in the spatial and temporal availability SM FAQ's. It was less important in this study (figure 46) but for other regions and time periods the differences can be much larger. Any user comparing with model data should strongly be recommended to do mask the model data.
- It would be useful to have a presentation similar to that presented at the CMUG 5th integration meeting available at the FAQ link or somewhere else at the website.

General thoughts on satellite and model soil moisture comparisons

The ESA SSM usually represents a very shallow layer corresponding to the top two centimetres of the soil, but the observed depth depends on the soil moisture content (deeper for drier soils). It is not easy to characterize this top layer but in many regions it is some

combination of active or dormant vegetation mixed by some dead vegetation material mixed with mineral soil. In the model, depending on the exact parameterization applied, the top SSM layer may be purely mineral soil or some weighted value between mineral soil, soil carbon and vegetation material.

As stated on ESA Web page "the statistical comparison metrics like root-mean-square-difference and bias based on our combined dataset are scientifically not meaningful. However, the CCI SM products can be used as a reference for computing correlation statistics or the unbiased root-mean-square-difference". This would support the anomaly analysis of SSM in this report although the absolute simulated SSM values are sometimes at the uncertainty limit of the ESA SSM.

The most important soil moisture in models is represented by the layer occupied by roots since this is the soil moisture limiting the transpiration. Methods do exist which can be used to integrate ESA SSM in time to reach a soil moisture representing a thicker layer but assumptions, sometimes difficult to control, are needed for such methods. ESA SSM can be nudged or assimilated in a land-surface model to compile a deep soil moisture product but such a product will always be model dependent and must be used carefully when compared to other models. A soil moisture product representing the degree of saturation rather than volumetric soil moisture would limit, or even exclude, any model dependence. We argue that such a product is preferable. The SM team at the CMUG 5th integration meeting informed that such products are planned to be made, we support that work.

4.11 Fire & Burned Area

This section summarises the results from [WP3.4] Integrated assessment of CCI terrestrial ECVs impact in the MPI-ESM.

Contrasting the burned area with soil moisture reported from CCI_SM (figure 47), we found a distinct relationship between burned area and soil moisture with low burned area for low soil moistures (fuel limitation) and low burned areas for high soil moistures (moisture limitation).

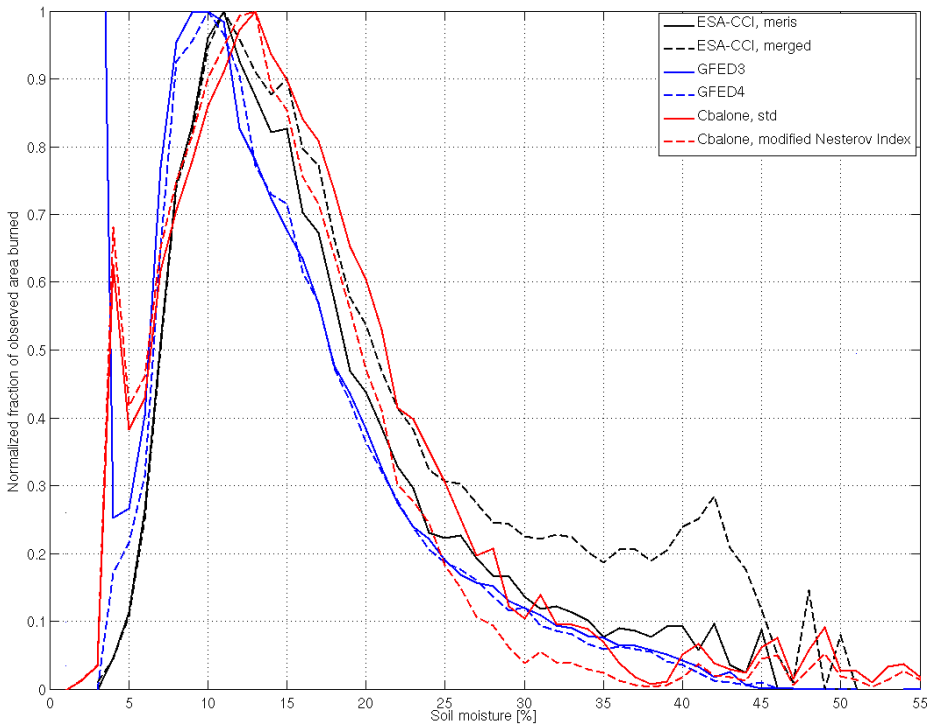

Figure 48: ESA CCI Soil Moisture against fraction of observed burned area with the peak normalized to one. Burned area data is taken from the CCI Fire MERIS and MERGED product, as well as from GFEDv3/v4. Simulated data is shown for JSBACH-SPITFIRE in its standard version (Cbalone, std) and in the modified version JSBACH-SPITFIRE (Cbalone, modified Nesterov Index).

The comparison shows that all products have a very similar distribution with the exception of the CCI MERGED product, for which substantial burned areas are reported in regions with soil moistures exceeding 25%. The CCI-MERIS product peaks at a higher soil moisture compared to GFED products and the distribution is wider. Both versions of JSBACH-SPITFIRE overestimate maximum soil moisture and the width of its distribution.

In a first step we identified two parameters (conversion soil moisture to fuel moisture and ignition rate) in SPITFIRE-JSBACH that are not well constrained by observations, which we systematically varied over a reasonable parameter space to optimize width and peak position of the soil moisture / burned area relationship. JSBACH-SPITFIRE was optimized to run a

large number of experiments with varying parameter settings in a reasonable amount of time. figure 49 shows the deviations in peak position and distribution width for 70 experiments with CCI-MERIS as reference.

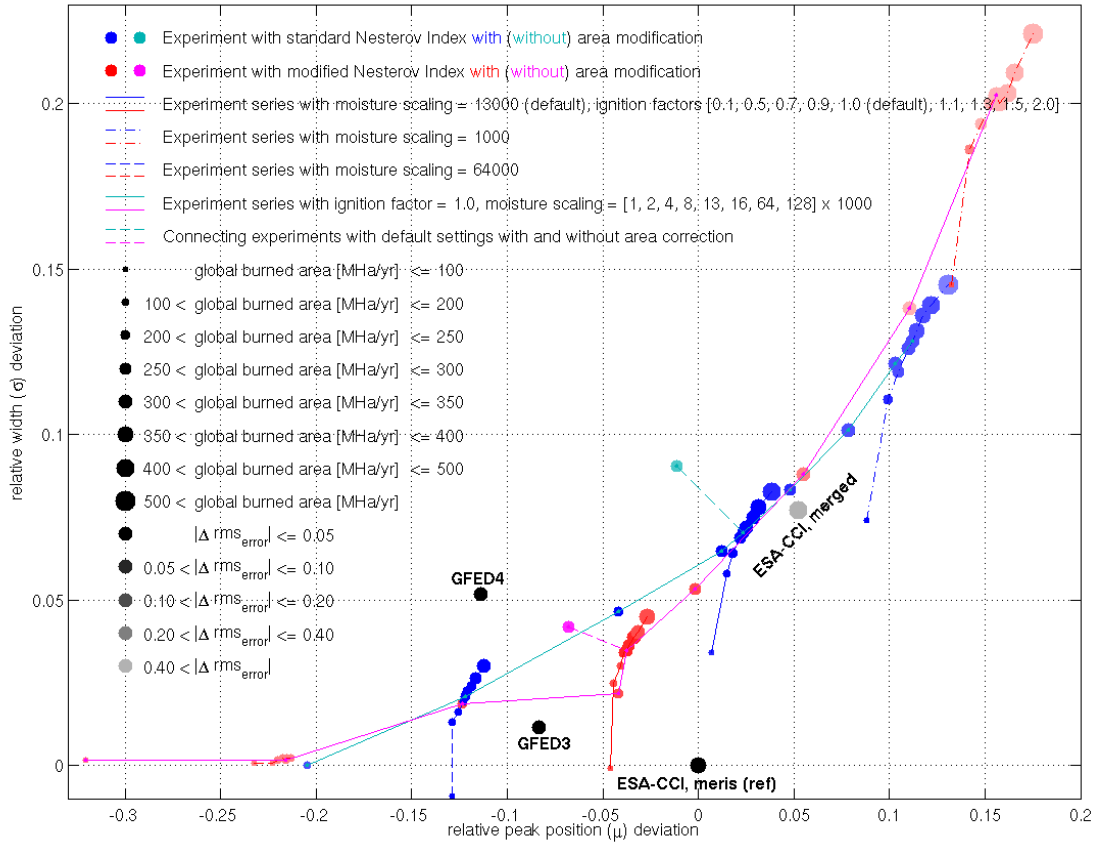

Figure 49: Relative difference in peak position and width of the burned area – soil moisture relationship for 70 experiments performed with JSBACH-SPITFIREv1/v2 compared to GFEDv3/v4, CCI MERGED and CCI MERIS (reference).

The analysis shows that lower fuel moisture improves the peak position, while lower ignition rates improve the width of the distribution. The improvements are however small, i.e. default values perform already reasonable well. Other less well-constrained parameters in the fire model are currently being tested for their relevance in the burned area - soil moisture relationship, for which the analysis will be separated into different land cover types.

In WP3.4 only the gridded FIRE_CCI products were used. The FIRE_CCI gridded products from phase 1 were only available for a 3 year period (2006-2008), which limits their applicability for climate studies. To test the functional relationships, such as that between burned area and soil moisture, global coverage was available reducing the dependency on having a long times series. A further assessment for fire model development will require categorization by land cover type to optimize land cover dependent parameters, which will benefit from a longer time series. A first assessment showed that the CCI-MERGED product

reports unrealistic high burned fraction for regions with soil moistures exceeding 25%. We therefore chose the CCI-MERIS product as reference. The CCI-MERIS product shows a very similar soil moisture dependency distribution compared with the MODIS based GFEDv3/GFEDv4 product which was applied in previous studies. These findings agree with the analysis of the FIRE CCI team reported in the Product Validation Report II as well as the Climate Assessment Report. Due to the limited time period covered by the global product we did not assess the temporal stability of the product.

4.12 Glacier

This section summarises the results from [WP3.9] Assessment of ESA CCI glacier, land cover and sea level data for hydrological modelling of the Arctic Ocean drainage basin.

- CCI Glacier data (Randolph Glacier Inventory, RGI v4.0) was found to be very useful for evaluating and improving the setup of the glacier sub-model in the Arctic-HYPE model:
  - RGIv4 glacier outlines was used for calculating total glacier area within the sub-basins of the hydrological model, and compared to glacier area estimated from CCI Land Cover and the pre-cursor data set ESA GlobCover 2004-2006.
  - RGIv4 glacier outlines could be further used for improving sub-basin delineation following the glacier outlines.
  - RGIv4 includes additional information that will be further used to improve the glacier sub-model: mean, maximum and minimum elevation, slope and length.
- Glacier area estimated from the class "permanent snow and ice" from CCI Land cover and Glob cover was found to largely overestimate the glacier area derived from CCI Glacier data (figure 50; table 4).

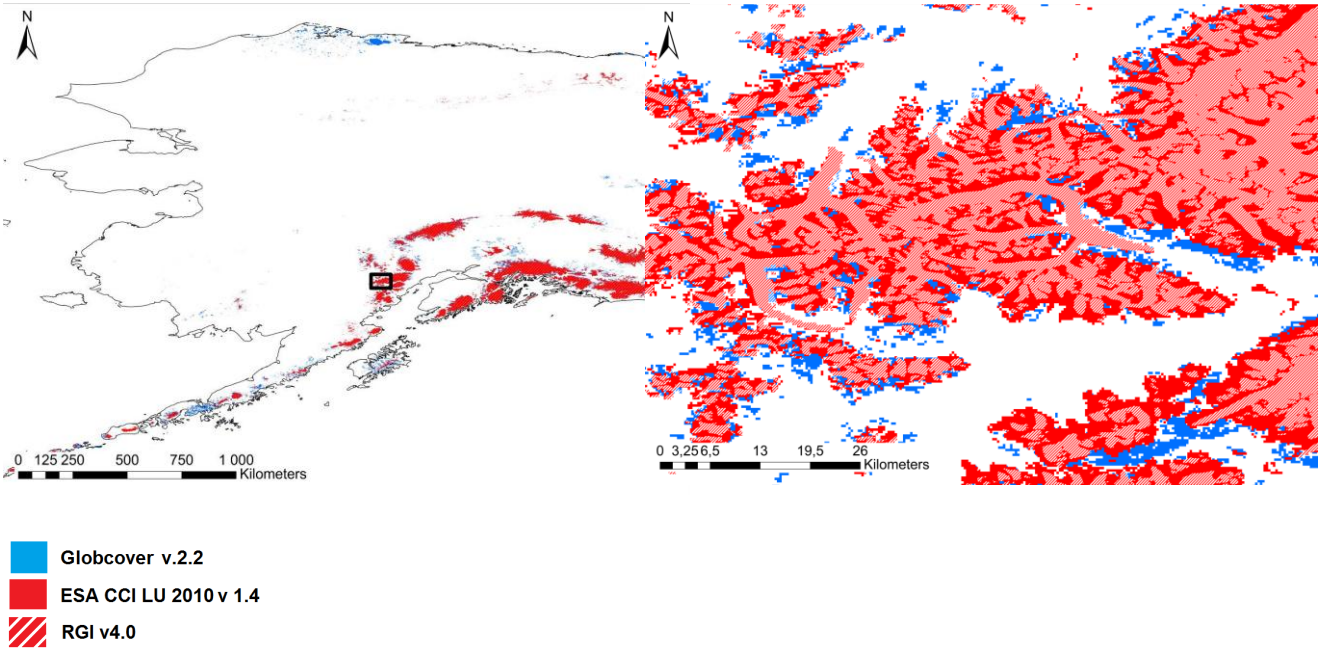

Figure 50: Comparison of glacier area in Alaska derived from CCI land cover and ESA GlobCover 2004-2006 (permanent snow and ice) and the glacier outlines from CCI Glacier (RGIv4).

RGI region	RGI glacier area (km2)	RGI glacier area (fraction of total model area)	Glacier area based on CCI Land cover (fraction of RGI area)	Glacier area based on GlobCover (fraction of RGI area)
01 Alaska	1232	0.007	1.359	1.569
02 Western Canada/US	315	0.001	**3.152**	**17.114**
03 Arctic Canada North	104074	0.291	**1.272**	**2.4**
04 Arctic Canada South	41303	0.036	**1.607**	**2.647**
06 Iceland	11060	0.109	**1.009**	**2.079**
07 Svalbard	32342	0.542	1.185	1.65
08 Scandinavia	1805	0.006	1.56	1.311
09 Russian Arctic	50756	0.346	**1.198**	**2.286**
10 North Asia	759	0	**2.039**	**8.599**
Total	243646	0.014	1.315	2.424

Table 4: Glacier area in the Arctic-HYPE model per RGI region, comparing data from CCI glacier (RGIv4) and estimations based on the land cover class "permanent snow and ice" from CCI land cover and GlobCover 2004-2006.

Quality relevant outcomes:

- Disagreement between CCI Glacier and CCI Land cover:
  - The CCI Land cover class "permanent snow and ice" is larger than the glacier area derived from the glacier outlines in CCI Glacier - in some regions the more than 30% too large (figure 50; table 4).
  - The CCI Land cover documentation reveals that the CCI Glacier outlines have been used to assign "permanent snow and ice" to all land cover pixels within the outlines – however, areas outside of the CCI Glacier outlines classified as "permanent snow and ice" have not been reset to "unclassified" or any other land cover class.
  - Discussions with Science Leaders from CCI Glacier and Land cover confirmed this situation, and it was suggested to include a sub-class under "permanent snow and ice" separating pixels under ice and other snow pixels.
- No ice thickness in CCI Glacier data (RGIv4):
  - Glacier thickness is not included in RGIv4 even though estimates of each glacier exist based on modelling and observations (Farinotti & Huss, 2012).
  - The model estimates can be requested from the CCI Glacier team on request. However this information is not clear in the CCI Glacier documentation.
- No temporal information in CCI Glacier (RGIv4):
  - The information in RGIv4 is only a snapshot in time representing the most recent available data. Information needed for initialization, calibration and evaluation of glacier models for long-term hydrological or climate model simulations are missing. Such information has to be compiled by the user from other sources, for instance from the other activities linked to CCI Glacier.

4.13 Land Cover

This section summarises the results from [WP3.9] Assessment of ESA CCI glacier, land cover and sea level data for hydrological modelling of the Arctic ocean drainage basin.

CCI land cover was compared to the precursor data GlobCover 2004-2006 with regard to differences in land cover distribution. The "climate quality" of the information in the land cover time series (2000, 2005, 2010) was of special interest, since the on-going changes in the Arctic regions (mainly climate related) are expected to be expressed for instance in the distribution of vegetation, surface water, and snow and ice.

Preliminary results to date:

- More surface water in CCI Land cover compared to the pre-cursor GlobCover 2004-2006):
    - CCI Land cover was found to include more surface water (about 6-20% more), which might be important for understanding Arctic hydrology (figure 51) dominated by large rivers and a large number of small and large lakes. Impact in the model still to be analyzed.

- The fraction of deciduous needle leaf trees (larches) was reduced in the latest epoch (2008-2012) compared to previous periods in eastern Siberia.
    - Field observations suggest that this might be due to increasing precipitation during the period.
    - This affects the "climate quality" of the time-series land cover data.
    - Analysis of relation to observed and simulated river discharge still to be analyzed.

- The class "water bodies" is constant throughout the three epochs and water bodies are not included in the seasonal products.
    - From a "climate quality" perspective, it would be interesting to get information on the trends and seasonal variation in the spatial distribution of surface water. Variation in small water bodies is a relevant ECV related to permafrost melting, which is of highest interest in the Arctic region.

- The difference between the CCI glacier area and the area with "permanent snow and ice" is much improved in the CCI land cover data compared to the GlobCover data, which apparently is based on data from only one complete melting period. However, CCI land cover data for "permanent snow and ice" still overestimates glacier area with up to more than 30%, as discussed above.

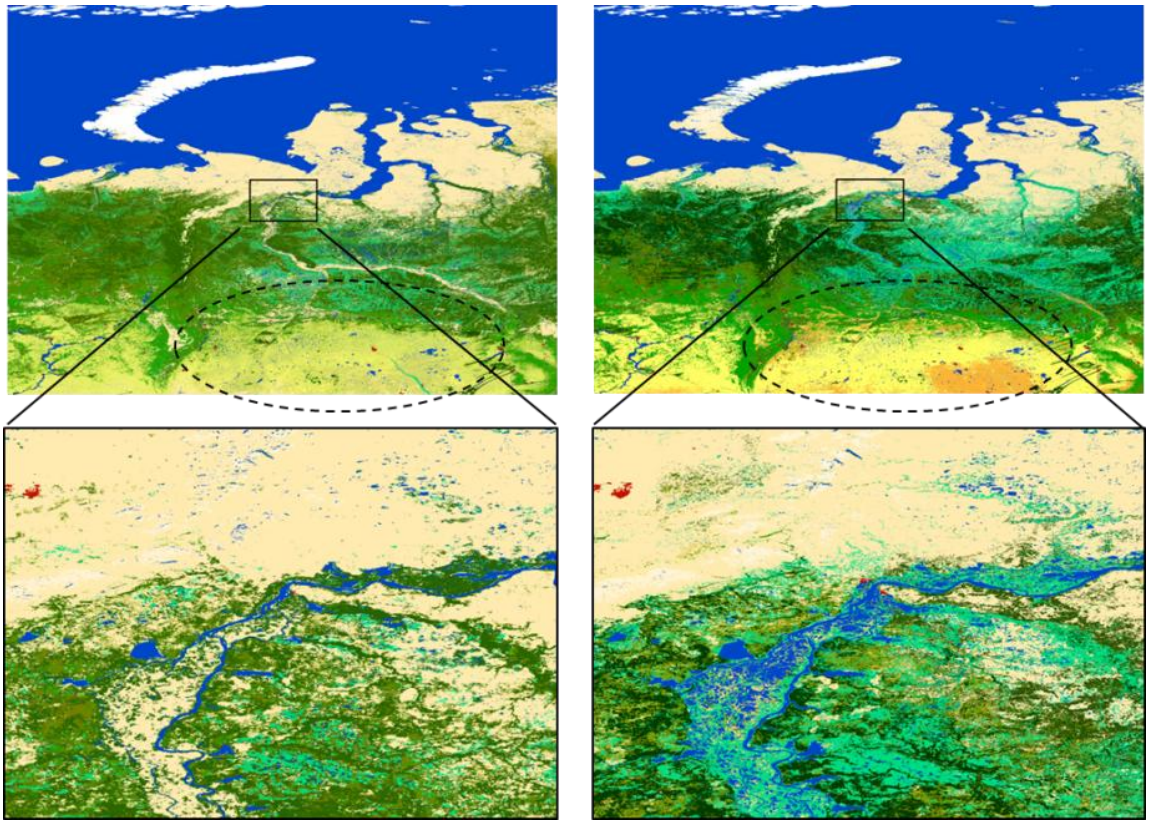

Figure 51: Land cover data from the area around the Ob River showing a clear increase in surface water area from Left: GlobCover to Right: CCI land cover.

Quality relevant outcomes

- Disagreement between CCI Glacier and CCI Land cover:
  - The CCI Land cover class "permanent snow and ice" is larger than the glacier area derived from the glacier outlines in CCI Glacier - in some regions the more than 30% too large (figure 50; table 4).
  - The CCI Land cover documentation reveals that the CCI Glacier outlines have been used to assign "permanent snow and ice" to all land cover pixels within the outlines – however, areas outside of the CCI Glacier outlines classified as "permanent snow and ice" have not been reset to "unclassified" or any other land cover class.
  - Discussions with Science Leaders from CCI Glacier and Land cover confirmed this situation, and it was suggested to include a sub-class under "permanent snow and ice" separating pixels under ice and other snow pixels.

5. References

Auligné T, McNally AP, Dee D. 2007. Adaptive bias correction for satellite data in a numerical weather prediction system. *Q. J. R. Meteorol. Soc.* **133**: 631–642.

Bakker, D. C. E., Pfeil, B., Smith, K., Hankin, S., Olsen, A., Alin, S. R., Cosca, C., Harasawa, S., Kozyr, A., Nojiri, Y., O'Brien, K. M., Schuster, U., Telszewski, M., Tilbrook, B., Wada, C., Akl, J., Barbero, L., Bates, N. R., Boutin, J., Bozec, Y., Cai, W.-J., Castle, R. D., Chavez, F. P., Chen, L., Chierici, M., Currie, K., De Baar, H. J. W., Evans, W., Feely, R. A., Fransson, A., Gao, Z., Hales, B., Hardman-Mountford, N. J., Hoppema, M., Huang, W.-J., Hunt, C. W., Huss, B., Ichikawa, T., Johannessen, T., Jones, E. M., Jones, S., Jutterstrøm, S., Kitidis, V., Körtzinger, A., Landschützer, P., Lauvset, S. K., Lefèvre, N., Manke, A. B., Mathis, J. T., Merlivat, L., Metzl, N., Murata, A., Newberger, T., Omar, A. M., Ono, T., Park, G.-H., Paterson, K., Pierrot, D., Ríos, A. F., Sabine, C. L., Saito, S., Salisbury, J., Sarma, V. V. S. S., Schlitzer, R., Sieger, R., Skjelvan, I., Steinhoff, T., Sullivan, K. F., Sun, H., Sutton, A. J., Suzuki, T., Sweeney, C., Takahashi, T., Tjiputra, J., Tsurushima, N., Van Heuven, S. M. A. C., Vandemark, D., Vlahos, P., Wallace, D. W. R., Wanninkhof, R. and Watson, A. J. 2014. An update to the Surface Ocean CO2 Atlas (SOCAT version 2). Earth Syst. Sci. Data, 6: 69-90.

Balmaseda, M. A., K. Mogensen, and A. T. Weaver, 2013: Evaluation of the ECMWF ocean reanalysis system ORA-S4. Quarterly Journal of the Royal Meteorological Society, 139 (674) 1132–1161.

Balmaseda, M. A., K. Mogensena, and A. T.Weaver, 2013: Evaluation of the ECMWF ocean reanalysis system ORAS4, Q. J. R. Meteorol. Soc., 139, 1132–1161.

Bhartia, P.K., OMI Algorithm Theoretical Basis Document, Volume II, Version 2.0, August 2002, OMI Ozone Products, NASA, available from http://eospso.gsfc.nasa.gov/sites/default/files/atbd/ATBD-OMI-02.pdf

Bormann, N., A. Collard, and P. Bauer, 2010: Estimates of spatial and inter-channel observation error characteristics for current sounder radiances for NWP, part II: Application to AIRS and IASI. *Q. J. R. Meteorol. Soc.*, **136**, 1051-1063.

Bormann, N., M. Bonavita, R. Dragani, R. Eresmaa, M. Matricardi, and T. McNally, 2015: Enhancing the impact of IASI observations through an updated observation error covariance matrix. ECMWF Technical Memorandum, in preparation.

Carli B, Carlotti M, Ceccherini S, Ho¨pfner M, Raspollini P, Ridolfi M, Santurri L. 2011. MIPASATBD, IFAC_GA_2007_12_SC. Technical report, ESA.

Cavalieri, D. J., P. Gloersen, and W. J. Campbell, 1984: Determination of sea ice parameters with the NIMBUS 7 SMMR. Journal of Geophysical Research: Atmospheres (1984–2012) 89 (D4), 5355–5369.

Comiso, J. C., 1995: SSM/I sea ice concentrations using the Bootstrap algorithm, Vol. 1380. National Aeronautics and Space Administration, Goddard Space Flight Center.

Dee, DP. 2005. Bias and data assimilation. *Q. J. R. Meteorol. Soc.* **131**: 3323–3343.

Dee, D., et al., 2011: The ERA-Interim reanalysis: Configuration and performance of the data assimilation system. Quarterly Journal of the Royal Meteorological Society, 137 (656), 553–597.

Desroziers, G., Berre, L., Chapnik, B. and Poli, P. (2005), Diagnosis of observation, background and analysis-error statistics in observation space. *Q.J.R. Meteorol. Soc*., **131**: 3385–3396. doi: 10.1256/qj.05.108.

Dethof A, Hólm E. 2004. Ozone assimilation in the ERA-40 reanalysis project. *Q. J. R. Meteorol. Soc*. **130**: 2851–2872.

Dragani R. 2009. Variational bias correction of satellite ozone data. Technical report R43.8/RD/0934. Technical report, ECMWF. Available from R. Dragani (rossana.dragani@ecmwf.int).

Dragani R. 2013. Validation of the reprocessed MIPAS and SCIAMACHY retrievals using ERA-Interim, and one-year assimilation of MIPAS ozone profiles at ECMWF. Final report for ESA contract 21519/08/I-OL CCN No 1: Technical support for global validation of ENVISAT data products. Technical report, ECMWF.

Dragani, R. and McNally, A. P. (2013), Operational assimilation of ozone-sensitive infrared radiances at ECMWF. *Q.J.R. Meteorol. Soc*., **139**: 2068–2080. doi: 10.1002/qj.2106.

ESA Web page - ESA soil moisture CCI Frequently Asked Questions. http://www.esa-soilmoisture-cci.org/node/136.

Eskes, H. J., R. J. van der A, E. J. Brinksma, J. P. Veefkind, J. F. de Haan, and P. J. M. Valks, Retrieval and validation of ozone columns derived from measurements of SCIAMACHY on Envisat, *Atmos. Chem. Phys. Discuss*, **5**, 4429-4475, 2005.

Ford, D. A., Edwards, K. P., Lea, D., Barciela, R. M., Martin, M. J., and Demaria, J. 2012. Assimilating GlobColour ocean colour data into a pre-operational physical-biogeochemical model, Ocean Sci., 8: 751-771.

Froidevaux L, Jiang YB, Lambert A, Livesey NJ, Read WG, Waters JW, Browell EV, Hair JW, Avery MA, McGee TJ, Twigg LW, Sumnicht GK, Jucks KW, Margitan JJ, Sen B, Stachnik RA, Toon GC, Bernath PF, Boone CD, Walker KA, Filipiak MJ, Harwood RS, Fuller RA, Manney GL, Schwartz MJ, Daffer WH, and1 R E Cofield BJD, Cuddy DT, Jarnot RF, Knosp BW, Perun VS, Snyder WV, Stek PC, Thurstans RP, , Wagner PA. 2008. Validation of Aura Microwave Limb Sounder stratospheric ozone measurement. *J. Geophys. Res.* **113.**

Giglio, L.; Randerson, J. T.; van der Werf, G. R. Analysis of daily, monthly, and annual burned area using the fourth-generation global fire emissions database (GFED4). *J. Geophys. Res. Biogeosci.* **2013**, *118*, 317–328.

Giglio, L.; Randerson, J. T.; Werf, G. R.; Kasibhatla, P. S.; Collatz, G. J.; Morton, D. C.; DeFries, R. S. Assessing variability and long-term trends in burned area by merging multiple satellite fire products. *Biogeosciences* **2010**, *7*, 1171–1186.

Groisman, P. Y.; Sherstyukov, B. G.; Razuvaev, V. N.; Knight, R. W.; Enloe, J. G.; Stroumentova, N. S.; Whitfield, P. H.; Førland, E.; Hannsen-Bauer, I.; Tuomenvirta, H.; Aleksandersson, H.; Mescherskaya, A. V.; Karl, T. R. Potential forest fire danger over Northern Eurasia: Changes during the 20th century. *Global and Planetary Change* **2007**, *56*, 371–386.

Hemmings, J. C. P., Barciela, R. M., and Bell, M. J. 2008. Ocean color data assimilation with material conservation for improving model estimates of air-sea CO_2 flux. J. Mar. Res., 66: 87-126.

Lasslop, G., K. Thonicke, and S. Kloster, SPITFIRE within the MPI Earth system model: Model development and evaluation, J. Adv. Model. Earth Syst., **2014**, 6, 740–755, doi:10.1002/ 2013MS000284.

Lindstedt, D., Lind, P., Jones, C., Kjellstr¨om, E., 2015. A new regional climate model operating at the meso-gamma scale; performance over Europe. Tellus A 67, 24138, doi: 10.3402/tellusa.v67.24138.

Liu, Y., Dorigo, W., Parinussa, R., de Jeu, R., Wagner, W., McCabe, M., Evans, J., van Dijk, A., 2012. Trend-preserving blending of passive and active microwave soil moisture retrievals. Remote Sensing of Environment 123, 280–297, doi: 10.1016/j.rse.2012.03.014.

Liu, Y., Parinussa, R., Dorigo, W., de Jeu, R., Wagner, W., van Dijk, A., McCabe, M., Evans, J., 2011. Developing an improved soil moisture dataset by blending passive and active microwave satellite-based retrievals. Hydrology and Earth System Sciences 15, 425–436, doi:10.5194/hess-15-425-2011.

Loyola, D. et al, 2013. ATDB (GDP 4.7) for O3M-SAF OTO and NTO, DLR/GOME-2/ATDB/01, issue 2, revision H, available from the O3M SAF web-site at:

Masson, V., et al., 2013. The SURFEXv7.2 land and ocean surface platform for coupled or offline simulation of earth surface variables and fluxes. Geosci. Model Dev. 6, 929–960, doi: 10.5194/gmd-6-929-2013.

Miles, G. M., Siddans, R., Kerridge, B. J., Latter, B. G., and Richards, N. A. D.: Tropospheric ozone and ozone profiles retrieved from GOME-2 and their validation, *Atmos. Meas. Tech.*, **8**, 385-398, doi:10.5194/amt-8-385-2015, 2015.

Palmer, J. R., and Totterdell, I. J. 2001. Production and export in a global ocean ecosystem model, Deep-Sea Res. Pt. I, 48: 1169-1198.

Samuelsson, P., Gollvik, S., Jansson, C., Kupiainen, M., Kourzeneva, E., van de Berg, W., 2014. The surface processes of the Rossby Centre regional atmospheric climate model (RCA4). Report in Meteorology 157, SMHI, SE-601 76 Norrk¨oping, Sweden.

Sevault F., S. Somot, A. Alias, C. Dubois, C. Lebeaupin-Brossier, P. Nabat, F. Adloff, M. Déqué, and B. Decharme, 2014: A fully coupled Mediterranean regional climate system model: design and evaluation of the ocean component for the 1980-2012 period, Tellus A, 66, 23967, http://dx.doi.org/10.3402/tellusa.v66.23967.

Sofieva, V. F., N. Rahpoe, J. Tamminen, E. Kyro, N. Kalakoski, M. Weber, A. Laeng, T. von Clarmann, G. Stiller, S. Lossow, D. Degenstein, A. Bourassa, C. Adams, C. Roth, N. Lloyd, P. Bernath, R. J. Hargreaves, J. Urban, D. Murtagh, A. Hauchecorne, M. Van Roozendael, N. Kalb, and C. Zehner, Harmonized dataset of ozone profiles from satellite limb and occultation measurements, *Earth Syst. Sci. Data Discuss.*, **6**, 189–222, 2013.

Stevens, B., et al., 2013: Atmospheric component of the MPI-M Earth System Model: ECHAM6. Journal of Advances in Modeling Earth Systems, 5 (2), 146–172.

Storkey, D., Blockley, E. W., Furner, R., Guiavarc'h, C., Lea, D., Martin, M. J., Barciela, R. M., Hines, A., Hyder, P., and Siddorn, J. R. 2010. Forecasting the ocean state using NEMO: The new FOAM system. Journal of Operational Oceanography, 3: 3-15.

Strandberg, G., Barring, L., Hansson, U., Jansson, C., Jones, C., Kjellstrom, E., Kolax, M., Kupiainen, M., Nikulin, G., Samuelsson, P., Ullerstig, A., Wang, S., 2014. CORDEX scenarios for Europe from the Rossby Centre regional climate model RCA4. Reports Meteorology and Climatology 116, SMHI, SE-601 76 Norrkoping, Sweden.

Takahashi, T., Sutherland, S. C., Wanninkhof, R., Sweeney, C., Feely, R. A., Chipman, D. W., Hales, B., Friederich, G., Chavez, F., Watson, A., Bakker, D. C. E., Schuster, U., Metzl, N., Yoshikawa-Inoue, H., Ishii, M., Midorikawa, T., Nojiri, Y., Sabine, C., Olafsson, J., Arnarson, T. S., Tilbrook, B., Johannessen, T., Olsen, A., Bellerby, R., Körtzinger, A., Steinhoff, T., Hoppema, M., de Baar, H. J. W., Wong, C. S., Delille, B., and Bates NR. 2009. Climatological mean and decadal changes in surface ocean pCO_2, and net sea-air CO_2 flux over the global oceans, Deep-Sea Res. Pt. II, 56, 554-577.

Tietsche, S., Notz, D., Jungclaus, J. H., & Marotzke, J., 2013. Assimilation of sea-ice concentration in a global climate model – physical and statistical aspects. *Ocean science*, *9*, 19-36.

Van Roozendael, M., R. Spurr, D. Loyola, C. Lerot, D. Balis, J-C. Lambert, W. Zimmer, J. van Gent, J. van Geffen, M. Koukouli, J. Granville, A. Doicu, C. Fayt, C. Zehner, Fifteen years of GOME/ERS2 total ozone data: the new direct-fitting GOME Data Processor (GDP) Version 5: I. Algorithm Description, *J. Geophys. Res.*, **117**, D3, doi:10.1029/2011JD016471, 2012.

Wagner, W., Dorigo, W., de Jeu, R., Fernandez, D., Benveniste, J., Haas, E., Ertl, M., 25 August-1 September 2012. Fusion of active and passive microwave observations to create an essential climate variable data record on soil moisture. In: XXII ISPRS Congress, Volume I-7. ISPRS Annals of the Photogrammetry, Remote Sensing and Spatial Information Sciences (ISPRS Annals), Melbourne, Australia, pp. 315–321.